

**SYNTHESIS AND CHARACTERISATION OF  
SOLUTION PROCESSABLE  
ACENES**

A thesis submitted to The University of Manchester for the degree of

Doctor of Philosophy

in the Faculty of Engineering and Physical Sciences.

**2010**

**Gonzalo Rincon LLorente**

**School of Chemistry**

# LIST OF CONTENTS

<b>LIST OF CONTENTS</b> .....	<b>2</b>
<b>LIST OF FIGURES</b> .....	<b>6</b>
<b>ABSTRACT</b> .....	<b>14</b>
<b>DECLARATION</b> .....	<b>15</b>
<b>COPYRIGHT STATEMENT</b> .....	<b>15</b>
<b>ACKNOWLEDGEMENTS</b> .....	<b>17</b>
<b>1 INTRODUCTION</b> .....	<b>19</b>
<b>1.1 Context of the thesis</b> .....	<b>20</b>
<b>1.2 Organic thin film transistors</b> .....	<b>21</b>
1.2.1 Operation of thin film transistor .....	22
1.2.2 Main components in organic thin film transistors .....	26
<b>1.3 Organic semiconductors</b> .....	<b>28</b>
1.3.1 What makes a good organic semiconductor?.....	33
1.3.1.1 HOMO-LUMO levels .....	33
1.3.1.2 Structure and packing.....	34
1.3.1.3 Purity of the materials .....	37
1.3.1.4 Processability and film formation properties .....	37
<b>1.4 Types of organic semiconductors</b> .....	<b>39</b>
1.4.1 N-type and p-type materials.....	39
1.4.2 Polymers and small molecules.....	40
1.4.2.1 Conjugated polymers .....	41
1.4.2.2 Small crystalline molecules.....	43
<b>1.5 Pentacene derivatives</b> .....	<b>46</b>
<b>1.6 Aims and Objectives</b> .....	<b>52</b>
<b>2 SYNTHESIS OF NOVEL PENTACENE AND ANTHRACENE DERIVATIVES</b> .....	<b>53</b>
<b>2.1 Synthesis of 6,13-bis(triisopropylsilylethynyl) pentacene (TIPS-pentacene) (1)</b> .....	<b>54</b>
<b>2.2 Synthesis of 1,4,8,11-tetramethyl-6,13-bis(trialkylsilyl ethynyl) pentacene derivatives</b> <b>59</b>	
2.2.1 Attempted synthesis of the tetramethyl-pentacene derivatives via 1,4,8,11-tetrabromo- 6,13-pentacenequinone (7).....	60

2.2.2	Attempted synthesis of the tetramethyl-pentacene derivatives via dialdehydes .....	65
2.2.2.1	Synthesis of 1,4-dimethyl-7-oxabicyclo[2,2,1]hept-5-ene-2,3-dicarboxylic anhydride (11) .....	66
2.2.2.2	Synthesis of 3,6-dimethylphthalic anhydride (12) .....	67
2.2.2.3	Synthesis of 3,6-dimethylphthalyl alcohol (13) .....	69
2.2.2.4	Different attempts to Synthesise 3,6-dimethylphthaldialdehyde (14) .....	70
2.2.2.4.1	Swern oxidation of 3,6-dimethylphthalyl alcohol (14).....	70
2.2.2.4.2	Pyridinium chlorochromate (PCC) oxidation of 3,6-dimethylphthalyl alcohol (13) .....	72
2.2.2.4.3	Synthesis of 3,6-dimethylphthaldialdehyde (14) via 3,6-dimethylphthalyl chloride .....	73
2.2.2.4.4	Diisobutylaluminium hydride (DIBAL) reduction of 3,6-dimethylphthalic anhydride (12) .....	74
2.2.3	Synthesis of the tetramethyl-pentacene derivatives via 3,6-dimethyl-1,2-bis(bromomethyl)benzene (19) .....	75
2.2.3.1	Synthesis of 3,6-dimethyl-1,2-bis(bromomethyl)benzene (19).....	76
2.2.3.2	Synthesis of 1,4,8,11-tetramethyl-6,13-pentacenequinone (15).....	77
2.2.3.3	Synthesis of tetramethylated pentacene derivatives (3, 4 and 5).....	78
2.3	Synthesis of 9,10-bis(trimethylsilylethynyl) anthracene (20), Synthesis of 9,10-bis(triethylsilylethynyl) anthracene (21), 9,10-bis(triisopropylsilylethynyl) anthracene (22) ...	83

### **3 PHYSICAL AND ELECTRONIC CHARACTERISATION OF THE NEW PENTACENE DERIVATIVES .....85**

3.1	Background.....	86
3.2	Solution properties of substituted pentacene derivatives.....	87
3.3	Determination of HOMO-LUMO levels of TMTES-pentacene and TMTIPS-pentacene .....	88
3.4	Thermal analysis of TMTES-pentacene and TMTIPS-pentacene .....	93
3.5	Crystal structure of TMTES-pentacene and TMTIPS-pentacene .....	97
3.6	Thin Film deposition of TMTES-pentacene and TMTIPS-pentacene.....	100
3.7	Determination of saturated hole mobility of TMTES-pentacene and TMTIPS-pentacene .....	104
3.8	Summary and Conclusions .....	109

### **4 PHYSICAL AND ELECTRONIC CHARACTERIZATION OF LOW MOLAR MASS SEMICONDUCTOR-INSULATOR BLENDS..... 110**

4.1	Introduction .....	111
4.2	Blends containing TIPS-pentacene and side-chain aromatic polymers.....	113
4.2.1	Materials .....	113
4.2.2	Solution processing.....	114
4.2.3	OFET performance of TIPS-pentacene-insulator blends. ....	114
4.2.4	Morphology of TIPS-pentacene-insulator blends. ....	117

4.3	Blends containing TMTES-pentacene and i-polyvinyl naphthalene .....	125
4.4	Conclusions .....	126
<b>5</b>	<b>AGGREGATION STUDIES OF ANTHRACENE DERIVATIVES AND THEIR INTERACTIONS WITH SINGLE WALLED CARBON NANOTUBES (SWNTS) .....</b>	<b>128</b>
5.1	Introduction to Single wall carbon nanotubes (SWNTs) .....	129
5.1.1	Non-covalent SWNTs functionalisation .....	131
5.1.1.1	Non covalent SWNTs functionalisation using biomolecules .....	132
5.1.1.2	Non covalent SWNTs functionalisation using polymers .....	133
5.1.1.3	Non covalent SWNTs functionalisation using small poly-aromatic materials ....	134
5.2	Single walled carbon nanotubes aims .....	135
5.3	Aggregation studies of 9,10-disubstituted anthracene derivatives .....	136
5.3.1	Fluorescence spectroscopy .....	137
5.3.2	Aggregation studies for anthracene and its derivatives.....	138
5.4	Dispersion of SWNTs using anthracene derivatives.....	145
<b>6</b>	<b>EXPERIMENTAL CHAPTER .....</b>	<b>150</b>
6.1	Materials .....	151
6.2	Synthetic characterisation techniques .....	151
6.3	Synthesis .....	153
6.3.1	Synthesis of 6,13-pentacenequinone (2) <sup>[131]</sup> .....	153
6.3.2	Synthesis of 6,13-bis(triisopropylsilylethynyl)pentacene (TIPS-Pentacene) (1) <sup>[60]</sup> .....	153
6.3.3	Synthesis of 1,4,8,11-tetrabromo-6,13-pentacenequinone (7) .....	154
6.3.4	Attempted synthesis of 1,4,8,11-tetrabromo-6,13-bis(triethylsilylethynyl) pentacene (23)	155
6.3.5	Attempted synthesis of 1,4,8,11-tetrabromo-6,13-bis(triisopropylsilylethynyl) pentacene (8)	156
6.3.6	Synthesis of 1,4-dimethyl-7-oxabicyclo[2,2,1]hept-5-ene-2,3-dicarboxylic anhydride (11) <sup>[132]</sup>	156
6.3.7	Synthesis of 3,6-dimethylphthalic anhydride (12) <sup>[132]</sup> .....	157
6.3.8	Synthesis of 3,6-dimethylphthalyl alcohol (13) <sup>[66]</sup> .....	158
6.3.9	Attempted synthesis of 3,6-dimethylphthalaldehyde (Swern oxidation) (14) <sup>[67]</sup> .....	159
6.3.9.1	Synthesis of phthalaldehyde (16) .....	160
6.3.9.2	Synthesis of 4,5-dimethylphthalaldehyde (17).....	160
6.3.10	Attempted synthesis of 3,6-dimethylphthalaldehyde (Pyridinium chlorochromate) (14)	161
6.3.11	Attempted synthesis of 3,6-dimethylphthalaldehyde (14) <sup>[69-70]</sup> .....	161
6.3.12	Attempted synthesis of 3,6-dimethylphthalaldehyde (14) .....	162
6.3.13	Synthesis of 3,6-dimethyl-1,2-bis(bromomethyl)benzene (19) <sup>[66]</sup> .....	163
6.3.14	Synthesis of 1,4,8,11-tetramethyl-6,13-pentacenequinone (15).....	163
6.3.15	Synthesis of 1,4,8,11-tetramethyl-6,13-bis(triethylsilylethynyl) pentacene (TMTES-pentacene) (4).....	164
6.3.16	Synthesis of 1,4,8,11-tetramethyl-6,13-bis(triisopropylsilyl ethynyl) pentacene (TMTIPS-pentacene) (5).....	165
6.3.17	Synthesis of 9,10-bis(triisopropylsilylethynyl) anthracene (22) .....	166

6.3.18	Synthesis of 9,10-bis(trimethylsilylethynyl) anthracene (20) .....	167
6.3.19	Synthesis of 9,10-bis(triethylsilylethynyl) anthracene (21) .....	167
<b>6.4</b>	<b>Materials Characterisation techniques.....</b>	<b>168</b>
<b>6.5</b>	<b>Organic field effect transistors device fabrication.....</b>	<b>170</b>
6.5.1	Solution preparation.....	171
<b>6.6</b>	<b>TMTES-pentacene and TMTIPS-pentacene crystallisation.....</b>	<b>172</b>
<b>6.7</b>	<b>Aggregation studies of anthracene and its derivatives .....</b>	<b>172</b>
<b>6.8</b>	<b>Anthracene derivatives-SWNTs interaction .....</b>	<b>173</b>
<b>7</b>	<b>CONCLUSIONS AND FURTHER WORK .....</b>	<b>174</b>
<b>8</b>	<b>REFERENCES .....</b>	<b>177</b>
<b>9</b>	<b>APPENDIX .....</b>	<b>187</b>
9.1	X-rays crystallographic data for TMTES-pentacene (4). .....	188
9.2	X-rays crystallographic data for TMTIPS-pentacene (5). .....	200

**Total words 37004**

# LIST OF FIGURES

<b>Figure 1.1</b> Cross section of basic structure for organic thin film transistors presenting bottom gate top contact structure (left hand side) and bottom gate bottom contact structure (right hand side) <sup>[10]</sup> . .....	22
<b>Figure 1.2</b> Operation diagram of an organic thin film transistor. Showing from top to bottom linear regime, pinch off point and saturated regime <sup>[2]</sup> . .....	23
<b>Figure 1.3</b> Classic output (a) and transfer (b and c) characteristics for an organic thin film transistor <sup>[2]</sup> . .....	25
<b>Figure 1.4</b> Bands diagram for an insulator, semiconductor and conductor material at 0 kelvin. Valence band are represented in red and conduction bands in blue. ....	29
<b>Figure 1.5</b> Polaron formed after removing one electron from polythiophene <sup>[21]</sup> . .....	31
<b>Figure 1.6</b> Transformation of a poly (phenylenevinylene) into the corresponding exciton due to the action of energy. ....	32
<b>Figure 1.7</b> Energy levels diagram showing the different types of polarons and excitons and the corresponding spin for each of them <sup>[22]</sup> . ....	32
<b>Figure 1.8</b> Simplified energetic diagram showing work function of gold and aluminium and HOMO-LUMO levels of an organic semiconductor <sup>[24]</sup> . ..	34
<b>Figure 1.9</b> Regioregular semicrystalline poly(3-hexylthiophene) (P3HT) <sup>[28]</sup> ....	35
<b>Figure 1.10</b> Distribution of highly ordered TIPS-pentacene molecules on a silicon oxide substrate. The highly ordered distribution and the close packing between the $\pi$ orbital of the pentacene cores are ideal for electronic carrier transport <sup>[31]</sup> . ....	36
<b>Figure 1.11</b> Represented p-type semiconductors. ....	40
<b>Figure 1.12</b> Represented n-type semiconductors. ....	40
<b>Figure 1.13</b> Amorphous semiconducting polymers. Polytriarylamine (left hand side), Polyphenylenevinylene (center) and Polythienylenevinylene (right hand side). ....	41
<b>Figure 1.14</b> Structure of MEH-PPV. ....	43

Figure 1.15 Structure of 5,11-trialkylsilylethynyl anthradithiophenes.....	45
Figure 1.16 6,13-disubstituted pentacene derivatives.....	48
Figure 1.17 Herringbone structure for pentacene <sup>[3b]</sup> .....	49
Figure 1.18. 1-D “Slip-Stack” structure <sup>[3b]</sup> . The arrows indicate the direction in which the charge transport can take place.....	49
Figure 1.19. 2-D “Brickwork” structure <sup>[3b]</sup> . The arrows indicate the directions in which the charge transport can take place.....	50
Figure 2.1 Synthesis of 6,13-bis(triisopropylsilylethynyl)pentacene (TIPS- pentacene) from Anthony’s method <sup>[34]</sup> .....	54
Figure 2.2 Synthesis of 6,13-pentacenequinone.....	55
Figure 2.3 Mechanism for the formation of 6,13-pentacenequinone. ....	55
Figure 2.4 Nuclear magnetic resonance (NMR) spectrum of 6,13- pentacenequinone in deuterated chloroform.....	56
Figure 2.5 Mechanism for the first step in the synthesis of TIPS-pentacene. The same process takes place at the other quinone to form the disubstituted species.....	57
Figure 2.6 Two different isomers of the dimerised molecules of TIPS- pentacene <sup>[61]</sup> .....	58
Figure 2.7 Products of the oxidation of pentacene (left hand side) and mass spectra corroborating their existence <sup>[62]</sup> .....	59
Figure 2.8 TMTMS-pentacene (3), TMTES-pentacene (4) and TMTIPS- pentacene (5).....	60
Figure 2.9 Attempted synthetic route for 1,4,8,11-tetramethyl-6,13-trialkyl silylethynyl pentacene derivatives via 1,4,8,11-tetrabromo-6,13- pentacenequinone (7).....	61
Figure 2.10 Proposed mechanism for the synthesis of quinone 7.....	62
Figure 2.11 Mass spectra of 1,4,8,11-tetrabromo-6,13-pentacenequinone (7). 63	
Figure 2.12 <sup>1</sup> H NMR spectra of the monosubstituted tetrabromo pentacene derivative. ....	63

<b>Figure 2.13 Diagram representing estimation of the atomic volumes for tetrabromoTIPS-pentacene when the bromine atoms are in the outer position (left hand side) an in the inner positions (right hand side).....</b>	<b>64</b>
<b>Figure 2.14 Proposed synthetic route for the synthesis of TMTIPS-pentacene (5) and TMTES-pentacene (4) and TMTMS-pentacene (3).....</b>	<b>65</b>
<b>Figure 2.15 Diels Alders reaction involving furan and maleic anhydride.....</b>	<b>67</b>
<b>Figure 2.16 Proposed mechanism to form 3,6-dimethylphthalic anhydride (12). .....</b>	<b>68</b>
<b>Figure 2.17 Mechanism for the reaction of LiAlH<sub>4</sub> with succinic anhydride to produce alcohols. It has been only represented in one side for extra clearness. The OR group attached to the aluminium corresponds to the intermediate A which appears from other equivalent reaction. The lithium has not been included in the mechanism but it forms part of the product as ionic salts. ....</b>	<b>69</b>
<b>Figure 2.18 Swern oxidation mechanism. In the common swern oxidation the oxalyl chloride transforms the dimethylsulfoxide (DMSO) into dimethylchlorosulphonium ion. This cation reacts with the alcohol to form an alkoxysulphonium ion and is this ion the one that in the presence of triethylamine (base) forms the desired aldehydes. In this mechanism only the reaction in one of the aldehydes is described. ....</b>	<b>71</b>
<b>Figure 2.19 Photo-catalysed formation of lactone. ....</b>	<b>72</b>
<b>Figure 2.20 PCC oxidation. From primary alcohols to aldehydes. The reaction is drawn taking place only in one of the sides for extra clarity. ....</b>	<b>73</b>
<b>Figure 2.21 Reaction structure for the formation of 3,6-dimethylphthaldialdehyde (14) <sup>[69], [70]</sup>.....</b>	<b>74</b>
<b>Figure 2.22 Mechanism for the reduction of esters to form aldehydes using DIBAL.....</b>	<b>75</b>
<b>Figure 2.23 Synthetic route towards the tetramethyl-pentacene derivatives<sup>[71]</sup>. .....</b>	<b>76</b>



Figure 2.24 Reaction mechanism for the synthesis of 3,6-dimethyl-1,2-bis(bromomethyl)benzene (19). Once more the reaction mechanism has been drawn only in one of the sides of the molecule for clarity.....	77
Figure 2.25 Reaction scheme for the synthesis of 1,4,8,11-tetramethyl-6,13-pentacenequinone (15).....	77
Figure 2.26 Mass spectrum of the crude TMTES-pentacene analysed after the column. Peak for the monomer and the dimers can be observed.....	79
Figure 2.27 Dimer taking place between the ethynyl group of one pentacenedithiophene molecule and one of the aromatic rings of another <sup>[47]</sup> .....	80
Figure 2.28 Vacuum sublimation system.....	80
Figure 2.29 Mass spectrum for TMTES-pentacene after the purification using silica plug. ....	82
Figure 2.30 9,10-Bis(trimethylsilylethynyl) anthracene (20), 9,10-bis(triethylsilylethynyl) anthracene (21) and 9,10-bis(triisopropylsilylethynyl) anthracene (22).....	83
Figure 2.31 Calculated HOMO, LUMO and band gaps for acenes <sup>[74]</sup> .....	84
Figure 3.1 Crystal lattice for TIPS-pentacene.....	87
Figure 3.2 Cyclic voltammetry of TMTES-pentacene (black dash line), TMTIPS-pentacene (red line) and ferrocene as the reference material (black solid line). The experiments were carried out in thin films on platinum electrodes using a scan rate of 100 mV/s (refer to experimental section for further details).....	89
Figure 3.3 Diagram explaining the calculation of $E_{1/2}$ ferrocene.....	90
Figure 3.4 Diagram explaining the how to obtain the offset of the UV-vis.....	91
Figure 3.5 UV-vis absorption diagram for TMTES-pentacene (black line) and TMTIPS-pentacene (red line). ....	91
Figure 3.6 From left to right, top to bottom thermal gravimetric analysis of TIPS-pentacene before drying, dry TIPS-pentacene, dry TMTIPS-pentacene and dry TMTES-pentacene. The samples were run at 5 °C/min heating rate under nitrogen atmosphere. ....	94

<b>Figure 3.7 DSC of TIPS-pentacene up to 200°C at a heating rate of 5 °C/min showing a reversible phase transition at 124 °C.....</b>	<b>95</b>
<b>Figure 3.8 DSC of TMTES-pentacene (left hand side) and TMTIPS-pentacene (right hand side) at 5 °C/min Heating rate. ....</b>	<b>96</b>
<b>Figure 3.9 Crystal lattice for TIPS-pentacene (left hand side) and pentacene (right hand side). ....</b>	<b>99</b>
<b>Figure 3.10 Crystal lattice for TMTES-pentacene (left hand side) and TMTIPS-pentacene (right hand side). ....</b>	<b>100</b>
<b>Figure 3.11 Optical micrographs (250 x 400 micron) of TMTIPS-pentacene (left hand side) and TMTES-pentacene (right hand side), drop cast onto OTS treated silica from a solution of 0.5 %w/w in toluene.....</b>	<b>101</b>
<b>Figure 3.12 Observation by atomic force microscopy in dynamic mode of a terraced film of TMTES-pentacene. The topographic scan (left hand side) and the dynamic mode amplitude image (right hand side) gives an enhanced viewing of the atomic step. ....</b>	<b>102</b>
<b>Figure 3.13 Diagram explaining the calculations of the tilt angle from the height obtained from AFM and the molecular length obtained by X-ray single crystallography.....</b>	<b>102</b>
<b>Figure 3.14 Out-of-plane XRD patterns (0,0,P) of TMTES-pentacene (left hand side) and TMTIPS-pentacene (right hand side) on OTS treated silicon substrates using a Cu K<sub>α</sub> source at 0.15405980 nm. ....</b>	<b>103</b>
<b>Figure 3.15 Bottom gate top contact organic thin film transistor structures.</b>	<b>105</b>
<b>Figure 3.16 Mechanism of coating of OTS on silica surface<sup>[84]</sup> .....</b>	<b>105</b>
<b>Figure 3.17 Transfer Characteristics for an OTFT made using TIPS-pentacene. ....</b>	<b>106</b>
<b>Figure 3.18 Transfer Characteristics for an OTFT made using TMTIPS-pentacene. ....</b>	<b>107</b>
<b>Figure 3.19 Transfer (left hand side) and output (right hand side) characteristics for an OFET using TMTES-pentacene.....</b>	<b>107</b>

<b>Figure 4.1 Maximum saturated hole mobility of TIPS-Pentacene–insulator blends as a function of weight fraction of TIPS-pentacene for PAMS, PS, iPS and iPVN.....</b>	<b>115</b>
<b>Figure 4.2 Output characteristics in the saturated regime (<math>V_G = -80V</math>) for TIPS-pentacene–insulator blends at (a) 0.8, (b) 0.5 and (c) 0.2 weight fraction TIPS-pentacene.....</b>	<b>115</b>
<b>Figure 4.3 Transfer characteristics in the saturated regime (<math>V_{sd} = -80V</math>) for TIPS-pentacene–insulator blends at (a) 0.8, (b) 0.5 and (c) 0.2 weight fraction TIPS-pentacene.....</b>	<b>116</b>
<b>Figure 4.4 Evolution of film morphology in thin films of TIPS-pentacene blended with (a) PAMS and (b) iPS as a function of TIPS-pentacene weight fraction.....</b>	<b>118</b>
<b>Figure 4.5 X-Ray Diffraction patterns (from top to bottom) of TIPS-pentacene–PAMS, TIPS-pentacene–iPS and TIPS-pentacene. Blends were containing 0.8 weight fraction of TIPS-pentacene .....</b>	<b>118</b>
<b>Figure 4.6 Infrared spectroscopic imaging of TIPS-pentacene–insulator blends at TIPS-pentacene weight fraction = 0.1: (a) TIPS:iPS bottom surface, (b) TIPS:iPS top interface, (c) TIPS:PS bottom surface, (d) TIPS:PS top interface, (e) TIPS:PAMS bottom surface, (f) TIPS:PAMS top interface. The absorbance image is focused on the stretch peak at <math>2130\text{cm}^{-1}</math> band consequently the contrast in the images represent the areas where TIPS-pentacene is present. ....</b>	<b>120</b>
<b>Figure 4.7 Optical images before etching and AFM topographic images of TIPS-pentacene–insulator blends for 0.9 and 0.2 weight fraction TIPS-pentacene before and after solvent etching. The contrast in the images represent crystals of TIPS-pentacene.....</b>	<b>121</b>
<b>Figure 4.8 Line profile of TIPS-pentacene-iPVN (0.2 weight fraction TIPS-pentacene) before (top) and after (bottom) selective chemical etching...</b>	<b>122</b>
<b>Figure 4.9 Comparison of high resolution XPS C1s spectra for TIPS-pentacene–insulator blend for 0.5 weight fraction TIPS-pentacene (a) PS and (b) iPS. ....</b>	<b>123</b>

<b>Figure 4.10 Maximum saturated hole mobility as a function of the weight concentration of compound TMTES-pentacene (■) and TIPS-pentacene (×) when blended with iPVN drop cast on OTS from tetralin solution at RT.....</b>	<b>125</b>
<b>Figure 4.11 Evolution of the (001) peak intensity of the powder diffraction XRD pattern of TMTES-pentacene as a function of weight concentration when blended with isotactic iPVN drop cast on OTS treated glass from tetralin solution at RT. ....</b>	<b>126</b>
<b>Figure 5.1 Basic structure of single wall carbon nanotubes<sup>[110]</sup>.....</b>	<b>129</b>
<b>Figure 5.2 Scheme representing chiral vector and angle<sup>[112]</sup>.....</b>	<b>130</b>
<b>Figure 5.3 Non covalent functionalisation using 1-pyrenebutanoic acid succinidyl ester (left hand side) and single stranded DNA (right hand side)<sup>[116a, 117]</sup>.....</b>	<b>132</b>
<b>Figure 5.4 Structure of PmPV. ....</b>	<b>133</b>
<b>Figure 5.5 Selective interactions of anthracene and terphenyl with armchair and zig-zag nanotubes respectively<sup>[126]</sup>.....</b>	<b>135</b>
<b>Figure 5.6 Anthracene derivatives used for the aggregation and SWNTs dispersion studies . ....</b>	<b>136</b>
<b>Figure 5.7 Jablonski Diagram<sup>[127]</sup>.....</b>	<b>138</b>
<b>Figure 5.8 Absorption (left hand side) and fluorescence (right hand side) spectrum of a 10<sup>-4</sup> M solution of anthracene in toluene. ....</b>	<b>139</b>
<b>Figure 5.9 Fluorescence intensity of anthracene at different concentrations in toluene. ....</b>	<b>140</b>
<b>Figure 5.10 Intensity of the fluorescence vs. concentration for anthracene..</b>	<b>141</b>
<b>Figure 5.11 Anthracene derivatives.....</b>	<b>142</b>
<b>Figure 5.12 Intensity of the fluorescence vs. concentration comparison. ....</b>	<b>143</b>
<b>Figure 5.13 Crystallographic cell for anthracene. ....</b>	<b>144</b>
<b>Figure 5.14 Crystallographic structure for TMS-anthracene. ....</b>	<b>144</b>
<b>Figure 5.15 Graphs showing the fluorescence intensity of anthracene and its derivatives at different concentrations and the intensity of the blends with SWNTs. ....</b>	<b>146</b>

**Figure 5.16 Percentages quenching of the fluorescence intensity for each derivative at different concentrations after the addition of the nanotubes.**

..... 147

## Abstract

The University of Manchester

Gonzalo Rincon LLorente

PhD

Synthesis and Characterisation of solution processable acenes.

30<sup>th</sup> of March 2010

Here we present the synthesis, characterisation and electronic evaluation of a new family of high performance solution processable 1,4,8,11-tetramethyl-6,13-bis(trialkylsilylethynyl) pentacene derivatives. 1,4,8,11 methyl substituted 6,13-bis(triethylsilylethynyl) pentacene shows extended  $\pi$ - $\pi$  overlap when deposited from solution yielding organic thin film transistors with high and reproducible hole mobility with negligible hysteresis.

The morphology and organic field effect transistor (OFET) properties of two component blends of semicrystalline 6,13-bis(triisopropylsilylethynyl)pentacene (TIPS-pentacene) with selected amorphous and semi-crystalline side chain aromatic low permittivity insulating binders deposited at room temperature under vacuum from a good solvent have been studied. When blended with an amorphous binder there is evidence from X-ray photoelectron spectroscopy (XPS) for a strong interaction between TIPS-pentacene and binder in the solidified film giving rise to twisted TIPS-pentacene crystals containing dislocations. Due to this strong interaction we see no evidence of segregation of TIPS-pentacene towards the active interface and hence we observe a rapid fall off in saturated hole mobility at an active concentration less than 50 wt-%. When blended with a crystalline binder there is no evidence from XPS of any interaction between TIPS-pentacene and binder in the solidified film. We propose that when a crystalline binder is used, which crystallizes more slowly from solution than TIPS-pentacene, we observe stratification of the active material to both interfaces and as a result retention of saturated hole mobility even down to 10 wt-%. The potential applications of the approach are in the formulation of low-cost organic semiconductors whose solution and solid state properties can be fine-tuned by careful binder selection.

To conclude, solution aggregation studies as a precursor to understanding crystallisation of a family of anthracene derivatives and their ability as single wall carbon nanotubes dispersants are presented.

## Declaration

No portion of the work referred to in the thesis has been submitted in support of an application for another degree or qualification of this or any other university or other institute of learning.

## Copyright Statement

- i. The author of this thesis (including any appendices and/or schedules to this thesis) owns certain copyright or related rights in it (the “Copyright”) and s/he has given The University of Manchester certain rights to use such Copyright, including for administrative purposes.
- ii. Copies of this thesis, either in full or in extracts and whether in hard or electronic copy, may be made **only** in accordance with the Copyright, Designs and Patents Act 1988 (as amended) and regulations issued under it or, where appropriate, in accordance with licensing agreements which the University has from time to time. This page must form part of any such copies made.
- iii. The ownership of certain Copyright, patents, designs, trade marks and other intellectual property (the “Intellectual Property”) and any reproductions of copyright works in the thesis, for example graphs and tables (“Reproductions”), which may be described in this thesis, may not be owned by the author and may be owned by third parties. Such Intellectual Property and Reproductions cannot and must not be made available for use without the prior written permission of the owner(s) of the relevant Intellectual Property and/or Reproductions.
- iv. Further information on the conditions under which disclosure, publication and commercialisation of this thesis, the Copyright and any

Intellectual Property and/or Reproductions described in it may take place is available in the University IP Policy (see <http://www.campus.manchester.ac.uk/medialibrary/policies/intellectual-property.pdf>), in any relevant Thesis restriction declarations deposited in the University Library, The University Library's regulations (see <http://www.manchester.ac.uk/library/aboutus/regulations>) and in The University's policy on presentation of Theses



## Acknowledgements

First of all I would like to thank Professor S. G. Yeates for his continuous support during all the time I have been working with. Especially I would like to thank him for his understanding during the last period of the PhD when the difficult circumstances made it particularly hard. I would also like to thank Marie Madec for her explanations and never-ending patience in the lab everyday during the PhD without whom the completion of it would have been especially hard. Thanks to John Morrison, Dolores Caras Quintero and Dave Crouch for the invaluable synthetic chemistry discussions.

I cannot forget the help offered by Barbara Sasso during the confusing first year of my PhD when the simplest thing looked impossible. As well I would like to thank Martin and Val, the people in the analysis and mass spectroscopy rooms, who helped me understanding a bit more about this crazy world that is chemistry. Thanks to Masaki for his explanations on cyclic voltammetry and to Robin Prichard for helping me with the crystallography.

I would like to thank and remember all the people who helped me enjoying life in Manchester. The good friends, who were there when I most needed them: Andromachi, Jesus, Irene, Lapo, Michela, Maite, Huete, Alex, Jordi, Dario, Afsar, my neighbours. Thanks to everyone who made me spend so many good moments in the lab during these years Henry, Khalid, Laura, Carol, Mark, Rex, Paul, Mike, Desheng, Siren, Sahreen, Andy, Abdul, Sean, Peter and all the people in OMIC.

The most sincere thanks to my parents and sisters that have been, from the distance, an invaluable source of love and support and of course to my loved Julia who has been by my side during all these years. Without them none of this could have been possible and for this I would be for ever thankful.

A mis padres y hermanas

A Julia

# 1 Introduction

## 1.1 Context of the thesis

Printed electronics<sup>[1]</sup> potentially offers relatively simple and low cost ways to fabricate electronic devices such as displays, identification tags, light emitting displays (LEDs), sensors, thin film transistors (TFTs) and photovoltaic cells. This is a complement to conventional silicon electronics not an alternative. The performance of organic electronics has improved over the last years that it is becoming comparable to the performance observed in amorphous silicon devices<sup>[2]</sup>. This organic circuits will not drive a PC but they can be used for many other applications, such as backplane drives for e-paper.

Printed electronics is used to describe the low temperature deposition of formulated “electronic” inks using a range of conventional printing techniques to make electronic components. These low temperature printing processes reduce material and energy usage compared with multi-step etches used in conventional silicon semiconductor manufacture<sup>[1a]</sup>. Printed electronics is a technique aimed for organic materials rather than inorganic counterparts and they can be printed onto flexible substrates such as plastics, stainless steel foils as well as glass substrates.

In the last decades, the scientific community has been interested in the development of organic semiconductors<sup>[3]</sup> which address the following performance requirements:

- Deliver cost effective manufacture at large scale using environmentally acceptable processes
- Allow a range of formulation such that it can be deposited using a variety of printing techniques including ink jet, flexographic and screen printing
- Chemically stable and capable of being processed under ambient conditions and at temperatures up to 180 °C.
- Be capable of being processed in a “typical” liquid crystal display (LCD) manufacture line

Organic semiconductors fall into two generic classes, conjugated polymers and small aromatic molecules<sup>[3c]</sup>. Polymeric organic semiconductors have the advantages of very good processing and film formation properties. However, the electronic mobilities reached are generally either low or require high temperature processing to achieve acceptable performance. A few examples of semiconducting polymers are poly(triarylamine)s (PTAA)<sup>[4]</sup>, poly(p-phenylenevinylene) (PPV)<sup>[5]</sup>, and poly(3-hexylthiophene) (P3HT)<sup>[6]</sup>. Semiconducting small molecules have been until few years ago poor in terms of processing or film formation properties but better in terms of electronic mobilities. Classic examples are pentacene<sup>[7]</sup> and rubrene<sup>[8]</sup>.

## **1.2 Organic thin film transistors**

Thin film transistors can be defined as electronic switches<sup>[9]</sup>. They are fundamental building blocks for electronic devices. As a key part of every electronic circuit they are essential for their operation and as a consequence they are present in all kind of electronic devices. Among their many applications, TFTs can be found in the backplane of every flat panel display or in memory applications.

Organic thin film transistors (OTFTs) have been fabricated with many different architectures trying to optimise their performance depending on the target application. The aim of this thesis was the synthesis and study of the electronic properties of new organic semiconductors. As a consequence only basic device structures were used in this study and these are the ones presented here, Figure 1.1.

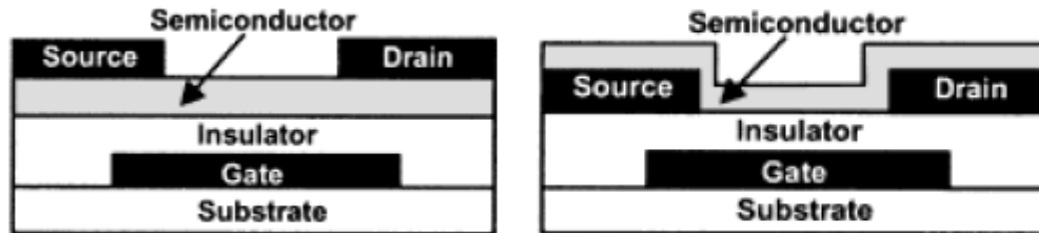


**Figure 1.1** Cross section of basic structure for organic thin film transistors presenting bottom gate top contact structure (left hand side) and bottom gate bottom contact structure (right hand side)<sup>[10]</sup>.

Organic thin film transistors are layered structures. Here we present two basic structures, bottom gate top contact and bottom gate bottom contact, where the only difference is the order in which the source and drain electrodes are deposited. In the top contact structure, the source and drain electrodes are deposited as the last layer on top of the organic semiconductor. In the bottom contact structure, the electrodes are placed before the organic semiconductor and on top of the insulator layer.

### 1.2.1 Operation of thin film transistor

Applying<sup>[11]</sup> a voltage to the gate electrode ( $V_G$ ) creates polarisation of the insulator. The polarisation induced in the insulator by the gate voltage generates into the organic semiconductor a very thin layer of mobile charges concentrated at the OSC-insulator interface. This interface is the accumulation layer. The mobile charges in the organic semiconductor will be either electrons or holes depending on the sign of the voltage applied on the gate. A negative gate voltage originates holes as mobile charge carriers and a positive gate voltage originate electrons as mobile charge carriers. The first charges injected fill deep traps existing in the organic semiconductor. These charges are the origin of threshold voltage ( $V_{TH}$ ).

When a bias is applied between the source and drain electrodes ( $V_{SD}$ ) the mobile charges move from drain to source generating so a current ( $I_D$ ). When  $V_{SD} \ll V_G - V_{TH}$  a linear representation can be obtained in a plot  $I_D$  vs  $V_{SD}$ . This is known as the

linear regime. Then as the voltage applied between source and drain is increased the point where  $V_{SD}=V_G-V_{TH}$  is reached. This is known as the “pinch off” point. At this point a depletion region is observed next to the drain electrode due to saturation of charges being injected into the system. This is the beginning of the saturated regime and it is where the current saturates reaching a maximum point  $I_{D,SAT}$ . If  $V_{SD}>V_G-V_{TH}$  no increase in the current  $I_D$  will be observed. Instead the depletion region will increase under the influence of the strong electric field, Figure 1.2.

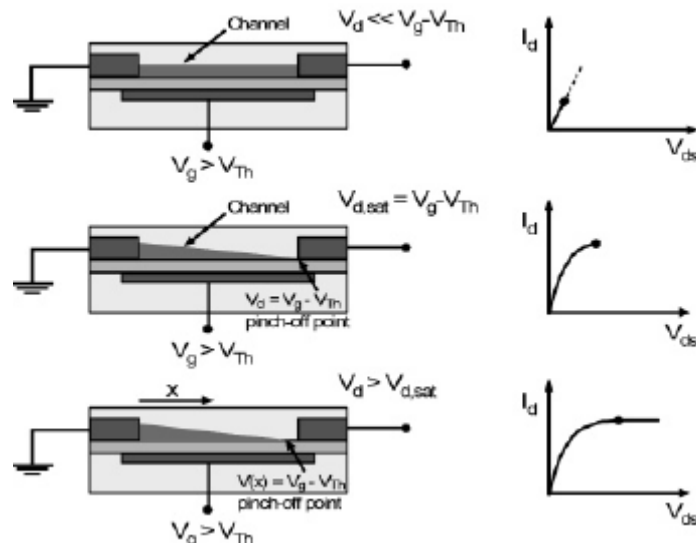


**Figure 1.2 Operation diagram of an organic thin film transistor. Showing from top to bottom linear regime, pinch off point and saturated regime<sup>[2]</sup>.**

There are two main parameters providing information about TFTs performance. The first one is the carrier mobility ( $\mu$ ) [ $\text{cm}^2/\text{Vs}$ ] which provides information about how fast the carriers move through the semiconductor channel depending on the voltage applied. This parameter is defined by Equation 1.1 and Equation 1.2 depending if the measurement is made either in the linear or saturated regime.

$$I_D = \frac{\mu_{FET}WC_i}{L} \left[ (V_G - V_{TH})V_{SD} - \frac{V_{SD}^2}{2} \right] \text{ for } |V_{SD}| \ll |V_G - V_{TH}| \quad \mathbf{1.1}$$

$$I_D = I_{sat} = \frac{\mu_{FET}WC_i}{2L} (V_G - V_{TH})^2 \text{ for } |V_{SD}| \geq |V_G - V_{TH}| \quad \mathbf{1.2}$$

Where  $W$  is the width of the channel,  $L$  the length of the channel,  $C_i$  is the equivalent capacitance of the dielectric intercepting the channel,  $V_{SD}$  and  $V_G$  are the voltage applied to drain and gate respectively and  $V_{TH}$  the threshold voltage.

If the voltage applied between the source and drain electrodes is much smaller than  $|V_G - V_{TH}|$  then Equation 1.1 is used, being defined as the linear regime. On the other hand, when the voltage applied between the source and drain electrodes is equal or bigger than  $|V_G - V_{TH}|$  then Equation 2 is used and this section is defined as the saturated regime.

The second parameter providing essential information about the TFT performance is the on/off ratio. This quantifies the current ratio between the on and off states. A good on/off ratio in an organic thin film transistor would be around  $10^6$  considering the on state when the saturation is reached and off state when no bias is applied to the device.

To characterise the behaviour of a thin film transistor and to understand the influence of the changes in the gate and source voltages two type of measurements can be carried out. These are the output and the transfer characteristics, Figure 1.3.



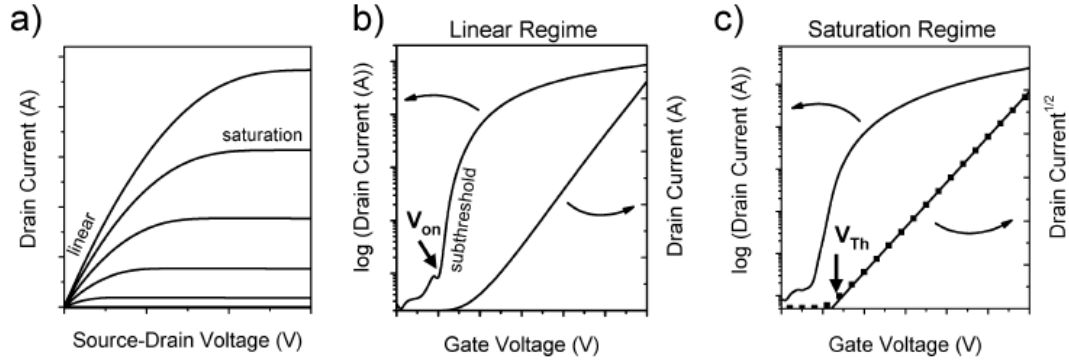


**Figure 1.3 Classic output (a) and transfer (b and c) characteristics for an organic thin film transistor<sup>[2]</sup>.**

The output characteristics are represented as a family of curves  $I_D$  vs  $V_{SD}$  at different constants  $V_G$ . The transfer characteristics are represented as a family of curves  $I_D$  vs  $V_G$  at different constant  $V_{SD}$ . Commonly the transfer characteristics are presented with a double Y axis and the  $I^{1/2}$  vs  $V_G$  is also represented, Figure 1.3.

The transfer characteristics contain fundamental information to understand the behaviour of the semiconducting material in the transistor. Among the most important ones are the threshold voltage ( $V_{TH}$ ), which correspond to the minimum gate voltage required to turn on the device, the saturated mobility ( $\mu_{sat}$ ) that correspond to the slope of the plot root square of the current vs gate voltage ( $I^{1/2}$  vs  $V_G$ ) and the on/off ratio that can be obtained by calculating the ratio between the currents in the on and off state.

From the output characteristics information about the injection of charges from the electrodes into the semiconducting material can be obtained.

## 1.2.2 Main components in organic thin film transistors

The characteristics required for an organic semiconductor to achieve optimum performance in thin film transistors are discussed in section 1.3.1. Here, the other components forming part of organic thin film transistors are briefly described:

- Substrate/Gate: the most common substrate for bottom gate top contact thin film transistors are wafers of highly n-doped silicon. Substrates can be prepared as conducting materials. This way the step of adding a gate electrode, on top of it, could be avoided. Silicon is a semiconductor but by doping it (commonly with phosphorus), a conducting substrate is achieved.

Organic semiconductors have brought the possibility of using plastic flexible substrates and a wide range of materials are now been used as OTFTs substrates. Polymer such as (Poly[3,4-ethylenedioxythiophene] Poly-styrenesulfonate) PEDOT:PSS or polyaniline (PANI) are good examples of conducting polymers that can be used as solution deposited electrodes on plastic substrates<sup>[1a]</sup>. Flexible substrates based on polyethylenephtalate (PET) with already deposited indium thin oxide (ITO) electrode layer are already commercially available<sup>[12]</sup>. Due to its transparency ITO has been widely used for the fabrication of organic light emitting diodes (OLEDs).

- Insulator: the insulator has a very important role to play in the operation of an organic thin film transistor<sup>[13]</sup>. In first place its morphology and composition determine the distribution and crystallisation of the semiconducting material molecules deposited on top of it. The accumulation layer occupies only a few nanometres in the semiconductor-insulator interface. If this interface is not well defined then the transport of carriers would be worsened<sup>[14]</sup>.

Another factor to consider is the importance of the insulator dielectric constant ( $\kappa$ ). This dielectric constant is related with the capacitance of the insulator by Equation 1.3 and the capacitance of the insulator is directly proportional to the current as can be observed in Equations 1.1 and 1.2.

$$C_i = \frac{\epsilon_0 \kappa}{d} \quad \mathbf{1.3}$$

In Equation 1.3  $C_i$  correspond to the capacitance of the insulator,  $\epsilon_0$  is the permittivity of the vacuum,  $\kappa$  is the dielectric constant and  $d$  is the thickness of the insulator.

The dielectric constant ( $\kappa$ ) gives an indication of how good is the polarisation of a material under the influence of an electric field. Debate is still open between supporters of low and high dielectric constant insulators. When using high dielectric constant insulators lower gate voltages are required to operate the devices and as a consequence lower voltages are necessary to run the devices<sup>[13]</sup>. This is essential to decrease the power consumption of the devices. The main inconvenience of high  $k$  dielectrics is that they enhance the localisation of electronic states through which the carrier transport takes place in organic semiconductors (increase of traps) and as a consequence a decrease in the mobility is observed.

On the other trend, and the most widely practised, suggests that this decrease in mobility arising from dipolar disorder could be avoided by using low dielectric constant insulators<sup>[15]</sup>. In order to be able to operate a thin film transistor at low voltages, using a low dielectric constant insulator, a thin insulator layer is required. This reduces the break down voltage and as a consequence the operation of the TFT is limited to low voltages.

The most common insulator used is silicon oxide ( $\text{SiO}_2$ ), which is grown on the surface of the doped silicon gate/substrate. However, nowadays the desire towards flexible substrates is taking the scientific community to use polymeric insulators which are solution processable such as poly(methyl methacrylate) (PMMA). The application of soluble polymeric dielectrics will enable all the layers of the thin film transistor to be printed.

- Source and drain electrodes: Deposition of the metallic electrodes can take place above or below the organic semiconductor layer. The deposition technique will depend on the nature of the material used as electrode. Insoluble materials such as gold or other metals are normally deposited by vacuum deposition through a shadow mask. Soluble conducting polymers such as PEDOT:PSS are seen as possible candidates for flexible devices and solution deposition techniques are used in these cases.

The width (W) and length (L) of the channel, which are factors of major importance, are decided at the electrodes deposition stage. The importance of the work function energetic level of the metallic electrodes with respect to the HOMO and LUMO of the organic semiconductor is defined later in this chapter. The injection of carriers into the semiconductor is defined by these parameters<sup>[16]</sup>.

### 1.3 Organic semiconductors

Band theory explains the electrical conductivity of inorganic materials<sup>[17]</sup>. In a molecule, the location of the electrons in the molecular orbitals is commonly represented using the molecular orbital diagram. When this representation is extended to the bulk material, the discrete individual molecular orbitals lead to the formation of bands. The higher occupied molecular orbitals (HOMO) represent the valence band and the lower unoccupied molecular orbitals (LUMO) correspond to the conduction band.

Depending on the energetic band gap between the valence and the conduction bands materials can be classified as metallic, insulators or semiconductors, Figure 1.4. When in a material valence and conduction bands overlap they are known as metals. The overlapping of these bands makes metallic materials good electronic conductors. Insulators present opposite characteristics since the distance between valence and conduction bands is so large that the promotion of one electron from the valence to the conduction bands is energetically forbidden. Semiconductors are materials that even when the valence and conduction bands do not overlap promotion of electrons from the valence into the conduction band can be achieved by applying heat, light or an electric field.

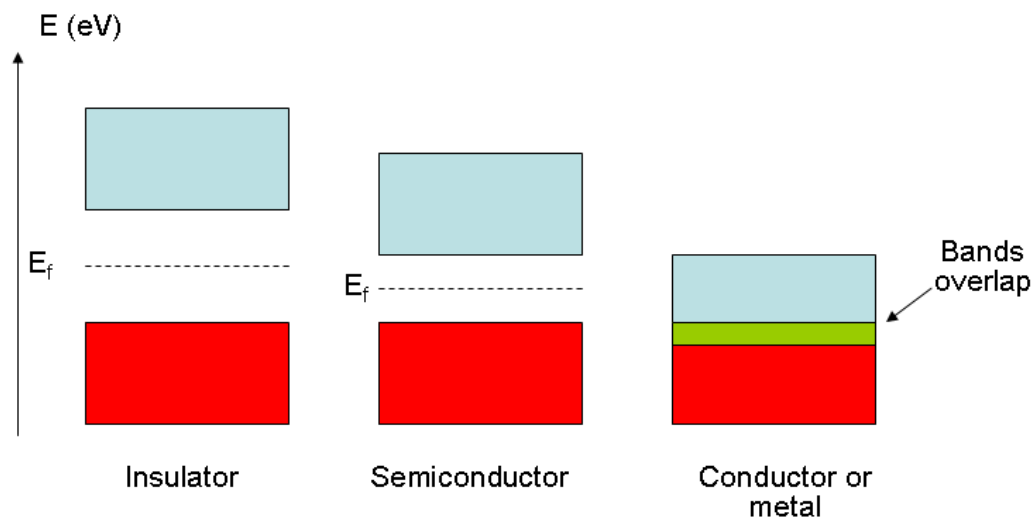


**Figure 1.4 Bands diagram for an insulator, semiconductor and conductor material at 0 kelvin. Valence band are represented in red and conduction bands in blue.**

The Fermi level ( $E_f$ ) at 0 Kelvin corresponds in a metal to the energy level that separates the filled from the empty electronic states. In metals it is known as the work function  $\Phi$ . In the case of semiconductors and insulators that the bands are not overlapped the Fermi level is placed equidistant from valence and conduction bands.

Organic materials are generally insulators. However, a few of them, so called conjugated materials, can behave as semiconductors. Conjugated materials are those which contain triple or double bonds alternated with single ones. This creates an overlap of the  $\pi$  orbitals which allows delocalization of electrons through the molecule. This conducting behaviour in organic materials was first observed by Heeger<sup>[18]</sup> et al. in 1977. They observed that when doping trans-polyacetylene with different halogens an increase in the electrical conductivity was observed. It was not until few years later when Ebisawa, Kurokawa and Nara used this technology for the construction of organic film transistors<sup>[19]</sup>.

There is controversy in the field of charge transport through organic semiconductors. A satisfactory theory to explain the phenomena in all kind of organic semiconductors has not been found. In amorphous materials such as conjugated polymers the transport of carriers seems to follow a hopping like transport between well defined states of energy<sup>[9b]</sup>. In the case of crystalline materials the transport seems to be following a band like behaviour between delocalised states of energy<sup>[2]-[20]</sup>.

Here we present an introduction to the hopping like transport which is the preferred theory explaining charge transport process in organic semiconductors.

The main difference between the charge transport in inorganic and organic semiconductors is that in inorganic semiconductors the transport takes place through delocalised states of energy emerging from the creation of the bands and in the case of organic semiconductors it occurs through localised states of energy. In hopping like transport theory the transport of carriers does not take place through a cloud of delocalised electrons like in the bands theory. Instead the charges hop through a number of localised states which are the polarons, Figure 1.5.

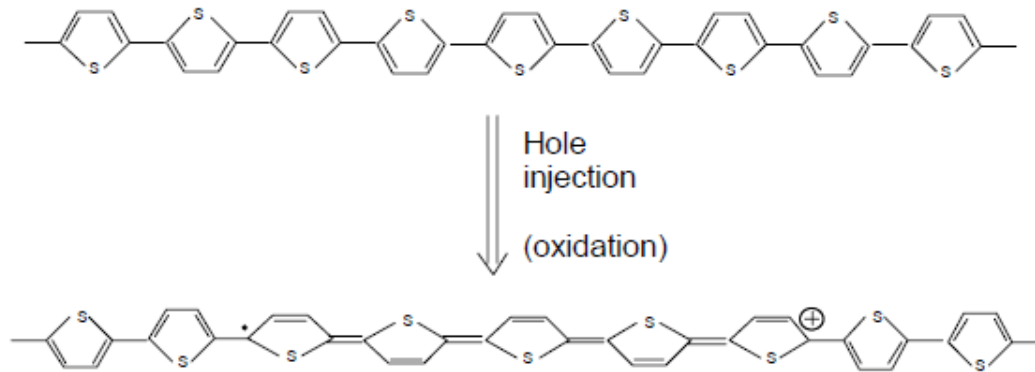


**Figure 1.5 Polaron formed after removing one electron from polythiophene<sup>[21]</sup>.**

The hopping type theory takes into account the nature of the organic material. The interaction between organic semiconductors molecules is much weaker than the covalent interaction observed in inorganic semiconductors. Therefore when a carrier is added to an OSC (removing electrons from the HOMO, which means adding a hole, or adding electrons to the LUMO) the structure of the molecules suffers a relaxation to reach a new state of minimum energy. The molecule with an extra electron, or hole, forms a radical ion which is called polaron, Figure 1.5. Therefore, a polaron is the result of the deformation of a conjugated compound under the presence of a charge<sup>[9b]</sup>. The charge transport takes place then as charges hopping from chain/molecule to another chain/molecule.

Another important difference between both theories is that in inorganic semiconductors increasing the temperature decreases the mobility since it causes lattice vibrations that would scatter the free flow of carriers. In the case of organic semiconductors the phonons improve the mobilities as it induces the formation of excitons. When a phonon excites a molecule but without enough energy as for the electron to leave the molecule, the electron is directed to the LUMO. In this case, as in the case of the polarons, the structure of the molecule suffers an energetically driven relaxation giving place to the so called exciton. The molecule is then in an excited state and it needs then less energy to be ionised, Figure 1.6.

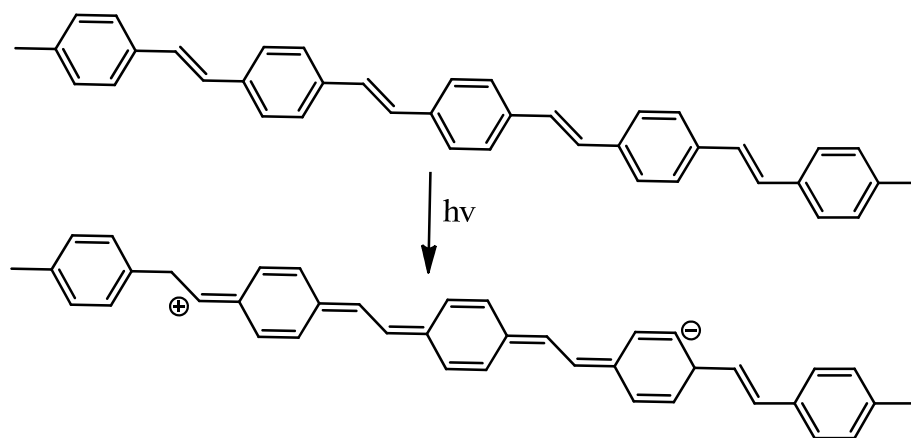


**Figure 1.6 Transformation of a poly (phenylenevinylene) into the corresponding exciton due to the action of energy.**

Below is presented for extra clarity an energy levels diagram where the different types of polarons and excitons are shown, Figure 1.7.

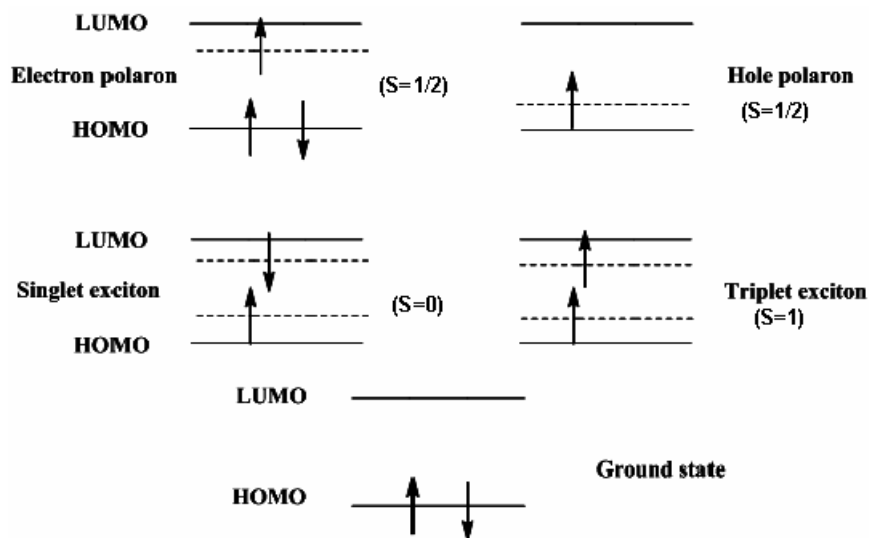


**Figure 1.7 Energy levels diagram showing the different types of polarons and excitons and the corresponding spin for each of them<sup>[22]</sup>.**



### 1.3.1 What makes a good organic semiconductor?

Several factors affect the performance of organic semiconductors in electronic devices. This thesis is focused in the application of organic semiconductors in thin film transistors. Hence, only the characteristic required to build up and optimise the operation of OTFTs are discussed. These influential factors can be comprised in four points:

- HOMO-LUMO levels
- Structure and packing
- Purity of materials
- Processability and film formation properties

#### 1.3.1.1 HOMO-LUMO levels

Injection of carriers from the electrodes into the organic semiconductors is determined by the HOMO-LUMO energetic levels of the semiconductor and by the work function ( $\Phi$ ) of the metal used in the electrodes. The work function of a metal represents the energy required to extract one electron from the metal surface, in metals the work function is equivalent to the ionisation potential<sup>[20]</sup>. One of the advantages of using organic semiconductors is that their HOMO-LUMO levels can be tuned by the addition of electron donor or electron acceptor groups into the semiconductor structure<sup>[23]</sup>. Their relative position respect to the work function of the electrodes would determine how easy would be the injections of charges into the material<sup>[24]</sup>.

In the ideal transistor, the Fermi level of the source should be very close in energy to the HOMO of the semiconductor. If  $\Phi - E_{\text{HOMO}} \leq 0.3\text{eV}$  then, the carriers can flow freely into the semiconductor. In these cases there is a minimum resistance in the injection process. This kind of contact between the metal and the semiconductor is called Ohmic contact, Figure 1.8.

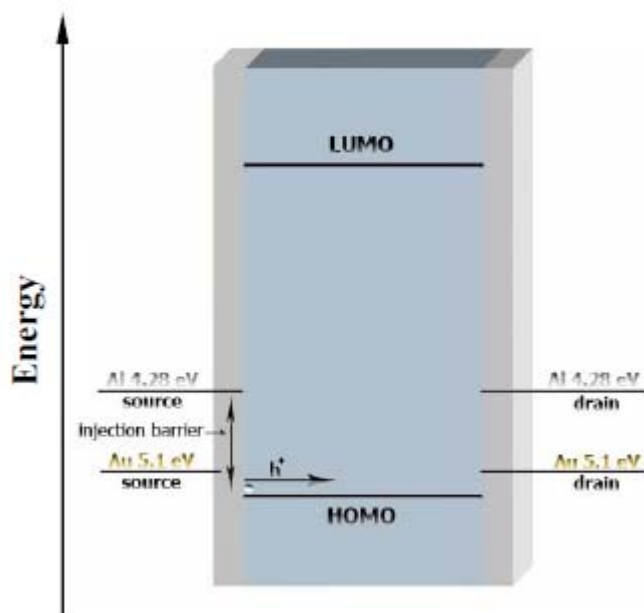


**Figure 1.8 Simplified energetic diagram showing work function of gold and aluminium and HOMO-LUMO levels of an organic semiconductor<sup>[24]</sup>.**

It is possible to use different metals for the fabrication of the electrodes or even in the same transistor have the drain made of one metal and the source made of a different one. This would change the energy of the Fermi level allowing a wider range of possibilities in the synthesis of new material.

### 1.3.1.2 Structure and packing

The molecular structure of organic semiconductors is perhaps the most important parameter to consider when designing new materials for organic electronics. High crystalline materials which maximise the  $\pi$  orbitals overlap are highly desired<sup>[25]</sup>. The close overlap of these orbitals allows the movement of carriers through the material. However, not only the close packing will determine the ability of the material as charge transporters. The overlapping of HOMO-LUMO levels of adjacent molecules is a factor that also must be considered<sup>[26]</sup>.

There are three types of OSC in terms molecular order: amorphous conjugated polymers, semi-crystalline polymers and crystalline small molecules.

The low electronic mobilities observed in amorphous polymeric materials are consequence of the disorder in the polymeric matrix. Charges can not easily travel in the desired direction between the electrodes as the hopping is in some cases is energetically impeded.

Semicrystalline polymers are those in which certain regions of their structure the molecular chains pack together showing some kind of order. These packed substructures can be conceived as micro-crystallites inside an amorphous polymeric matrix. Possibly the most studied semicrystalline polymer in electronics terms is the regioregular poly(3-hexylthiophene) (P3HT)<sup>[27]</sup>.

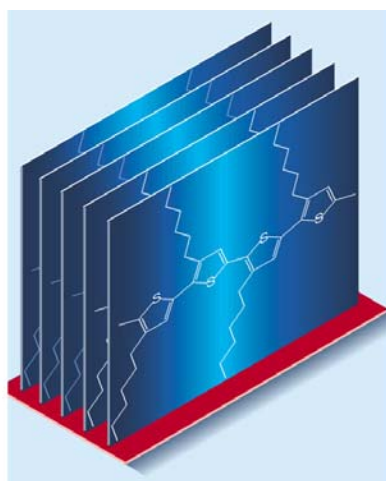


**Figure 1.9 Regioregular semicrystalline poly(3-hexylthiophene) (P3HT)<sup>[28]</sup>.**

It has been reported that the regioregularity of P3HT has a massive influence in how the lamellar structure is formed and its disposition towards the substrate<sup>[27]</sup>. In the case of P3HT when the  $\pi$  orbitals are parallel to the substrate mobilities as high as  $0.1 \text{ cm}^2/\text{Vs}$  have been obtained. This molecular order is only partial in this kind

of material and has been observed that a larger amount of these ordered micro-crystalline structures in the film yields better mobilities results<sup>[29]</sup>.

An increase in the molecular order leads us into crystalline small molecules. In this case all the molecules are in a determined place in the crystal lattice. This high degree of molecular order favours the movement of charges through the material. As described in section 1.2 the main part of a thin film transistor is the OSC-insulator interface at the channel. High degree of crystallisation should be aimed here to guarantee good device performance. A rough insulator would promote the growth of isolated crystals with the consequent apparition of grain boundaries and decrease of electronic mobility.

The nature of the insulator can also influence the disposition of the semiconductors towards it. Many different treatments, consisting in growing self assembled monolayers (SAMs)<sup>[30]</sup>, have been applied to substrates in order to improve crystallisation.

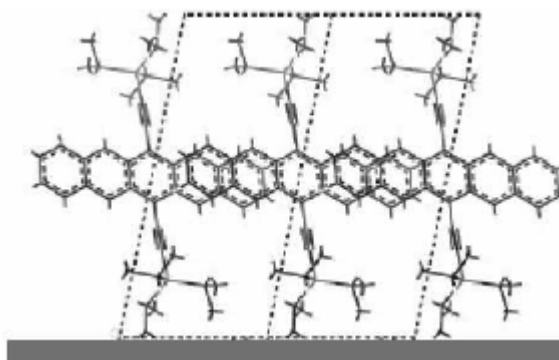


**Figure 1.10 Distribution of highly ordered TIPS-pentacene molecules on a silicon oxide substrate. The highly ordered distribution and the close packing between the  $\pi$  orbital of the pentacene cores are ideal for electronic carrier transport<sup>[31]</sup>.**

### **1.3.1.3 Purity of the materials**

Considering that molecular order is essential to achieve high performance devices the addition of impurities into the system only decreases the TFT operation by disruption of the semiconductor crystal structure. High purity materials are a requirement to obtain efficient devices.

Apart from the disruption in the crystallographic structure of the semiconductors, there are two well defined effects that can be introduced by impurities. The first one is doping of the semiconductor. Doping occurs when traces of a conducting material are left in the semiconductor bulk. This kind of impurity hinders the semiconducting behaviour of the materials and it is noticed in the on/off currents.

The other effect that takes place in organic semiconductors when traces of impurities are present is traps. Traps occurs when the impurity have lower conducting properties than the semiconductor bulk<sup>[32]</sup>. In the case of p-type semiconductors traps are defined as a site with lower ionisation potential than the bulk material<sup>[24]</sup>.

An important consequence of the presence of traps in the system is the increase of the threshold voltage. This increase in the threshold voltage implies an increase in the voltage that is required to run the device. This involves an increase in the power consumption.

The presence of grain boundaries within organic semiconductor film will induce the presence of traps in the system.

### **1.3.1.4 Processability and film formation properties**

Ink jet printing is seen as the short-term future cheap mass scale production technique for organic electronic devices. Solution processability is then an

indispensable requirement for the new generation organic semiconductor. The soluble high performance materials developed in the last years leave behind the expensive evaporation deposition techniques.

Thin film transistors are multi-layer structures. Deposition techniques for each layer have a critical influence in their operation and fabrication cost. Until the recent development of efficient soluble small molecules there have been two well differentiated ways of depositing OSC depending on the solubility of the material<sup>[33]</sup>.

Conjugated polymers which possess solubilising groups are normally solution processable materials. Solution deposition techniques which may include drop casting or spin coating are cheap and easy to scale up. In addition to their high solubility conjugated polymers form homogeneous films which are another key factor required to obtain large area coverage and reproducible devices.

On the other hand, the small molecules used traditionally for organic electronics, pentacene or rubrene, are not solution processable. The addition of solubilising groups used to disrupt their structure and to worsen the face to face distribution which improves the overlap of the  $\pi$  orbitals. The only technique available to obtain continuous and reproducible films was vacuum evaporation. Vacuum deposition is expensive and difficult to scale up since it requires high temperatures and very low vacuum.

Recently the solution processability of small molecules has been greatly improved by the addition of solubilising groups which do not interfere in the overlap of the  $\pi$  orbitals. In fact, in molecules such as 6,13-bis(triisopropylsilylethynyl) pentacene (TIPS-pentacene), the addition of the silyl groups improves the overlap of the  $\pi$  orbitals promoting a face to face distribution<sup>[34]</sup>.

Large area and continuous coverage of crystalline materials is challenging and the formation of grain boundaries is commonly observed. To overcome this problem blends mixing the good carrier transport properties of small molecules and the good film formation properties of polymers are being studied<sup>[35]</sup>. Blends will be discussed in chapter four.

The nature of the substrate plays a fundamental role in the film formation properties of the materials. A good way of controlling the nature and morphology of the substrate is by using self assembled mono-layers (SAMs). The chemical configuration of the SAM can be tuned to match the organic semiconductor. Possibly the most common SAM used in organic thin film transistors has been octadecyltrichlorosilane (OTS)<sup>[36]</sup>. This material forms hydrophobic continuous films and helps some semiconductors to achieve better crystallisation and surface coverage.

## **1.4 Types of organic semiconductors**

Organic semiconductors can be classified based on the preferred type of carriers the material can carry (p-type or n-type semiconductors) or on the nature of the material (small molecules or polymers).

### **1.4.1 N-type and p-type materials**

Depending on the kind of charges they can transport OSC are classified as p-type or hole carriers materials and n-type or electron carriers materials<sup>[2]</sup>. The great majority of organic semiconductors are p-type materials. Organic semiconductors, as conjugated materials, are electron rich materials and as a consequence they have a relatively low ionisation potential ( $I_p$ ). Therefore, it is relatively easy to remove an electron from the outer layers. The real meaning of hole transport in OSC is the transport of this positively charged species (polaron) that remains in the system after the extraction of an electron.

Molecular engineering can create n-type semiconductors by addition of electron withdrawing groups to the molecules, Figure 1.12. These groups lower the electron affinity ( $E_a$ ) of the molecules and as a consequence electrons are easily injected into the system. N-type materials are not the focus of this thesis and are not considered further.

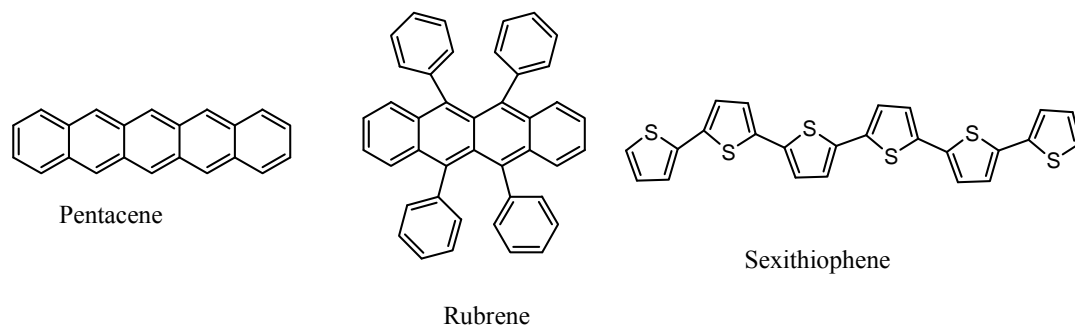


**Figure 1.11 Represented p-type semiconductors.**

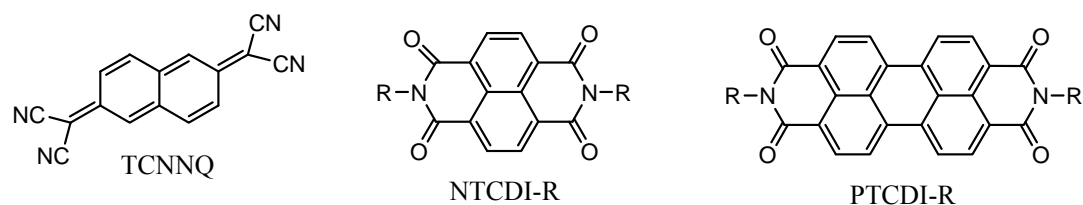


**Figure 1.12 Represented n-type semiconductors.**

## 1.4.2 Polymers and small molecules

Previously, in section 1.3.1 when describing the factors needed to obtain good organic semiconductors the two families, conjugated polymers and small molecules, have been introduced.

The aim of the thesis was the synthesis of 6,13-disubstituted pentacene derivatives, hence the polymer review only consists of a brief mention of the most important ones. Then, small molecules are described putting special emphasis in acenes and pentacenes.



### 1.4.2.1 Conjugated polymers

Conjugated polymers are those having alternated single and double bonds along their back bone. This allows the overlap of the  $\pi$  orbitals allowing delocalisation of electrons through the molecule<sup>[37]</sup>. Most conjugated polymers are amorphous material. This is one of the main reasons to understand the low charge mobilities they can reach.

Since the 1970's when Heeger et al. discovered the conducting nature of polyacetylene, under certain doping conditions<sup>[18]</sup>, the study of this kind of polymers has been widely developed. Among the most important families of amorphous semiconducting polymers are polytriarylamines (PTAA)<sup>[4]</sup>, polyphenylenevinylenes (PPV)<sup>[5]</sup>, polythienylenevinylenes (PTV)<sup>[38]</sup>, Figure 1.13. These materials by their self are totally insoluble. Different derivatives with diverse substitutions have been reported. The addition of alkyl chains to the polymer back bone creates soluble materials that can benefit from all the advantages of solution processability.

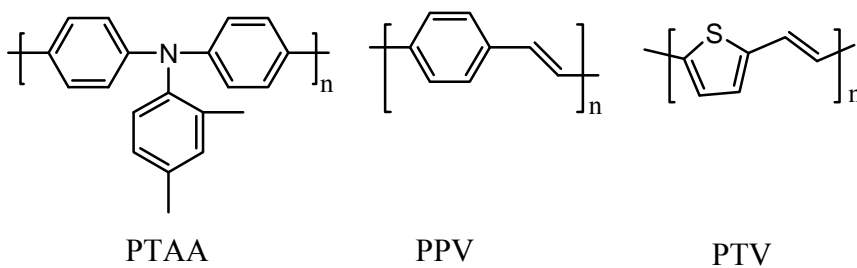


**Figure 1.13 Amorphous semiconducting polymers. Polytriarylamine (left hand side), Polyphenylenevinylene (center) and Polythienylenevinylene (right hand side).**

In Table 1.1 average mobilities for different polymeric materials are presented. Direct relation between the structure of the materials and electronic mobilities can be observed. Semicrystalline polymers show higher mobilities than the amorphous

ones. In the table are included the average mobility values for silicon graphene and single walled carbon nanotubes (SWNTs).

**Table 1.1 Electronic mobilities of main semiconducting polymers. In this table are included SWNTs, graphene and silicon.**

Organic Semiconductors	Structure in solid state	Mobilities ( $\mu$ in $\text{cm}^2/\text{Vs}$ )	References
Poly (triarylamine) (PTAA)	Amorphous	$10^{-6}$ to $10^{-3}$	[4]
Poly (phenylenevinylene) (PPV)	Amorphous	$10^{-6}$ to $10^{-3}$	[5]
Poly (thiophenevinylene) (PTA)	Amorphous	$10^{-6}$ to $10^{-3}$	[38]
poly(3-hexylthiophene) (P3HT)	Semi-crystalline	$10^{-2}$ to $10^{-1}$	[6]
SWNTs	-	$10^5$	[39]
Graphene	-	$10^4$	[40]
Silicon (inorganic)	Amorphous	1	[39]
Silicon (inorganic)	Crystalline	$10^2$	[39]

Triarylamines have been deposited as small molecules<sup>[41]</sup> using vacuum sublimation and have been polymerised and processed from solution. The mobilities achieved with these polymers were generally in the range of  $10^{-3}$   $\text{cm}^2/\text{Vs}$ . The main benefit of this kind of polymers comes from their stability and processability. As a consequence, recent publications of PTAA are focused in using this kind of polymers as hosts for other type of more sensitive materials<sup>[42]</sup>. The role of blends is described in detail in chapter four.

Polyphenylenevinylenes are used mainly in organic light emitting devices (OLED) due to the good emission efficiencies. One of the main problems with these polymers is the poor stability. As mentioned above, the unsubstituted material is

totally insoluble. However, the addition of alkyl chains can improve the solubility and it makes the polymer easily processable making possible the formation of homogeneous continuous films. The addition of the solubilising groups induces more instability to the polymer. This determines the low life times and the need of encapsulation. Possibly, the most studied PPV is poly(2-methoxy-5-(2'-ethylhexyloxy)1,4-phenylenevinylene) (MEH-PPV)<sup>[43]</sup>, Figure 1.14.

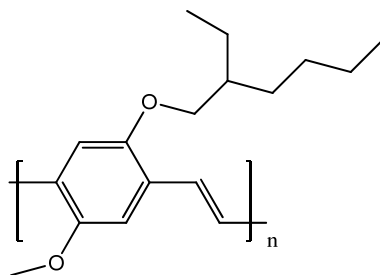


**Figure 1.14 Structure of MEH-PPV.**

As we have seen previously in this chapter, semicrystalline polymers are those which in certain regions of their structure the molecular chain packs together showing some kind of order. This improved order has an influence in the charge transport through the material. The most influential semicrystalline semiconducting polymer is the regioregular poly(3-hexylthiophene). The locations of the functionalising alkyl chains and the deposition technique used to process it have a massive influence in the device performance. When hexyl chains are used as substituents and they are located in a head to tail distribution, lamellar distribution is observed<sup>[27]</sup>.

#### 1.4.2.2 Small crystalline molecules

Polyaromatic crystalline small molecules have attracted the attention of scientific community as they possess very good charge transport abilities. However, their application in organic electronics has been limited by their poor processability. Most of the classic semiconducting small molecules are insoluble. In order to obtain

continuous and homogeneous films expensive vacuum deposition technique are required.

**Table 1.2 Electronic mobilities of crystalline small molecules. In this table are included SWNTs, graphene and silicon.**

Organic Semiconductors	Structure in solid state	Mobilities ( $\mu$ in $\text{cm}^2/\text{Vs}$ )	References
Pentacene	Crystalline	7	[44]
TIPS-pentacene	Crystalline	2-3	[45]
Rubrene (single crystal)	Crystalline	15	[46]
SWNTs	-	$10^4$	[39]
Graphene	-	$10^4$	[40]
Silicon (inorganic)	Amorphous	1	[39]
<i>Silicon (inorganic)</i>	<i>Crystalline</i>	$10^3$	[39]

During the last few years there has been a great interest in developing new soluble derivatives. The addition of solubilising groups, typically alkyl groups, can make these materials solution processable. Among the most important solution processable small molecules are the pentacenes and anthradithiophenes derivatives. Within the field of organic electronics TIPS-pentacene is perhaps the most studied pentacene derivative. This is due to its excellent thin film transistor performance. TIPS-pentacene can be easily synthesised and is soluble in most organic solvents.

To conclude the section on small crystalline molecules, and due to their similarity with the pentacene derivatives that are our main interest, a brief description on anthradithiophenes is presented, Figure 1.15. This kind of anthradithiophenes have been synthesised by Anthony et al<sup>[47]</sup> and excellent thin film transistor device characteristics using them have been measured.

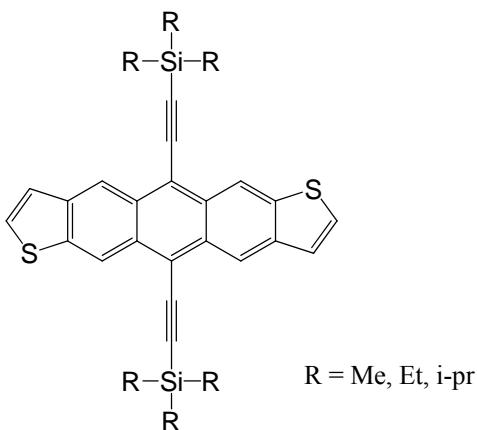


**Figure 1.15 Structure of 5,11-trialkylsilylethynyl anthradithiophenes.**

There is an obvious structural similarity between this kind of anthradithiophenes TIPS-pentacene derivatives. As happens with substituted pentacenes different behaviour was observed depending on the R groups. Being the ethyl derivative the only one presenting good thin film transistor performance. In this case mobilities as high as  $2 \text{ cm}^2/\text{Vs}$  were reached<sup>[48]</sup>.

Within this family, another interesting derivative results from the addition of fluorine atoms to the carbon next to the sulphur atom. This addition has increased the crystals formation speed and the photostability of these materials. The stability has been increased due to the F-F and F-S interactions that take place between the molecules in the crystal<sup>[49]</sup>.

Many other soluble small molecules are now available<sup>[3a]</sup>. The main area of this thesis is the synthesis and thin film transistor performance of new 1,4,8,11-tetramethyl-6,13-trialkylsilylethynyl pentacene derivatives. Hence, a review of only pentacene derivatives highlighting 6,13-trialkylsilylethynyl substitution is presented here.

## 1.5 Pentacene derivatives

Acenes such as pentacene have shown some of the highest mobilities observed in organic semiconductors<sup>[44]</sup>. Soluble pentacene derivatives maintaining the electronic properties of the mother pentacene material and capable of being processed from solution have been a target pursued by organic electronic researchers.

Many synthetic attempts towards solution processable pentacene derivatives to be used in thin film transistors have been reported<sup>[7, 50]</sup>. The addition of substituents to the pentacene core can improve their processability and stability. However, it might affect the crystalline structure of pentacene and consequently its semiconducting properties. The addition of alkyl groups can also decrease the oxidation potential pentacene and this involves lower stability.

The most important soluble pentacene derivatives according to their performance in thin film transistors are 6,13-trialkylsilylethynyl pentacene derivatives. In table 1.3 there are some examples of different disubstituted derivatives.

**Table 1.3 6,13-trialkylsilylethynyl soluble pentacene derivatives. The R groups are in accordance with Figure 1.16.**

R <sub>0</sub>	R <sub>1</sub>	R <sub>2</sub>	R <sub>3</sub>	R <sub>4</sub>	R <sub>5</sub>	R <sub>6</sub>	R <sub>7</sub>	R <sub>8</sub>	Mobilities (cm <sup>2</sup> /Vs)	Reference
i-pr	H	H	H	H	H	H	H	H	2-3	[48]
i-pr	H	Me	Me	H	H	Me	Me	H	patent, not mobility given	[51]
i-pr	H	H	H	H	H	Me	Me	H	patent, not mobility given	[52]
i-pr	H	CN	CN	H	H	CN	CN	H	-	[53]
i-pr	H	H	H	H	H	CN	CN	H	-	[53]
i-pr	F	F	F	F	F	F	F	F	0.045	[53]
i-pr	H	H	H	H	F	F	F	F	0.014	[53]
i-pr	H	F	F	H	H	F	F	H	patent, not mobility given	[51]
i-pr	H	H	H	F	H	H	H	F	Patent not mobility given	[51]
i-pr	H	H	H	F	F	H	H	H	Patent not mobility given	[51]
i-pr	H	Br	Br	H	H	Br	Br	H	-	[53]
i-pr	H	Br	Br	H	H	H	H	H	-	[53]
Me	H	H	H	H	H	H	H	H	10 <sup>-5</sup>	[54]
Me	H	C <sub>8</sub> H <sub>17</sub>	C <sub>8</sub> H <sub>17</sub>	H	H	C <sub>8</sub> H <sub>17</sub>	C <sub>8</sub> H <sub>17</sub>	H	-	[55]
Me	H	TMS ethynyl	TMS ethynyl	H	H	TMS ethynyl	TMS ethynyl	H	-	[56]
Me	H	TIPS ethynyl	TIPS ethynyl	H	H	TIPS ethynyl	TIPS ethynyl	H	-	[56]
Et	H	H	H	H	H	H	H	H	10 <sup>-5</sup>	[54]
Ph	H	H	H	H	H	H	H	H	-	[54]

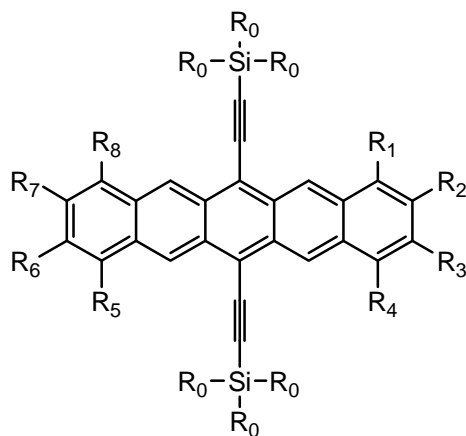


**Figure 1.16 6,13-disubstituted pentacene derivatives**

Many derivatives were synthesised and for some of them their performance in TFTs was measured. The one attracting more attention due to its device performance was TIPS-pentacene.

Notice that derivatives containing electron withdrawing groups in an attempt to obtain n-type semiconductors have also been synthesised.

The substituents in the 6,13 positions of pentacene have an influence in different aspects of the material. Three main changes will take place by the addition of these groups. The first change observed is the effect on molecular packing. The second change is the influence of the added groups in the HOMO and LUMO energetic levels in the molecular orbital diagram and the third one is that substitution in the 6,13-positions improves the stability of pentacene by protecting the most sensitive part of its structure<sup>[57]</sup>.

The improved electronic characteristics of the 6,13-triisopropylsilylethynyl are directly related to its molecular packing. TIPS-pentacene packs in the 2-D “brickwork” arrangement which favours the  $\pi$ - $\pi$  stacking and enhanced the mobility of carriers through the crystalline material by allowing the transport to take place in more than one direction.

Pentacene crystallises in the herringbone structure. The  $\pi$ - $\pi$  stacking is not favoured, Figure 1.17. The herringbone structure is characterised by an edge to face distribution (52° edge to face angle for pentacene)<sup>[50]</sup>.



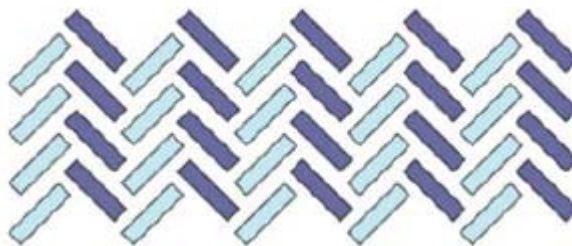


**Figure 1.17 Herringbone structure for pentacene<sup>[3b]</sup>.**

Depending on the size of the  $R_o$  groups the molecules will pack in a different manner. In the case of  $R_o$  groups having a diameter smaller than the half of the length of the pentacene core, the molecule will pack in a 1-D “Slip-stack” distribution<sup>[25b]</sup>, Figure 1.18. In this case the charge transport can only take place in one direction.

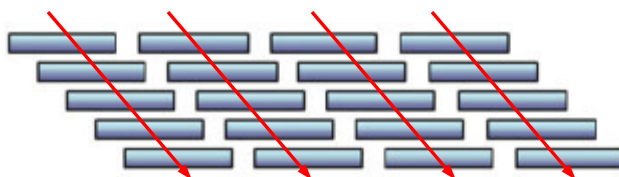


**Figure 1.18. 1-D “Slip-Stack” structure<sup>[3b]</sup>. The arrows indicate the direction in which the charge transport can take place.**

However, if the  $R_o$  groups are approximately half of the length of the pentacene core, the configuration will be 2-D “Brickwork” distribution. For bigger  $R_o$  groups herringbone structure is observed. In the case of 2-D “brickwork” arrangement the molecules are packed in such a way that charge transport can take place in two different directions through the crystal lattice, Figure 1.19. This makes easier the charge transport taking place in the channel of an organic thin film transistor improving consequently the organic semiconductor performance.

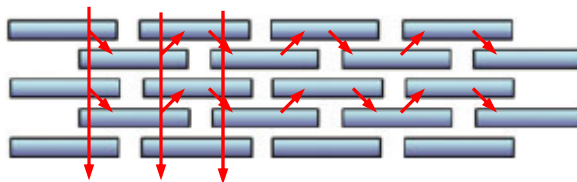


**Figure 1.19. 2-D “Brickwork” structure<sup>[3b]</sup>. The arrows indicate the directions in which the charge transport can take place.**

2-D “brickwork” distribution enhances overlap of the  $\pi$ -orbitals among different molecules. This distribution is preferred because the charges can move through the material more easily independently of the direction of the crystal growth on the substrate. TIPS-pentacene packs following this distribution. 6,13-Triethylsilylethynyl pentacene (TES-pentacene) and 6,13-trimethylsilylethynyl pentacene (TMS-pentacene) packs in a 1D structure. This distribution of the molecules in the solid state is the origin of the poor electronic behaviour measured for methyl and ethyl derivatives. The design of new pentacene derivatives should aim for a 2-D “brickwork” configuration.

The second property affected by the addition of solubilising groups is the location of the HOMO-LUMO levels in a molecular orbital diagram (MO diagram)<sup>[58]</sup>. As we have seen in section 1.3.1.1, to achieve maximum performance in a thin film transistor, the energetic HOMO-LUMO levels of the semiconductor respect to the location of the metallic electrode work function is a factor of major importance. This factor will determine how easy would be to inject charges from the electrodes into the semiconductor. In the case of TIPS-pentacene the addition of the TIPS groups in the 6,13 positions of pentacene lowers the energy of the HOMO level from 4.96 eV to 5.11 eV. Considering that the work function of gold is 5.1 eV, the injection of carriers into the semiconducting material from gold electrodes will be favoured. The energetic barrier required to inject carriers into the system have been minimised. When synthesising new materials ohmic contacts are preferred.

In resume, crystalline low molar mass materials possess most of the desired properties to become optimum organic semiconductors. The addition of the ethynyl groups in the 6,13 positions in pentacene have improved, not only the solubility but also the overlap of the  $\pi$ -orbitals. These reasons drove us to consider pentacene derivatives as the starting reference materials for this thesis. The remaining problem is the difficulty in achieving continuous films. To overcome this problem the materials have been blended with commodity low permittivity dielectric constant ( $\kappa$ ) polymers. These blends keep the characteristics of both materials. Presenting the good film formation properties of the polymers and the good carrier transport properties observed in crystalline small molecules. Blends are discussed in chapter 4.

## 1.6 Aims and Objectives

1. 6,13-Disubstituted pentacene derivatives are showing great potential as solution processable organic semiconductors. In this thesis for the first time the effect of 1,4,8,11 tetrasubstitution on the solubility, solid state packing and p-type semiconductor behaviour is considered. Synthesis, characterisation and electrical properties are presented in chapters two and three respectively.
2. It has been reported that blending low molar mass organic semiconductors with dielectric polymers can give improvements in film processing and electrical properties. For the first time in the open literature we investigate the effect of blend structure and morphology of 6,13-disubstituted pentacene derivatives with side chain aromatic dielectric polymers and the effect on the electrical properties. This is discussed in chapter four.
3. Single walled carbon nanotubes (SWNTs) offer the potential as high mobility p-type semiconductors but are limited by their processability. Preliminary results on the use of low molar mass soluble p-type semiconductors as dispersants are presented. The discussion of this topic is in chapter five.

## **2 Synthesis of novel pentacene and anthracene derivatives**

In this chapter we discuss the results on the synthesis of novel solution processable pentacene and anthracene derivatives. The main objectives are:

1. First reported synthesis of 1,4,8,11-tetramethyl-6,13-bis(trialkylsilylethynyl) pentacene derivatives as potential solution processable ambient stable organic semiconductors for use in organic thin film transistors.
2. Synthesis of 9,10-bis(trialkylsilylethynyl) anthracene derivatives as potential semiconducting dispersants for single wall carbon nanotubes.

## 2.1 Synthesis of 6,13-bis(triisopropylsilylethynyl) pentacene (TIPS-pentacene) (1)

As reference TIPS-pentacene was synthesised according to the procedure reported by Anthony et al.<sup>[34]</sup> (Figure 2.1) by addition of triisopropylsilylethynyl groups to 6,13-pentacenequinone.

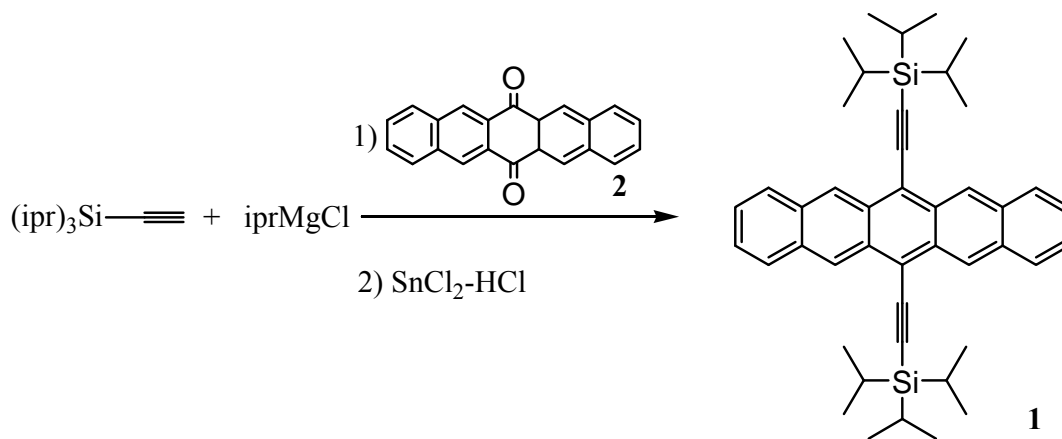


**Figure 2.1** Synthesis of 6,13-bis(triisopropylsilylethynyl)pentacene (TIPS-pentacene) from Anthony's method<sup>[34]</sup>.

Although 6,13-pentacenequinone is commercially available it was effectively synthesised in one step and in quantitative yield, by condensation of o-

phthalaldehyde and 1,4-cyclohexanedione in the presence of strong base, Figure 2.2.

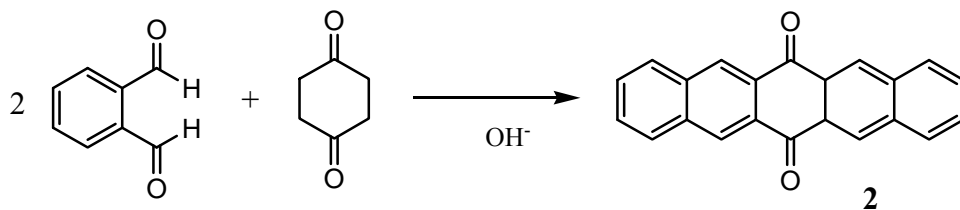


**Figure 2.2 Synthesis of 6,13-pentacenequinone.**

When base is added it reacts with the hydrogen attached to the  $\alpha$ -carbon atom in 1,4-cyclohexanedione and the reactive enolate attacks the carbonyl group of the o-phthalaldehyde. Loss of a water molecule yields the double bond that will yield the aromatic ring, Figure 2.3. This mechanism takes place sequentially to give 6,13-pentacenequinone.

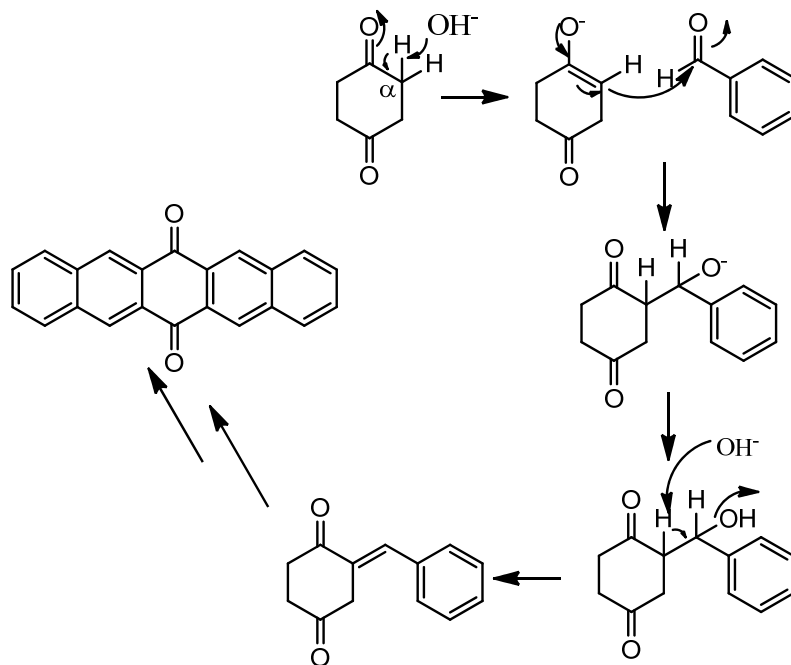


**Figure 2.3 Mechanism for the formation of 6,13-pentacenequinone.**

Since the quinone is insoluble in water and most organic solvents clean-up was carried out simply by filtering the yellow solid and washing several times with water and acetone yielding the intractable final quinone.

Due to low solubility the material it is difficult to effectively characterise using solution based techniques. However, recent literature<sup>[59]</sup> where NMR of the material was present has shown that it was possible to dissolve it in minimal amounts just sufficient to characterise by both  $^1\text{H}$  and  $^{13}\text{C}$  NMR. Figure 2.4 shows the NMR of 6,13-pentacenequinone achieved

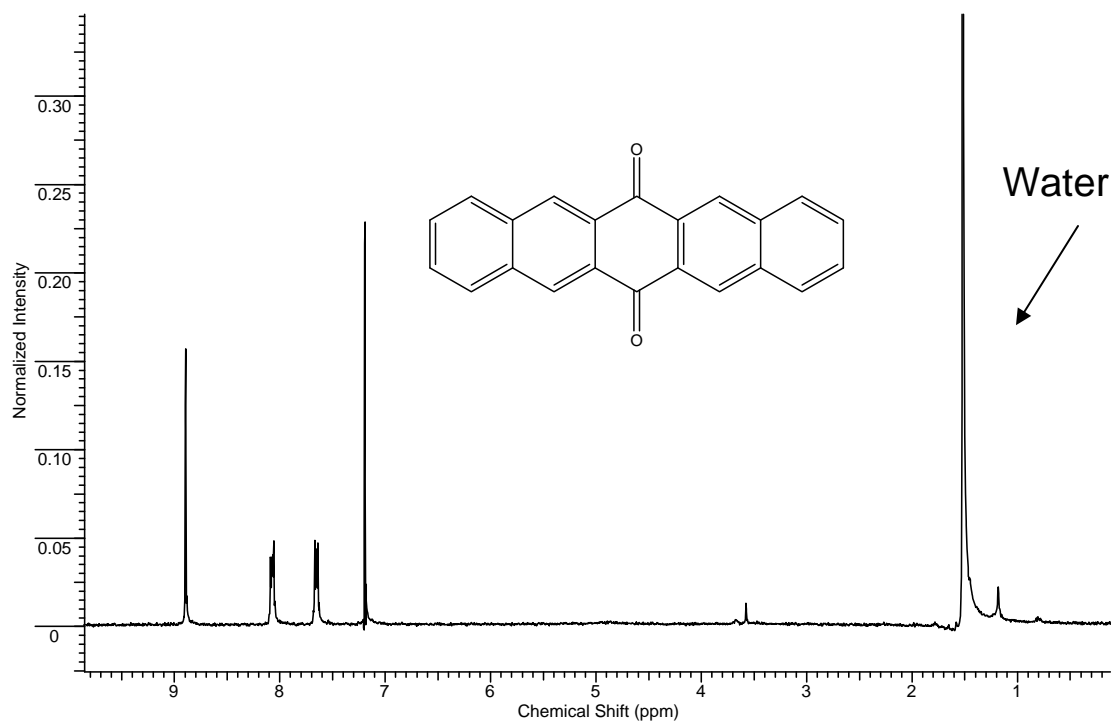


**Figure 2.4 Nuclear magnetic resonance (NMR) spectrum of 6,13-pentacenequinone in deuterated chloroform.**

The synthesis of TIPS-pentacene was subsequently accomplished in two steps<sup>[60]</sup>. Step one involves lithiation, using n-butyllithium (n-BuLi), of the triisopropylsilyl acetylene. Using the high basicity of n-BuLi, the C-H bond of the acetylene was deprotonated; this forms the reactive species that reacts with the quinone to give the anion. Once the anion was formed HCl was added to quench the reaction and form the alcohol. Figure 2.5 shows the mechanism for this reaction. The reaction takes place sequentially at both quinones. However, for simplicity only the first insertion is shown.



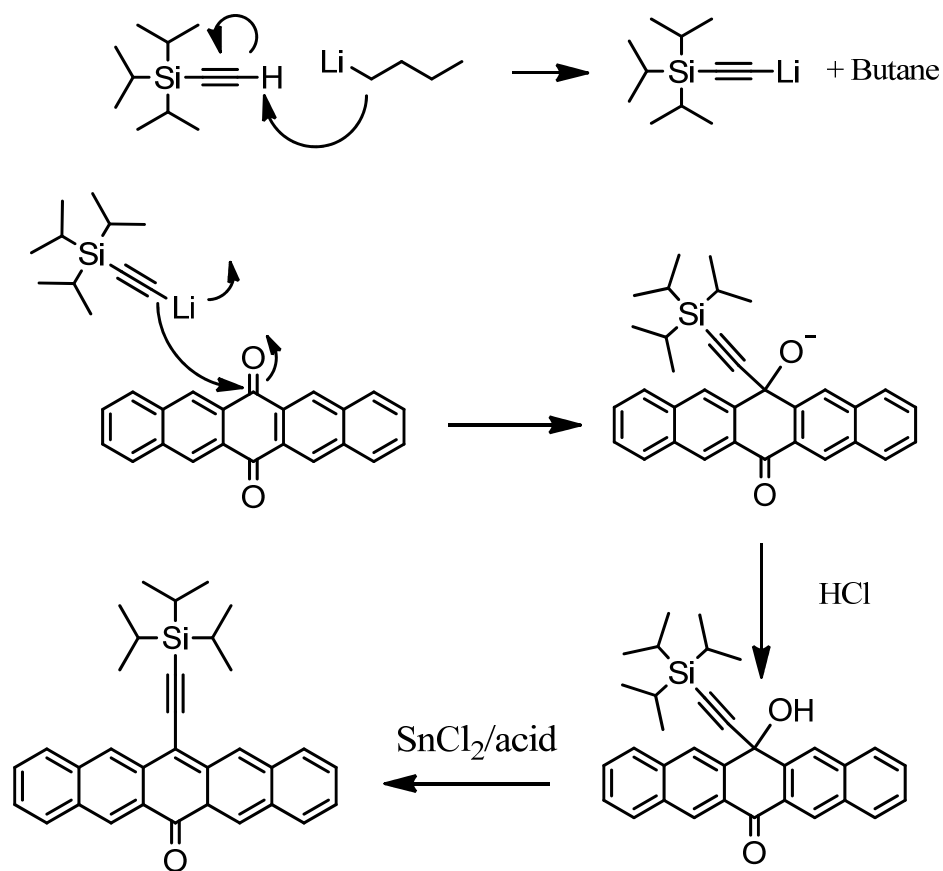


**Figure 2.5 Mechanism for the first step in the synthesis of TIPS-pentacene. The same process takes place at the other quinone to form the disubstituted species.**

At this stage the crude was subjected to a simple chloroform-water workup process to remove inorganic by-products of the reaction. Without this cleaning process decomposition of the final product was observed. When the workup was not performed, the yields of the reaction were much lower.

The second step involves the addition of the reducing agent tin (II) chloride dihydrated in acid solution (acetic acid). The tin chloride supplies the electrons to aromatise the ring yielding the desired TIPS-pentacene with the consequent release of two water molecules. The blue product was easily purified by column chromatography on silica using hexane as eluent. If the workup was not carried out after the formation of the alcohol decomposition was observed. At the beginning of this study a slightly different method was used. In this method the two steps were

carried out in one pot. Following this procedure, we found that on many occasions the desired product was not achieved, a green mixture resulting. We believe that this green crude was due to radical dimerisation of the TIPS-pentacene molecules in a similar fashion to the one observed when films of TIPS-pentacene were exposed to light<sup>[61]</sup>.

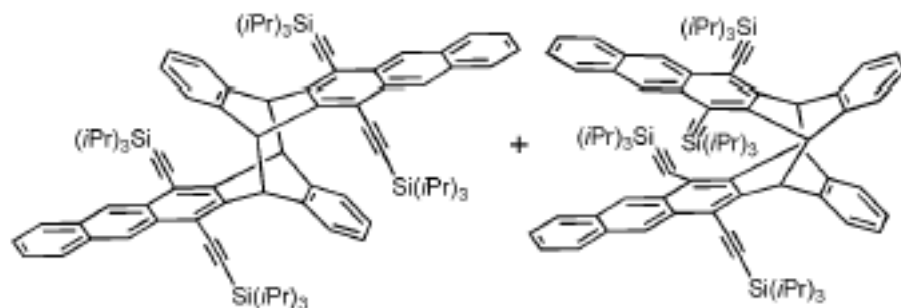


**Figure 2.6 Two different isomers of the dimerised molecules of TIPS-pentacene<sup>[61]</sup>.**

Therefore, when any synthetic protocol towards 6,13-pentacene derivatives is considered we should be aware that Diels-Alder reactions during the synthesis, and the consequent formation of dimers, can occur. We believe that these sub-products of the reaction are due to light (Diels alder) and oxygen degradation and they represent a critical issue in the synthesis of these kinds of compounds.

The poor stability of pentacene towards light, moisture and oxygen is well known. The oxidation of the pentacene molecule, in ambient conditions, may lead to the formation of alcohols or quinones as shown in Figure 2.7.

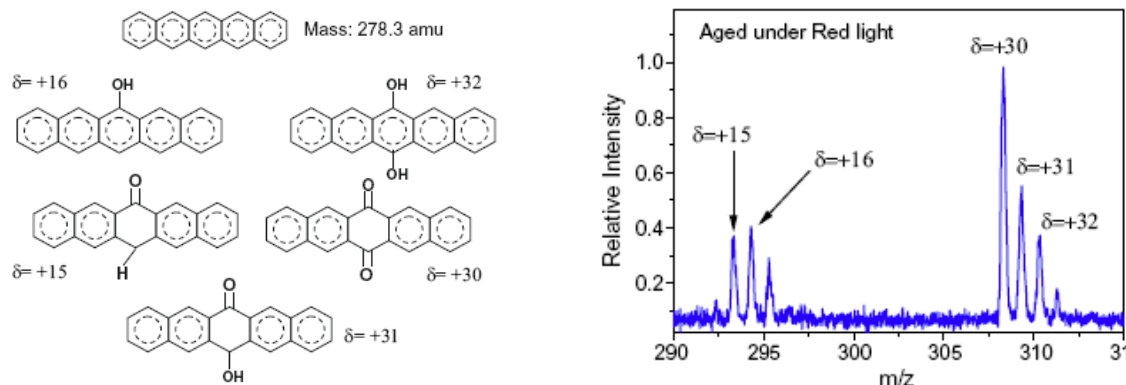


**Figure 2.7 Products of the oxidation of pentacene (left hand side) and mass spectra corroborating their existence<sup>[62]</sup>.**

However, the full process of decomposition is not fully understood<sup>[62]</sup>. Comparative studies of the degradation of TIPS-pentacene and pristine pentacene have been reported<sup>[63]</sup>. Improved stability has been demonstrated in the case of highly crystalline solution deposited TIPS-pentacene. Two main reasons have been given to support this argument. In first place, the large silyl groups may hinder the oxidation of the pentacene back bone. The second one makes reference to the closer packing observed in TIPS-pentacene. Pristine pentacene packs in a herringbone structure with intermolecular distances of  $\sim 4$  Å. These distances are larger than those measured for TIPS-pentacene and it is believed that oxygen or moisture can diffuse through the crystal with the subsequent oxidation of the material.

We believe that by the addition of substituents in the positions 1,4,8,11 to the reference material oxidation may be further hindered compared to TIPS-pentacene and this might improve the environmental stability of these pentacene derivatives.

## 2.2 Synthesis of 1,4,8,11-tetramethyl-6,13-bis(trialkylsilyl ethynyl) pentacene derivatives

1,4,8,11-Tetramethyl-6,13-bis(trialkylsilylethynyl) pentacene derivatives as potential solution processable ambient stable organic semiconductors for use in organic thin film transistors have not been previously reported. The potential for

improved oxidative stability and improved molecular packing makes them worthy of study

The following target molecules were identified, Figure 2.8.

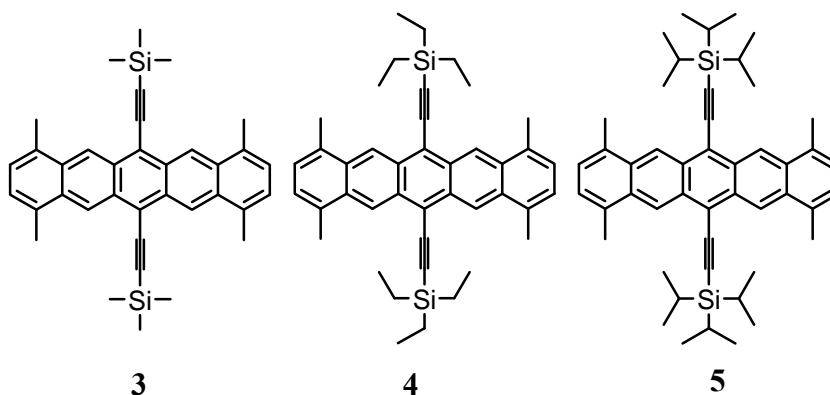


**Figure 2.8 TMTMS-pentacene (3), TMTES-pentacene (4) and TMTIPS-pentacene (5).**

### **2.2.1 Attempted synthesis of the tetramethyl-pentacene derivatives via 1,4,8,11-tetrabromo-6,13-pentacenequinone (7)**

The first attempted route to synthesise the tetra-methylated compounds was via 1,4,8,11-tetrabromo-6,13-pentacenequinone (7). The initial strategy consisted of the addition of the silylethynyl groups to 1,4,8,11-tetrabromo-6,13-pentacenequinone (7) and subsequent substitution via Kumada coupling of the bromine atoms with methyl groups. This route was chosen as the first possibility due to the small number of steps needed to accomplish the final product. A scheme of the proposed route is presented in Figure 2.9.

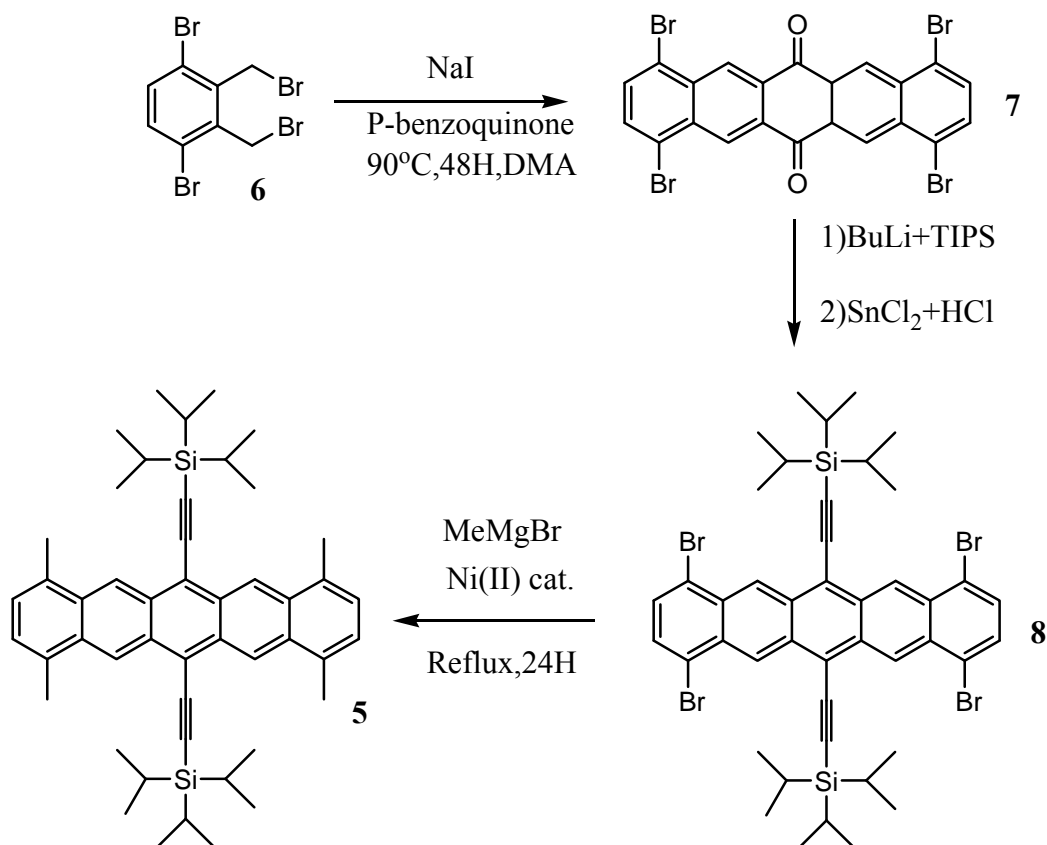


**Figure 2.9** Attempted synthetic route for 1,4,8,11-tetramethyl-6,13-trialkyl silylethynyl pentacene derivatives via 1,4,8,11-tetrabromo-6,13-pentacenequinone (**7**).

The synthesis of the quinone (**7**) took place in very low yields. Previously in this chapter we have discussed a more efficient way of synthesising pentacene quinones starting from phthalaldehydes instead of 1,6-dibromomethylbenzenes. This is the route followed for the synthesis of TIPS-pentacene where almost quantitative yields were achieved. However, the Cava reaction<sup>[64]</sup> using the dibromo starting material (1,6-dibromomethylbenzene) provided in all cases yields lower than 25 %. We believe that this might be due to the low yielding Diels-Alder reaction that takes place for the formation of the pentacene quinone. A proposed mechanism for this reaction has been presented in Figure 2.10. As before, the reaction is drawn taking place only in one of the side for extra clarity.

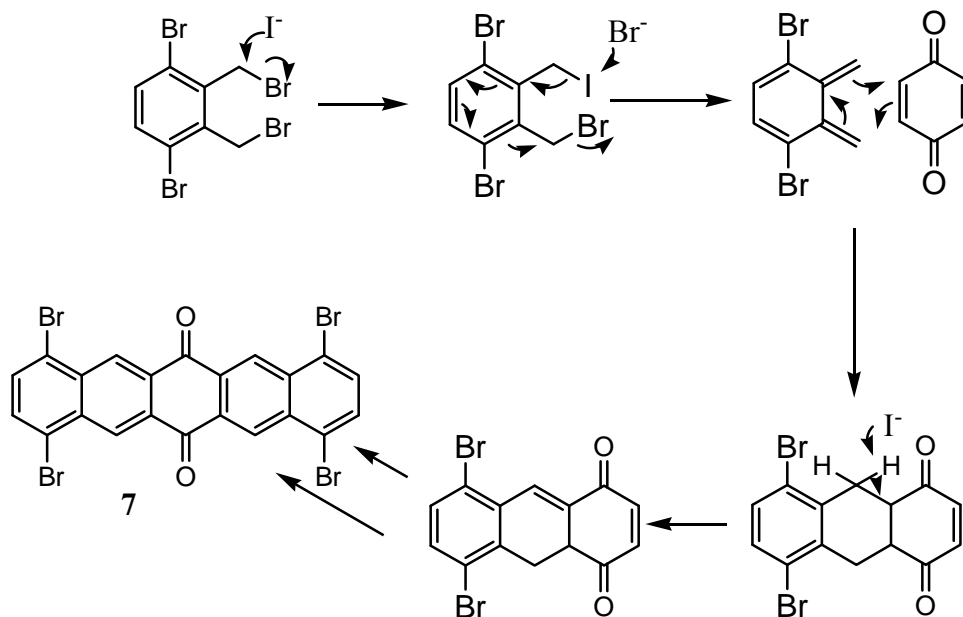


**Figure 2.10 Proposed mechanism for the synthesis of quinone 7.**

Theoretically, the Diels-Alder reaction is favoured when the diene is as electron rich as possible and when the dienophile is substituted with electron withdrawing groups. In this case, the diene is substituted with bromine atoms that due to their high electronegativity, withdraw the electrons from it making it difficult for the reaction to take place. The Cava reaction works best when the benzyl bromides are replaced with benzyl dibromides. However, the steric bulk of this system is unfavourable particularly when the bromine substituents are ortho on the ring.

The purification of the brominated pentacene quinone was carried out in a similar manner as for 6,13-pentacenequinone (**2**). A large number of soluble by-products arising from undesired Diels-alder reactions are formed and they are removed over the work up. As before, the low solubility of this kind of material precluded attempt to perform NMR characterisation but mass spectrometry confirmed the product, Figure 2.11.

mod98 in alpha

0407493 2 (0.184) Sb (2,2.00); Sm (Mn, 2x1.00)

TOF LD+  
177

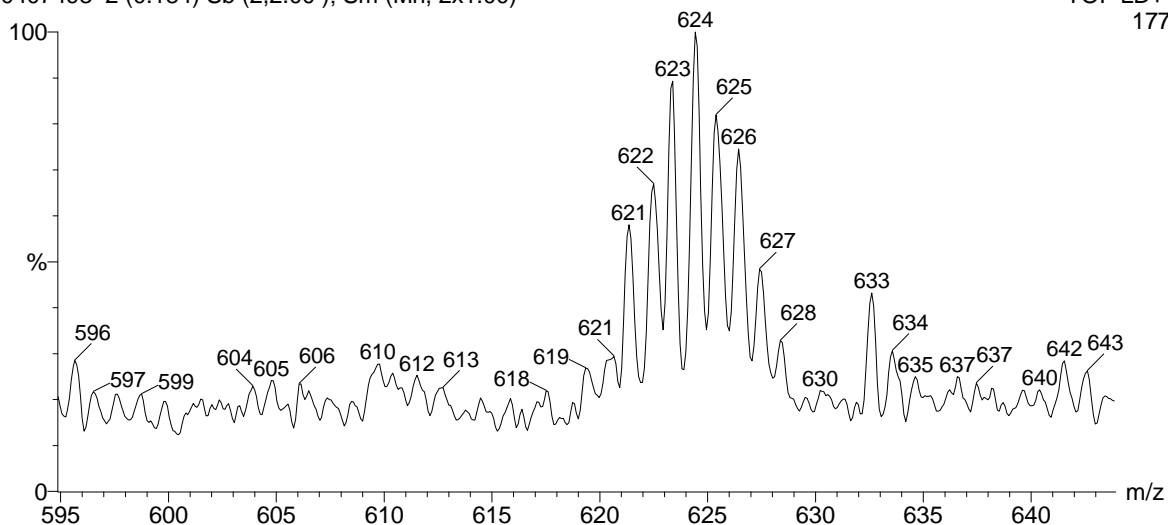


**Figure 2.11** Mass spectra of 1,4,8,11-tetrabromo-6,13-pentacenequinone (7).

Once the quinone was purified we attempted the addition of the silylethynyl groups following the same procedure used for the synthesis of TIPS-pentacene. However only mono substitution was achieved as shown by NMR where the integration of the peaks in the allylic region corresponds only to the mono-substituted species, Figure 2.12.

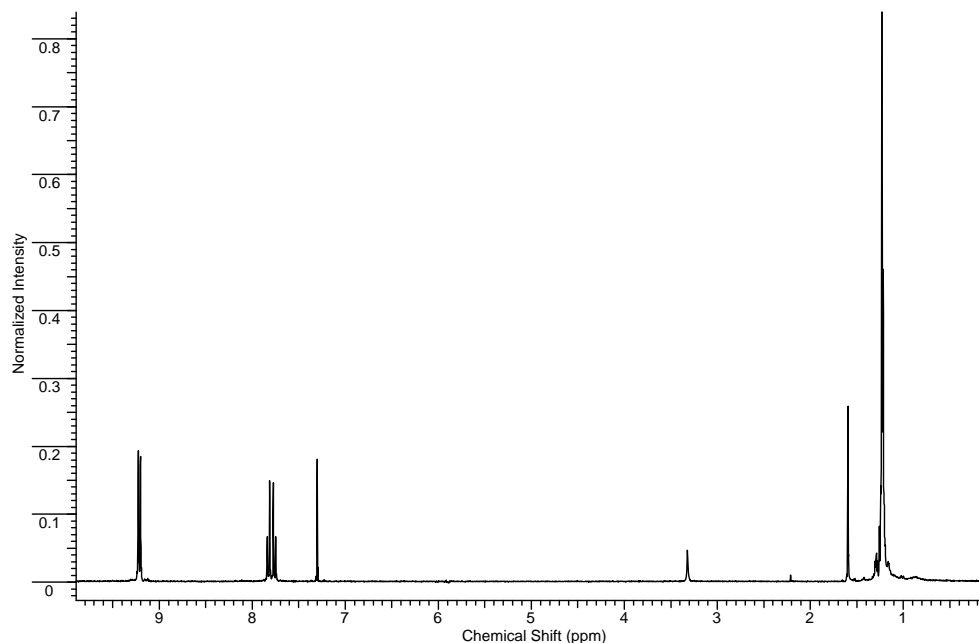


**Figure 2.12**  $^1\text{H}$  NMR spectra of the monosubstituted tetrabromo pentacene derivative.

We believe that the size and the position of the bromine atoms have a critical effect, making di-substitution difficult. 2,3,9,10-tetrabromo-6,13-bis (triisopropylsilyl ethynyl) pentacene has previously been reported<sup>[53]</sup> by the same procedure. This compound has the bromine atoms in the outer positions of the pentacene quinone and no problems were observed during its synthesis. Models calculated using Chem 3D Pro (2004 edition) show that when the bromine atoms are in the inner 1,4,8,11 positions the volumetric sphere representing the bromine atom are much closer to the isopropyl groups coming from the acetylene than when they are in the outer positions, Figure 2.13.

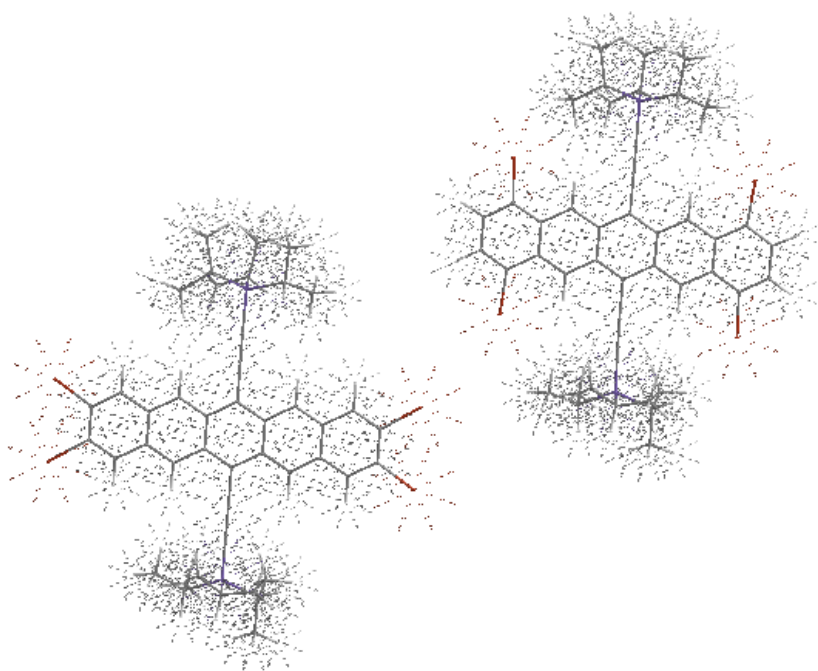


**Figure 2.13** Diagram representing estimation of the atomic volumes for tetrabromoTIPS-pentacene when the bromine atoms are in the outer position (left hand side) and in the inner positions (right hand side).

This synthetic route was not progressed further but given success at di-substitution it was subsequently appreciated that substitution of the bromine atoms with the methyl groups via the Kumada coupling would not be favoured in all the positions. The additional electron density in the aromatic ring, from replacement of bromine with methyl groups, when one of the substitutions takes place, would make



subsequent substitution in the para position more difficult. Therefore, a mixture of the mono, di, tri and tetra derivatives would be achieved making the separation challenging.

### 2.2.2 Attempted synthesis of the tetramethyl-pentacene derivatives via dialdehydes

Attempted synthesis of the tetramethyl-pentacene derivatives via 1,4,8,11-tetrabromo-6,13-pentacenequinone (7) showed that very low yields were obtained when synthesising the quinone starting from 1,6-dibromomethylbenzene. Additionally the bromine atoms impede the desired functionalisation in the 6,13 positions and that their substitution with methyl groups was complicated. Therefore a new route was proposed by formation of the quinone from dialdehydes already containing the methyl groups, Figure 2.14.

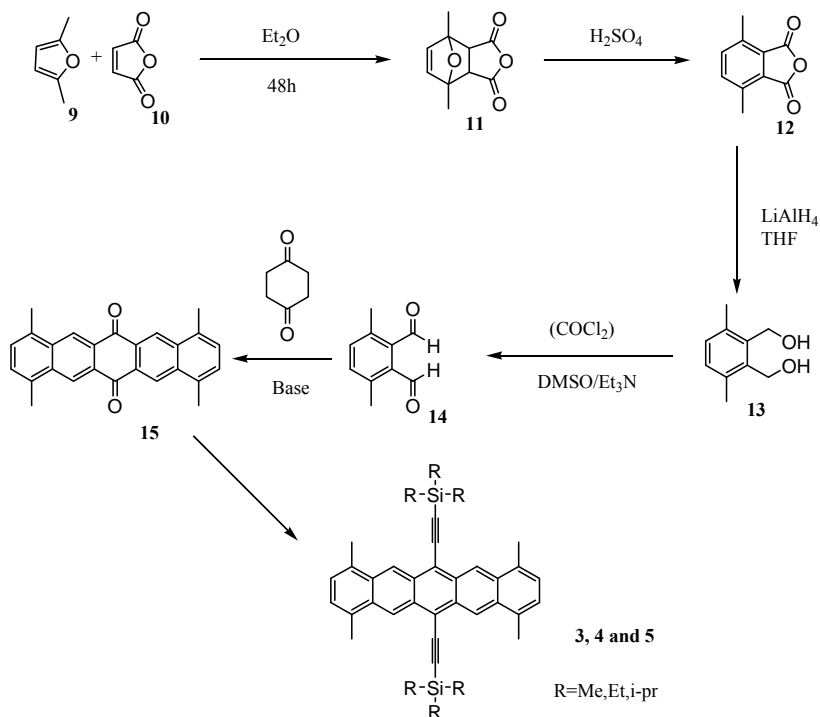


**Figure 2.14 Proposed synthetic route for the synthesis of TMTIPS-pentacene (5) and TMTES-pentacene (4) and TMTMS-pentacene (3).**

The starting materials for this synthetic route were the commercially available 2,5-dimethylfuran (**9**) and maleic anhydride (**10**). Diels-Alder reaction of these two materials yielded the corresponding anhydride (**11**). Compound **11** in presence of sulphuric acid dehydrates producing 3,6-dimethylphthalic anhydride (**12**). Then, Lithium aluminium hydride reduces compound **12** to yield the corresponding dialcohol (**13**). Conversion of the alcohols into the aldehydes turns out to be more complicated than expected.

As we have seen above, we have dealt with two different ways of synthesising 6,13-pentacenequinones. The base method involves synthesis via o-phthalaldehyde and 1,4-cyclohexanedione. In this case almost quantitative results were achieved. However, if the starting materials are 1,6-bromomethylbenzene and p-benzoquinone maximum yields of 25 % were obtained. Therefore, we have always tried to find a synthetic route which involves the formation of the quinone from the dialdehyde starting material. Nevertheless, formation of compound **14** was never achieved. A number of methods were tried without success and are described below.

#### **2.2.2.1 Synthesis of 1,4-dimethyl-7-oxabicyclo[2,2,1]hept-5-ene-2,3-dicarboxylic anhydride (11)**

The Diels Alders reaction involving furan and maleic anhydride is driven thermodynamically towards the minimum energy state thus leading to quantitative yields, Figure 2.15. The reason is that the  $\sigma$ -bonds are lower in energy than  $\pi$ -bonds. When this reaction takes place we decrease the number of  $\pi$ -bonds, going from three in the starting materials to one in the final product. Instead, two new  $\sigma$ -bonds have been created.

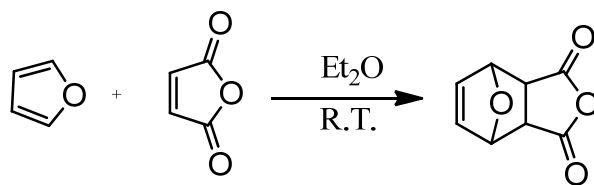


**Figure 2.15 Diels Alders reaction involving furan and maleic anhydride.**

In the case of our reaction we have used 2,5-dimethylfuran (**9**). The small difference induced by the two methyl groups had an effect on the reaction. Theoretically, the addition of the methyl groups lowers the energy of the LUMO and this should make the reaction easier<sup>[65]</sup>. However, the yields obtained for our reaction were lower than expected, of the order of 60 to 70 %.

At the end of the reaction a mixture of the starting materials and the final product was obtained. The mixture was then purified by rinsing off the crude with diethyl ether. The starting materials were highly soluble and washed through the filter paper, leaving the clean anhydride crystals. To make sure all the starting materials were removed a large quantity of solvent was required. Peak signals of the starting materials were observed in the NMR unless rinsed thoroughly. We believe that this dissolved part of the product and this is the reason for the lower than expected yields.

#### **2.2.2.2 Synthesis of 3,6-dimethylphthalic anhydride (**12**)**

In this step, dehydration of the compound **11** gives the anhydride **12**. The oxygen from compound **1** was removed and the six member ring was aromatised. Figure 2.16 shows a proposed mechanism.

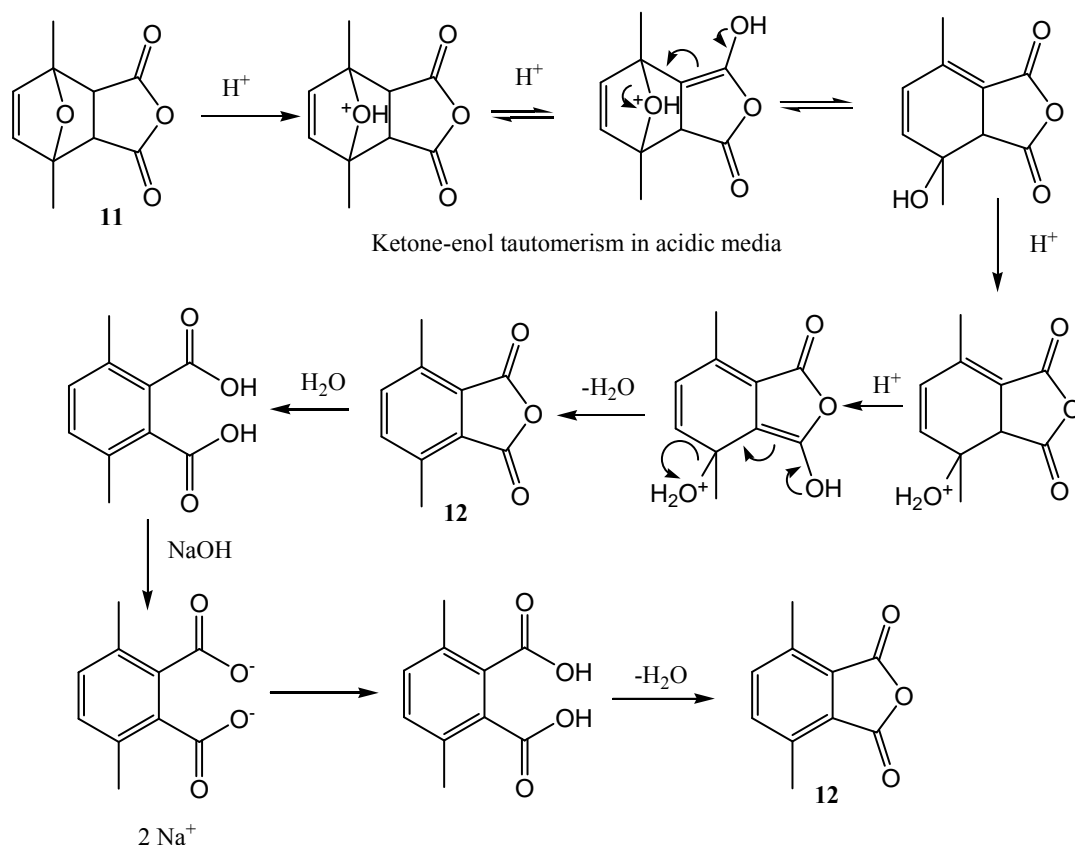


**Figure 2.16 Proposed mechanism to form 3,6-dimethylphthalic anhydride (12).**

The procedure involves the following steps:

1. Addition of anhydride **11** to concentrated sulphuric acid. We believe that compound **12** formation takes place at this stage. Therefore the subsequent steps are to remove the large amount of sulphuric acid and by-products.
2. The crude solution was poured into crushed ice. Aqueous solution with acidic pH transforms the crude into 3,6-dimethylphthalic acid which appeared as white crystals.
3. Those white crystals were dissolved in basic solution. The phthalic acid was converted to the disodium salts (soluble in water).

4. A small amount of acetic acid was added and the solution was filtered to remove insoluble parts. At this stage we got rid of undesired by-products.
5. To conclude the solution was acidified with HCl to obtain again phthalic acid and this was subjected to azeotropic distillation in toluene to form the desired anhydride **12**. With the distillation we liberated the final product of the water formed when the di-acid is dehydrated into the anhydride.

### 2.2.2.3 Synthesis of 3,6-dimethylphthalyl alcohol (**13**)

In this step lithium aluminium hydride ( $\text{LiAlH}_4$ ) reduces the carboxy groups in compound **12** into the dialcohol species **13**. In the ionic compound  $\text{Li}^+\text{AlH}_4^-$  the very low electronegativity of aluminium promotes the formation of the negatively charged hydrogens. This extremely reactive species acts directly in the reduction of the carboxy groups to form alcohols. To complete the reaction basic aqueous solution was added. This protonates the alkoxide oxygen and the alcohol are created. In our reaction an excess of the  $\text{LiAlH}_4$  was added and yields similar to that observed in literature were achieved<sup>[66]</sup>. The mechanism for this reaction is plotted in Figure 2.17.

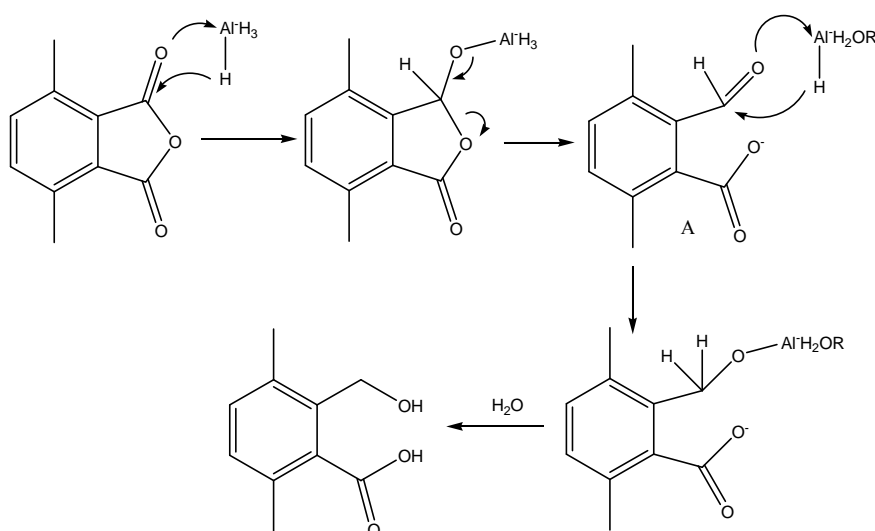


**Figure 2.17 Mechanism for the reaction of  $\text{LiAlH}_4$  with succinic anhydride to produce alcohols. It has been only represented in one side for extra clearness. The OR group attached to the aluminium corresponds to the intermediate A**

**which appears from other equivalent reaction. The lithium has not been included in the mechanism but it forms part of the product as ionic salts.**

The same procedure takes place on the other half of the molecule where the acid was formed. The aluminium complex can react with four molecules at the same time as it keeps being a source of negative hydrogens. At the end, when the reaction is quenched with water, four alcohols in four different molecules have been formed.

#### **2.2.2.4 Different attempts to Synthesise 3,6-dimethylphthaldialdehyde (14)**

Previously in this chapter we discussed the advantages of using the dialdehydes when synthesising 6,13-pentacenequinone. A number of oxidations of **13** to **14** were attempted and are discussed here.

##### ***2.2.2.4.1 Swern oxidation of 3,6-dimethylphthalyl alcohol (14)***

Literature precedence showed that 4,5-dimethylphthalyl alcohol could be converted into 4,5-dimethylphthaldialdehyde in a good 70 % yield using a Swern oxidation<sup>[67]</sup>, Figure 2.18. We thought that by changing the methyl groups from the 4,5 positions into the 3,6 positions would have little effect. However, the methyl groups in the para positions of the benzene ring have a critical effect and the reaction did not take place.

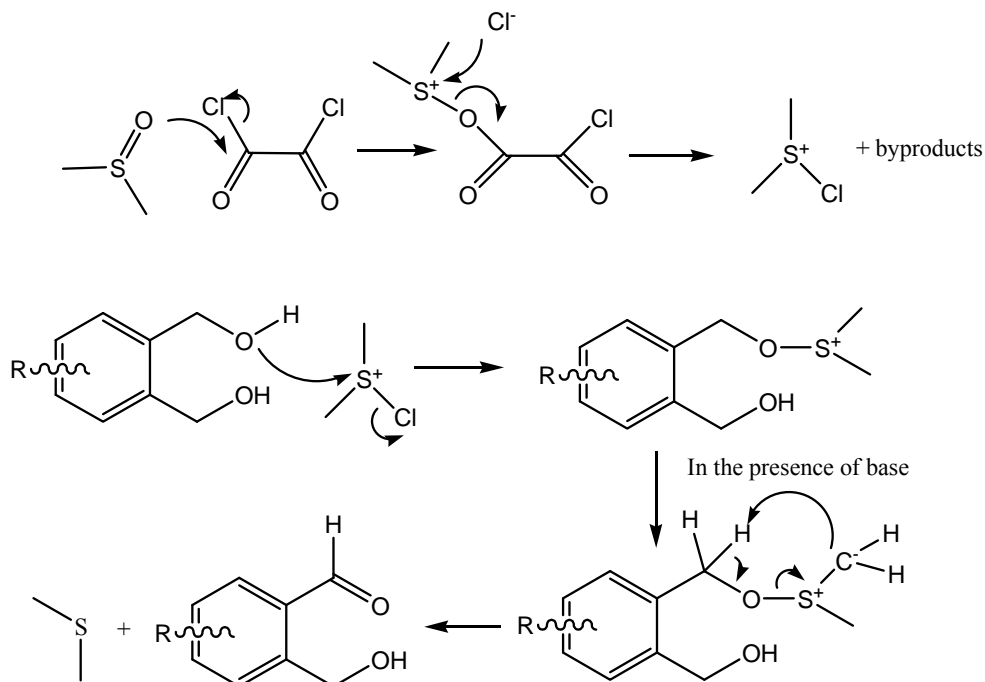


**Figure 2.18 Swern oxidation mechanism. In the common swern oxidation the oxalyl chloride transforms the dimethylsulfoxide (DMSO) into dimethylchlorosulphonium ion. This cation reacts with the alcohol to form an alkoxy-sulphonium ion and is this ion the one that in the presence of triethylamine (base) forms the desired aldehydes. In this mechanism only the reaction in one of the aldehydes is described.**

To make sure that the reaction was being carried out in the right way we repeated the reactions observed in literature using phthalyl alcohol and 4,5-dimethylphthalyl alcohol as starting materials. In those cases the reaction proceeded without problems and the phthaldialdehyde (**16**) and 4,5-dimethylphthaldialdehyde (**17**) were easily obtained in similar yields to those observed in literature.

In the case of the 3,6 substituted dialcohol the lactone 4,7-dimethyl-1(3H)-isobenzofuranone (**18**) was generated as sole product. Lactones are cyclic esters with a ketone located in one of the carbons next to the esteric oxygen. In our case,

we suggest a mechanism similar to the one proposed by Jacques Kagan et al. where the formation of the lactone is photocatalysed<sup>[68]</sup>, Figure 2.19.

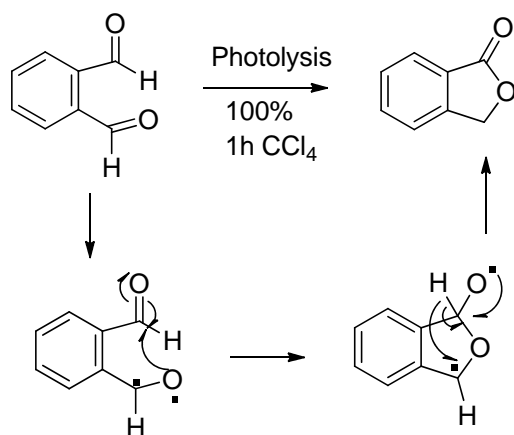


**Figure 2.19 Photo-catalysed formation of lactone.**

This method did not provide the desired product. A first thought towards the explanation of why this reaction is impeded when the methyl groups are present in the 3,6 positions could be steric hindrance. However, we believe that the small size of the methyl groups should be not a major problem as to consider steric hindrance.

Attention should also be focused on the donation of electrons into the system from the methyl electron donating groups. The mechanism for this process remains unknown and further research should be made in order to understand it.

#### **2.2.2.4.2 Pyridinium chlorochromate (PCC) oxidation of 3,6-dimethylphthalyl alcohol (13)**

Pyridinium chlorochromate is one of the catalysts used classically for the conversion of alcohols into aldehydes, Figure 2.20. Theoretically, in this reaction the chromium ion forms an ester with the primary alcohol. Then the formed compound undergoes elimination process of a water molecule and the aldehyde is formed.



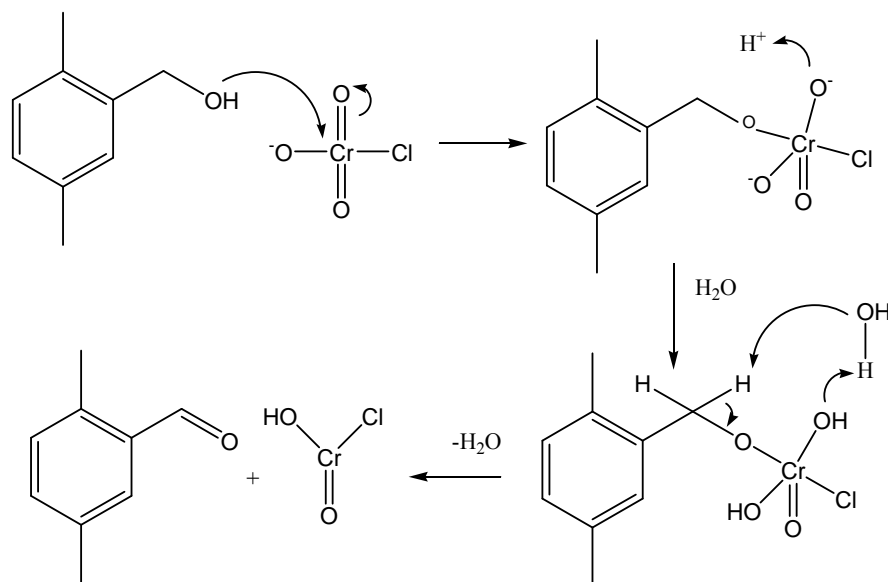


**Figure 2.20 PCC oxidation. From primary alcohols to aldehydes. The reaction is drawn taking place only in one of the sides for extra clarity.**

However in the case of 3,6-dimethylphthalyl alcohol (**11**) the desired dialdehyde was never formed. Instead, when the crude was analysed the same lactone obtained in previous methods (4,7-dimethyl-1(3H)-isobenzofuranone) was found to be the main product of the reaction.

#### 2.2.2.4.3 *Synthesis of 3,6-dimethylphthalaldehyde (14) via 3,6-dimethylphthalyl chloride*

The third alternative to synthesise the dialdehyde consisted of the synthesis of 3,6-dimethylphthalyl chloride starting from 3,6-dimethylphthalic anhydride (**12**), Figure 2.21. Once the chlorinated intermediate was obtained the idea was to transform it using an indium catalyst into the desired 3,6-dimethylphthalaldehyde.

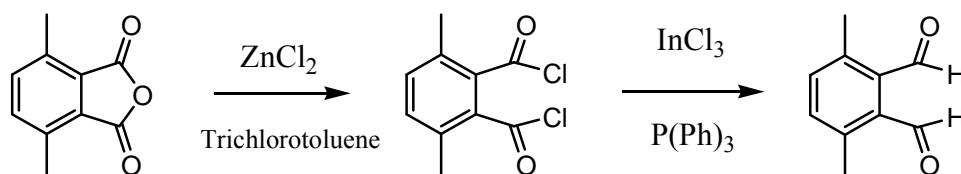


**Figure 2.21** Reaction structure for the formation of 3,6-dimethylphthalaldehyde (**14**)<sup>[69], [70]</sup>.

The first step of the synthesis did not succeed. The crude of the reaction was analysed by  $^1\text{H}$  NMR and the starting materials were detected. The lack of formation of the acid chlorides at this step meant that this route could not proceed. The mechanism of this reaction is unknown. We believe that the addition of the methyl groups in the three and six positions have a critical effect that might impede the reaction.

#### 2.2.2.4.4 *Diisobutylaluminium hydride (DIBAL) reduction of 3,6-dimethylphthalic anhydride (12)*

This time we tried to reduce 3,6-dimethylphthalic anhydride (**12**) directly using DIBAL to obtain 3,6-dimethylphthalaldehyde (**14**). In this reaction the aluminium compound reacts with the unpaired electrons of the ketone oxygen forming the aluminium complex, Figure 2.22. Then, the hydrogen attached to the aluminium atom is released and it is attached to the carbon of the carbonyl group. To conclude the complex is hydrolysed to form the aldehyde.

The usage of DIBAL is preferred than  $\text{LiAlH}_4$  because the size of the isobutyl substituents. These groups create a more hindered structure and therefore more selective and less reactive than  $\text{LiAlH}_4$ .

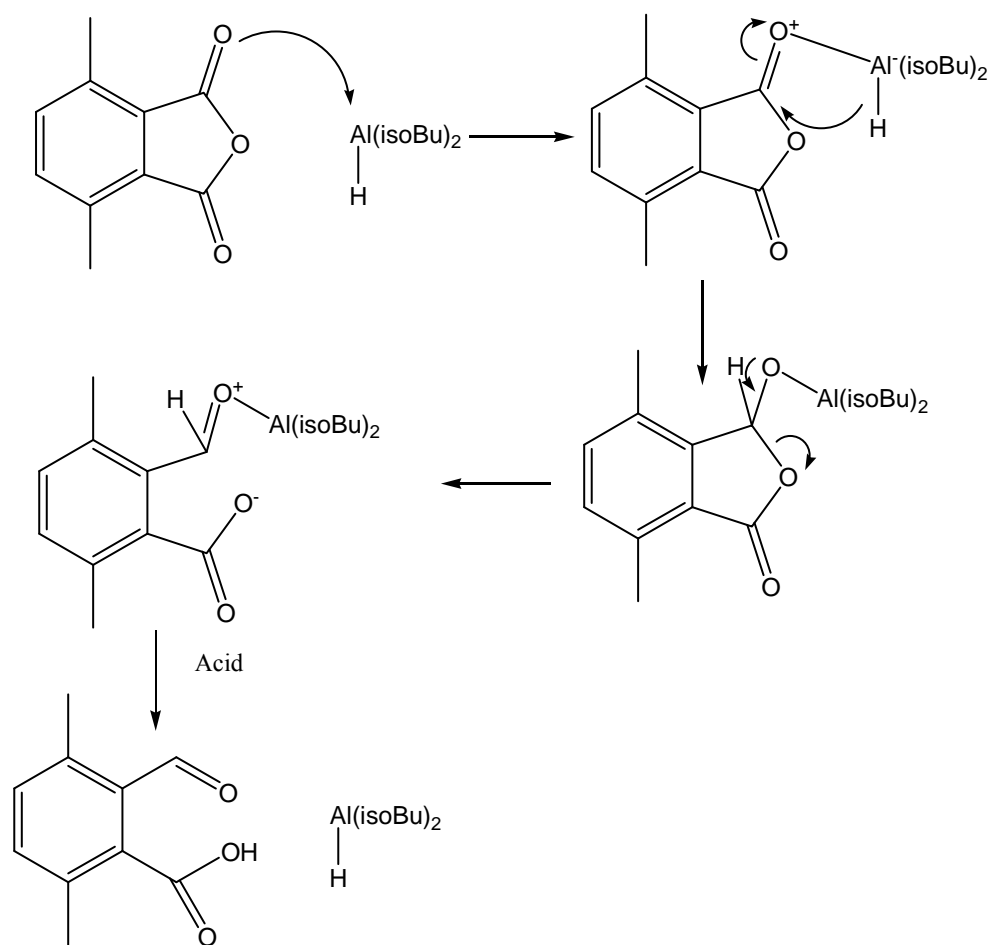


**Figure 2.22 Mechanism for the reduction of esters to form aldehydes using DIBAL.**

Once more the main product of the reaction was found to be the unchanged lactone. After many unsuccessful attempts of synthesising the desired 3,6-dimethylphthalaldehyde we decided to change strategy.

### 2.2.3 Synthesis of the tetramethyl-pentacene derivatives via 3,6-dimethyl-1,2-bis(bromomethyl)benzene (19)

Here we present the definitive route for the synthesis of the tetramethyl-pentacene derivatives. This route can be considered as a mixture of those proposed in the sections 2.2.1 and 2.2.2 since we are using the first three steps of the second route

to form compound **10** and the NaI driven quinone formation from the first one, Figure 2.23.

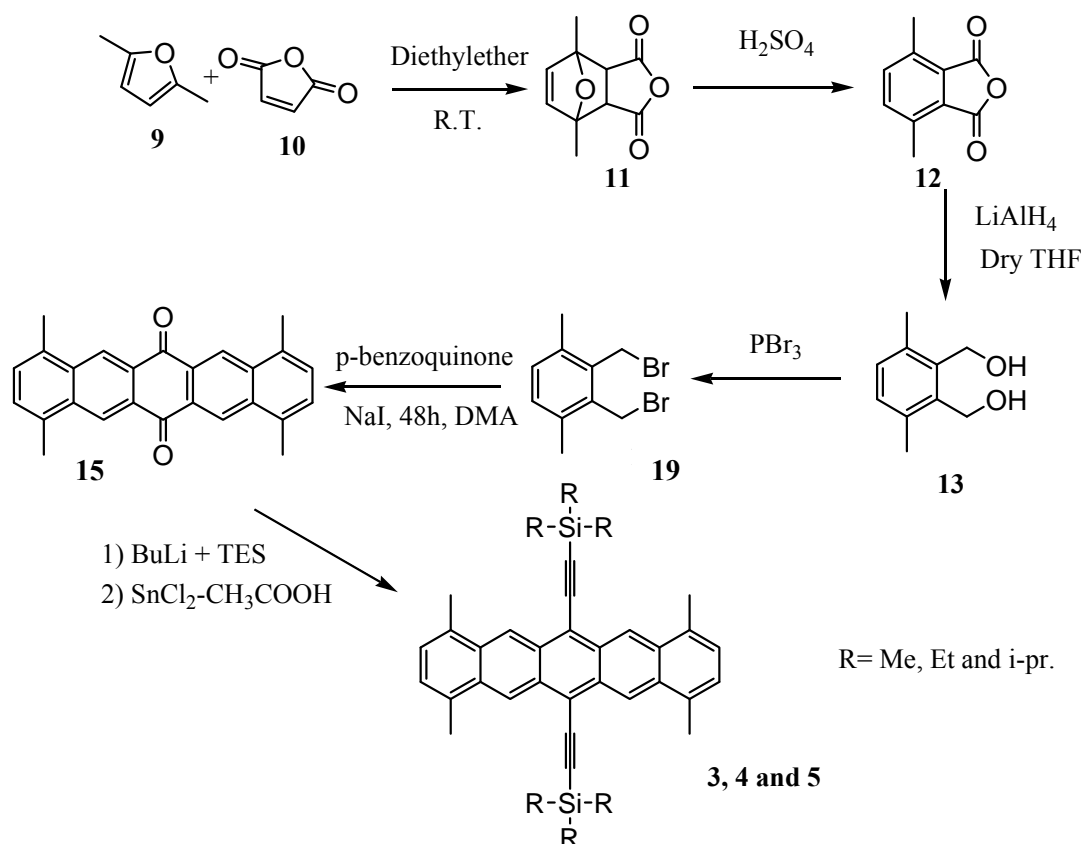


**Figure 2.23** Synthetic route towards the tetramethyl-pentacene derivatives<sup>[71]</sup>.

The principal bottleneck is the low yield reaction when synthesising the quinone **15**. But the final product could be achieved. The first steps of this new route have been described previously in this section.

### 2.2.3.1 Synthesis of 3,6-dimethyl-1,2-bis(bromomethyl)benzene (**19**)

The substitution of an alcoholic group with a bromine atom was carried out using phosphorus tribromide and proceeds in quantitative yield, Figure 2.24. The oxygen lone pair on the alcohol group attacks the phosphorus with the consequent release of a bromine anion. Then, the bromine anion links with the carbon with a positive density of charge to produce the final product.

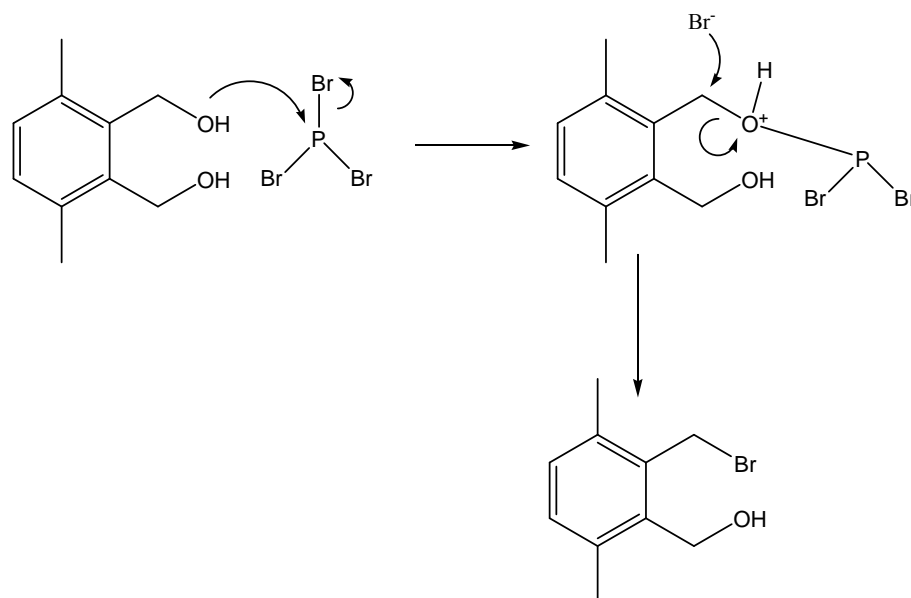


**Figure 2.24** Reaction mechanism for the synthesis of 3,6-dimethyl-1,2-bis(bromomethyl)benzene (19). Once more the reaction mechanism has been drawn only in one of the sides of the molecule for clarity.

### 2.2.3.2 Synthesis of 1,4,8,11-tetramethyl-6,13-pentacenequinone (15).

The procedure for this reaction is exactly the same than the one described in section 2.2.1 the only difference is that in this case instead of bromine atoms the molecule has methyl groups in the positions 1, 4, 8 and 11, Figure 2.25.

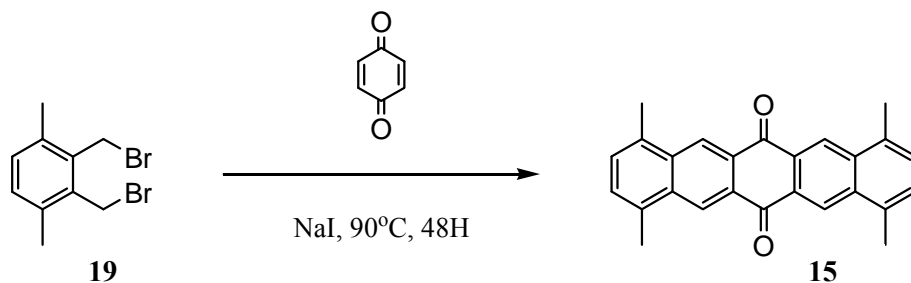


**Figure 2.25** Reaction scheme for the synthesis of 1,4,8,11-tetramethyl-6,13-pentacenequinone (15).

Despite having electron donor groups around the diene, the yield was consistently very low. Evidently a considerable amount of starting material is consumed by undesirable side reactions that result in products washed out over work up. Again these side reactions take place due to the highly reactive diene formed during the reaction mechanism. This diene might react via Diels alder with any carbon-carbon double bond that would act as dienophile.

### **2.2.3.3 Synthesis of tetramethylated pentacene derivatives (3, 4 and 5)**

The general conditions involved in the synthesis of the three target derivatives are presented (R= Me (**3**), Et (**4**) and i-pr (**5**)). Later specific details for each individual will be provided.

The reaction involving the addition of the silyl groups should be similar to the one observed in Section 2.1 which corresponds to the synthesis of TIPS-pentacene. The same procedure was used. However, we have found that the addition of the methyl groups in the 1,4,8,11 positions include some very important modification to the system. In the case of TIPS-pentacene, the purification was made straight forward using a silica plug or in cases of polluted reactions by using column chromatography. However, we found that the new compounds decompose on silica and this makes the cleaning of the new materials much more complicated.

Thin layer chromatography (TLC) of the crude (in the case of TMTES-pentacene (**4**)) and using only hexane as eluent showed that the spot of the desired materials moved slowly and only a little on the silica layer. Showing retardation factor ( $R_f$ ) of 0.11. The addition of a polar solvent to the eluent in an attempt to promote better separation dragged impurities and lead to streaks making the separation impossible. We believe that the material degrades when in prolonged contact with silica and the very slow elution exacerbates this.

Analysis of the crude obtained after the chromatography column carried out on silica and using hexane as eluent, was studied to understand what the problem could be. The characterisation techniques carried out were NMR and mass spectroscopy, Figure 2.26.

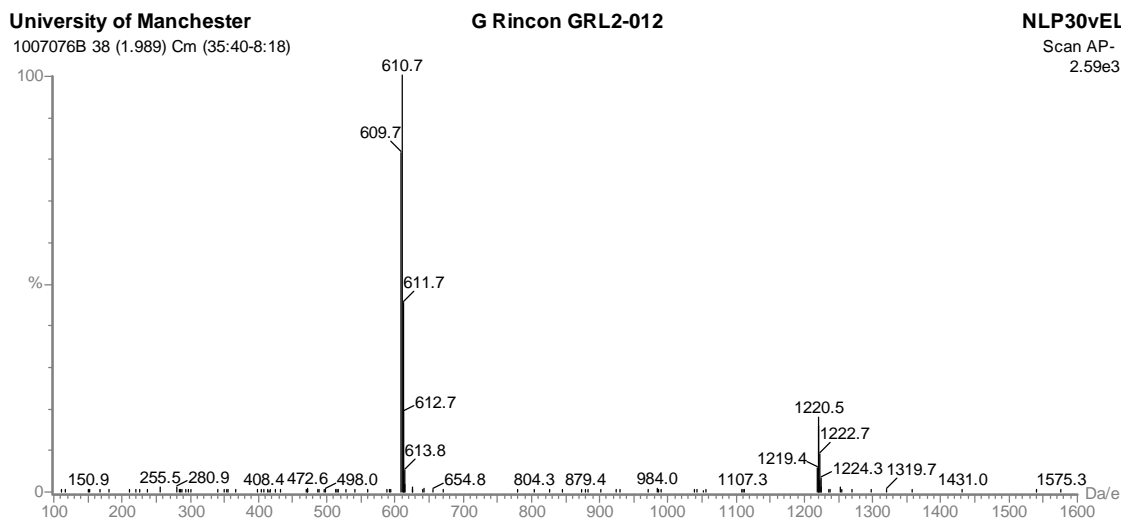


**Figure 2.26 Mass spectrum of the crude TMTES-pentacene analysed after the column. Peak for the monomer and the dimers can be observed.**

The proton NMR spectrum exhibited too many multiplets both in the aromatic and the alkyl region to be only attributed to the clean compound and a number of decomposition or side products are possible. The mass spectrum (APCI) reveals that dimers of the material were formed. This could explain the presence of the complex signals in the NMR spectra (take into account the presence of two different isomeric dimers<sup>[61]</sup> presented earlier in this chapter (Figure 2.6)).

In addition, to the dimers known for TIPS-pentacene, it is possible that others such as those reported by Anthony<sup>[47]</sup> can be formed in the solution. This kind of dimerisation takes place when the ethynyl group of one of the silyl groups undergoes cyclisation with one of the aromatic rings of another molecule via Diels-Alder reaction, Figure 2.27. This kind of dimers would possess an untouched pentacene core in its structure and this could make confusing the interpretation of

the thin film chromatography (TLC) since they would fluoresce in the same region of the spectrum than single molecules.

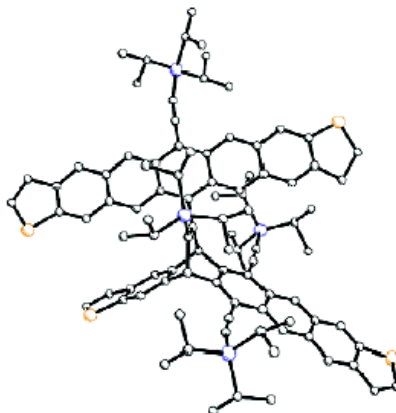
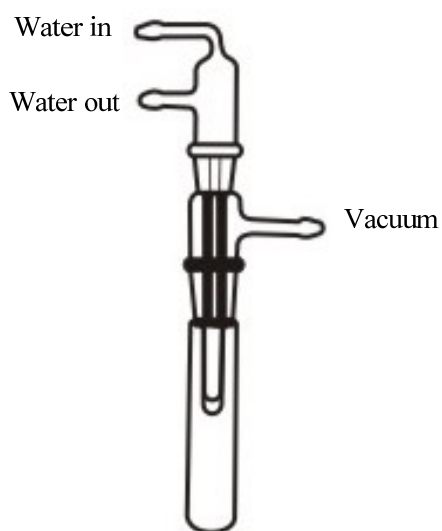


**Figure 2.27 Dimer taking place between the ethynyl group of one pentacenedithiophene molecule and one of the aromatic rings of another<sup>[47]</sup>.**

All these kinds of pentacene derivatives are very easily oxidised. The formation of dimers has been discussed previously in this chapter and it is probable that the presence of oxygen or the effect of light have a dramatic influence in this reaction<sup>[62]</sup>.



Vacuum sublimation was considered as an alternative method for the purification. This technique consisted on a glass chamber where the crude sample was added. This chamber was kept under high vacuum and the temperature of it was controlled using a sand bath. Above the sample (2 cm) and inside the vacuum chamber is the “cold finger” which is kept cold by a constant flow of water, Figure 2.28.

**Figure 2.28 Vacuum sublimation system.**



The operation of the system consisted on heating up the material until the sublimation temperature is reached. Then, the pure material vapours condensed on the surface of the cold finger from where it can be easily collected. The vacuum system that we used consisted of a rotary oil pump that was used to get primary vacuum of approximately  $10^{-2}$  Torr. Then the system was connected to a diffusion pump and pressures as low as  $10^{-6}$  Torr were reached. The sensor of the gauge was located next to the diffusion pump. Therefore, as it was connected to the glassware line slightly higher pressures should be considered at the apparatus it self. We thought that the pure material should condense on the cold finger of the sublimation system before the heavier dimers. TMTES-pentacene (**4**) was the first derivative to which this technique was applied.

As the sublimation temperature of this compound was unknown. We started the experiment at room temperature and it was increased in 25 °C increments up to 200 °C. At 150 °C a small amount of green material started to condense on the cold finger. This was analysed using proton NMR and the result showed clearly sign of decomposition (Multiplets on both the alkyl and aryl regions of the spectrum). Therefore, vacuum sublimation was discarded as possible purification technique. Subsequently has being found that at atmosphere pressure degradation occurs at less than 10 °C above the melting point.

To carry out the purification we used silica plugs on a sintered tube of 1 cm in diameter. The silica used was enough to form 1 cm in depth and the system was under reduced pressure to make the pentacene derivatives pass through it as fast as possible. The crude was then dissolved in hexane and it was pipetted into the plug. It was made one pipette at a time and it was flushed with hexane until most of the blue compound had come out. In this way the yield of the reaction compared to the one observed for normal TIPS-pentacene was much inferior. However, this has been the best way we found to purify the materials.

Below in Figure 2.29 is presented the mass spectra of TMTES-pentacene after the filtration through the silica plug and as we can see there is no sign of the dimer formation.

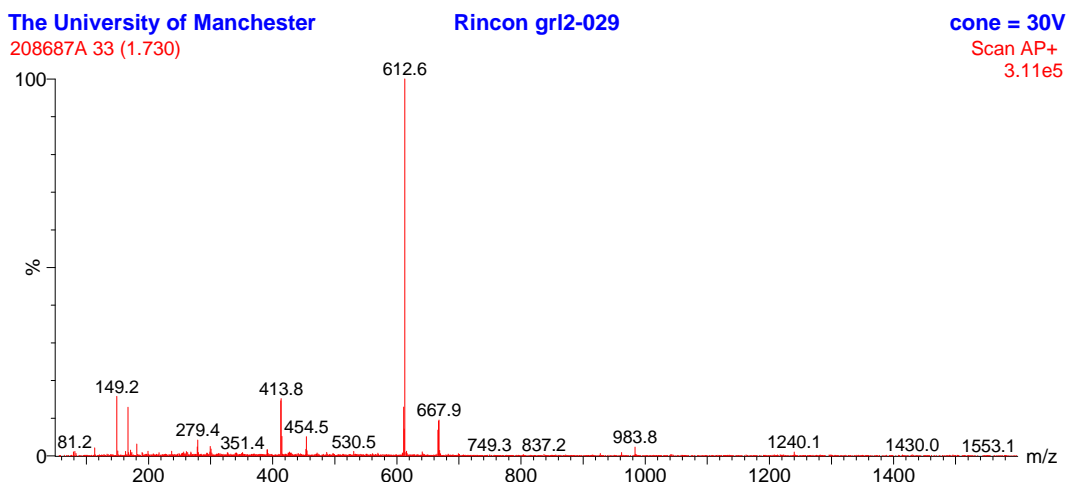


**Figure 2.29 Mass spectrum for TMTES-pentacene after the purification using silica plug.**

The aim of all these synthetic efforts was the synthesis of the three tetramethylated pentacene derivatives; R=Me (**3**), Et (**4**), i-pr (**5**). We found problems during the purification process and using the silica plug method we were able to purify only two of them TMTES-pentacene (**4**) and TMTIPS-pentacene (**5**). The purification of TMTMS-pentacene (**3**) was tried but without success. We believe that this might be due to the lower solubility that this material shows in hexane. This would have an effect in the speed of the material moving through the silica, increasing so the possibilities of decomposition.

### 2.3 Synthesis of 9,10-bis(trimethylsilylethynyl) anthracene (20), Synthesis of 9,10-bis(triethylsilylethynyl) anthracene (21), 9,10-bis(triisopropylsilylethynyl) anthracene (22)

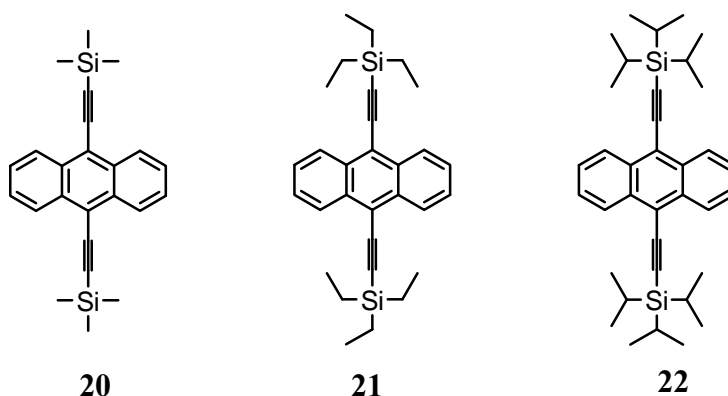


**Figure 2.30** 9,10-Bis(trimethylsilylethynyl) anthracene (20), 9,10-bis(triethylsilylethynyl) anthracene (21) and 9,10-bis(triisopropylsilylethynyl) anthracene (22).

The addition of the silyl groups on the 9,10-substituted anthracene derivatives<sup>[72]</sup> was carried out exactly in the same fashion as described previously for the 6,13 disubstituted pentacene derivatives.

There is one consideration that is worthy of comment and it is the better stability of the anthracene derivatives compared to their pentacene equivalents.

We believe that this can be explained by looking at the molecular orbitals diagrams and to the structure of the materials. In terms of molecular orbitals we observe that the band gap between HOMO and LUMO is smaller as the size of the acene increases, Figure 2.31. A smaller band gap makes the movement of electrons from bonding orbitals to anti-bonding ones easier and this can create instability in the molecules under certain conditions<sup>[73]</sup>.

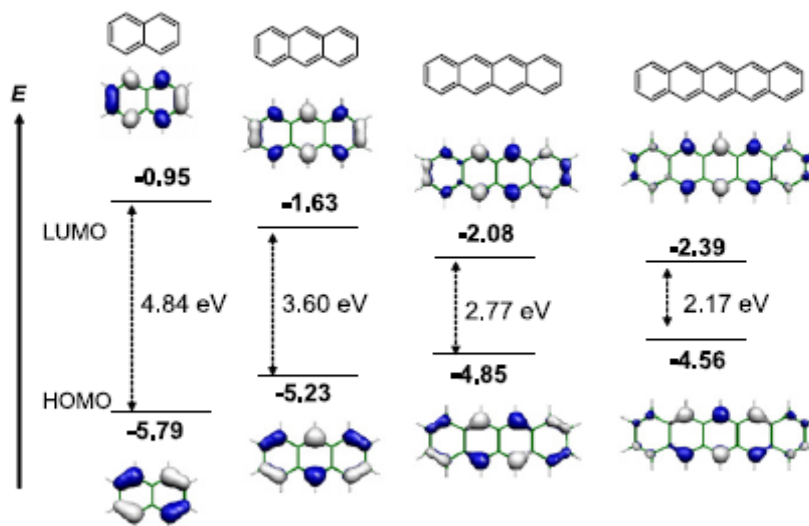


**Figure 2.31** Calculated HOMO, LUMO and band gaps for acenes<sup>[74]</sup>.

The crystallographic structure of the material has a very important influence over the stability too. Silyl pentacene derivatives are longer and they pack in a face to face fashion. This allows the close superposition of the aromatic rings and hence a clear  $\pi$ - $\pi$  interaction. In the case of anthracene derivatives, their crystalline structure shows clearly edge to face distribution. Structure is motivated more by silyl anchoring rather than weak  $\pi$ - $\pi$  stacking between the polyacene cores. These impede the close  $\pi$ - $\pi$  interaction. In the solid state the benzene cores are never close enough to initiate the dimerisation discussed in Section 2.1. In liquid state, the silyl groups are believed to occupy too much space to allow the core to be close long enough for the reaction to occur.

One of the first kinds of degradation observed among the pentacene derivatives is due to radical and Diels-Alder reactions taking place between the aromatic rings in the molecules. In the case of the anthracene derivatives, this reaction is impeded because the relative size of the silyl groups in comparison to the anthracene. This silyl groups avoid anthracene cores to approach each other therefore, making it much less likely for the Diels-Alders reaction to take place.

### **3 Physical and electronic characterisation of the new pentacene derivatives**

In this chapter the results on the physical and electronic characterisation of the novel solution processable pentacene derivatives (1,4,8,11-tetramethyl-6,13-triethylsilylethynylpentacene (TM TES-pentacene) (**4**) and 1,4,8,11-tetramethyl-6,13-triisopropylsilylethynylpentacene (TMTIPS-pentacene) (**5**)<sup>[71]</sup> are discussed.

### 3.1 Background

It is well known that molecular order and structure in organic semiconductors is a key factor which determines their hole or electron carrier mobilities. The overlap and distances between the  $\pi$  orbitals are a few of the many factors that need to be considered when designing new materials for these applications<sup>[3c, 9a]</sup>. Acenes and in particular soluble pentacene derivatives are the organic semiconductors of interest in this thesis. This kind of materials has been previously studied due to their known ability as hole carriers<sup>[25b, 34, 54]</sup>.

TIPS-pentacene has overcome the problem of the solubility of pentacenes with the addition of the 6,13 silyl groups making the compound soluble in most organic solvents<sup>[75]</sup>. More over, the silyl groups disrupt the three dimensional herringbone structure of pentacene, promoting face to face packing as shown in Figure 3.1 resulting in enhanced overlap of the  $\pi$  orbitals. This superior  $\pi$ - $\pi$  stacking interaction leads to an improvement in the hole mobilities. In the case of solution deposited TIPS-pentacene mobilities of  $1.5 \text{ cm}^2/\text{Vs}$  have been achieved<sup>[45]</sup>.

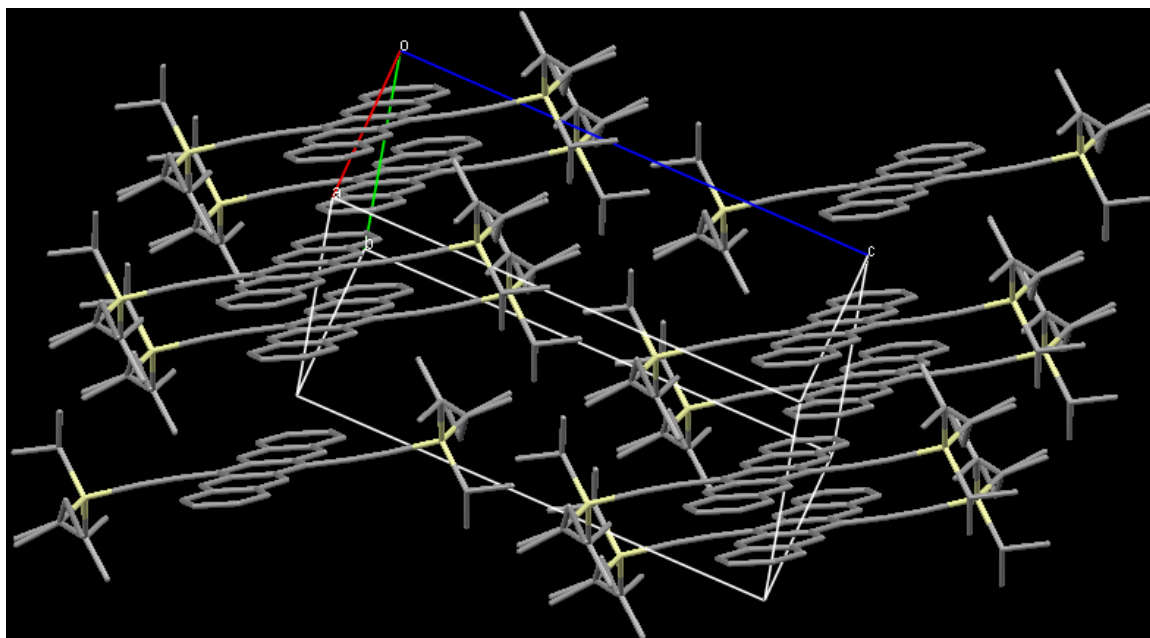


**Figure 3.1** Crystal lattice for TIPS-pentacene.

### **3.2 Solution properties of substituted pentacene derivatives**

The solubility of pentacene is increased by the addition of the trialkylsilylethynyl groups in the 6,13 positions of its structure. Three main alkyl groups have been used for the substitution methyl, ethyl and isopropyl. A detailed study of the solubility of TIPS-pentacene was presented by Anthony in 2007<sup>[75]</sup>. They found that TIPS-pentacene was highly soluble in toluene, tetrahydrofuran and chloroform. In solvents like hexane or diethylformamide TIPS-pentacene showed poorer solubility. Also, they suggest a direct relationship between how good the solvent was, related to TIPS-pentacene, and the quality of the TIPS-pentacene films formed after solvent evaporation. Good solvents yielded larger grain size crystals and as a consequence better films and better devices were obtained. Another influential factor in terms of film formation is the evaporation rate of the solvent. Since organic materials require time to crystallise<sup>[76]</sup> fully, higher boiling point solvents were found to be preferred.

TIPS-pentacene, compared with 6,13-bis(trimethylsilylethynyl) pentacene (TMS-pentacene) and 6,13-bis(triethylsilylethynyl) pentacene (TES-pentacene), was the pentacene derivative achieving best performance in thin film transistors. This was due to the improved two dimensional solid phase packing observed for this material<sup>[50]</sup>. As a consequence this has been the most studied derivative. There is no study so far of the solubility of TMS-pentacene and TES-pentacene derivatives. Both, like TIPS-pentacene, are soluble in most organic solvents. The rigidity of the TMS groups in TMS-pentacene and the freedom of movements of the TES groups in TES-pentacene should affect the solubility of these materials and as a consequence further study is required before any definitive statements can be made.

TMTES-pentacene and TMTIPS-pentacene are soluble in the same solvents as the reference material TIPS-pentacene. Toluene was chosen as the solvent in this study for two main reasons; toluene was one of the best solvents for the reference material, TIPS-pentacene<sup>[75]</sup> and is also a good solvent for the new materials and secondly, since the long term aim of this work is to use ink-jet printing as deposition technique, it is a requirement the usage of a suitable high boiling point solvent<sup>[77]</sup>. Toluene with a boiling point of 111 °C is a suitable candidate.

### **3.3 Determination of HOMO-LUMO levels of TMTES-pentacene and TMTIPS-pentacene**

An important factor that needs to be considered when designing new organic semiconductors is the molecular orbitals levels. This data provided us information about how easy is going to be injecting carriers from the electrodes into the material.

HOMO and LUMO levels were determined using a combination of cyclic voltammetry (CV) in thin film and UV-vis in solution and thin film. Using CV it is possible to obtain the HOMO and the LUMO of the materials from the oxidation and reduction potential respectively. However it was not possible to determine the onset of the reduction potentials using cyclic voltammetry since both materials



(TMTIPS-pentacene and TMTES-pentacene) decompose on reduction. As a consequence the LUMO could not be measured directly. Instead, the optical band gap was measured using UV-vis and the LUMO was calculated by simple addition of the HOMO and the band gap, Equation 3.1. We know of the limitations of this method since optical and electronic band gaps can be often different. The main difference arises from the fact that the optical band gap is obtained by the addition of photons to the material and the electronic band gap is given by the oxidation and reduction potentials, which are a measure of the potential required to withdraw or to add electrons to the molecule. However, this approximation has been used previously in literature for pentacene derivatives<sup>[78]</sup> and it is openly accepted.

$$|LUMO| = -Bandgap + |HOMO| \quad 3.1$$

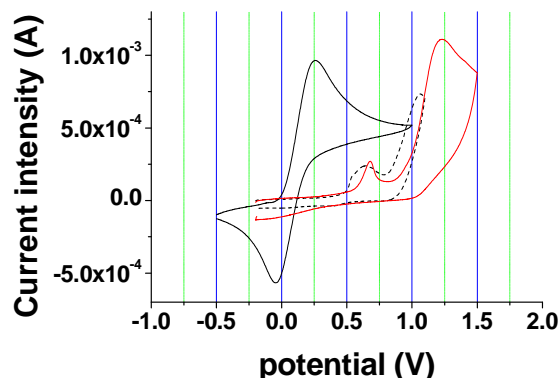


**Figure 3.2** Cyclic voltammetry of TMTES-pentacene (black dash line), TMTIPS-pentacene (red line) and ferrocene as the reference material (black solid line). The experiments were carried out in thin films on platinum electrodes using a scan rate of 100 mV/s (refer to experimental section for further details).

The oxidation onset observed in cyclic voltammetry matches with the HOMO level, Figure 3.2. Equation 3.2<sup>[79]</sup> provided the HOMO level for our materials.

$$|HOMO| = HOMO_{ferrocene} + (E_{onset} - E_{1/2,ferrocene}) \quad 3.2$$

The HOMO level of ferrocene ( $HOMO_{ferrocene}$ ) was used as reference 4.8 eV.  $E_{onset}$  is the energy at which the onset in the current can be observed when increasing the potential and  $E_{1/2,ferrocene}$  is the energy reached when the voltage is at half way between the maximum and the minimum current for the first oxidation potential in ferrocene, Equation 3.3 and Figure 3.3.

$$E_{1/2} = 1/2 \cdot (E_{max} - E_{min}) \quad 3.3$$

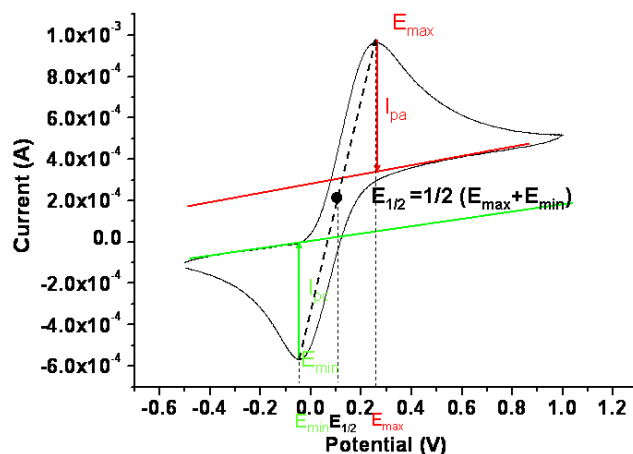


**Figure 3.3** Diagram explaining the calculation of  $E_{1/2}$  ferrocene.

The wavelength of the onset of the UV-vis spectra for organic thin films corresponds to the energy of the optical band gap, Figure 3.4 and can be calculated using Equation 3.4.

$$E = h \cdot \frac{c}{\lambda} \quad 3.4$$

Where  $E$  is the energy of the band gap,  $h$  is the Plank's constant,  $c$  is the speed of light and  $\lambda$  is the wavelength.

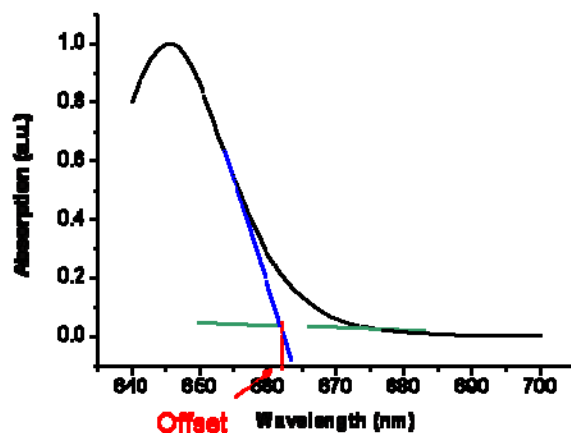


Figure 3.4 Diagram explaining the how to obtain the offset of the UV-vis.

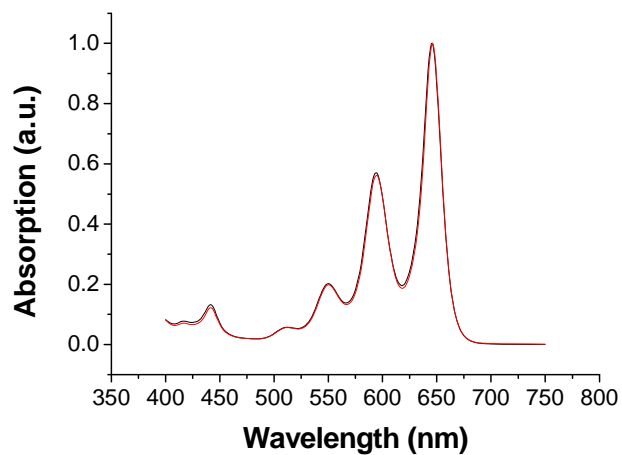


Figure 3.5 UV-vis absorption diagram for TMTES-pentacene (black line) and TMTIPS-pentacene (red line).

To conclude with the calculation of the molecular levels the addition of both, HOMO and band gap, provided the LUMO, Equation 3.1.

$$|LUMO| = -Bandgap + |HOMO| \quad 3.1$$

**Table 3.1 Table showing oxidation onset in comparison to ferrocene, HOMO from cyclic voltammetry, calculated LUMO and band gaps from UV-vis for TIPS-pentacene, TMTES-pentacene and TMTIPS-pentacene.**

Compound	TIPS-pentacene	TMTES-pentacene	TMTIPS-pentacene
$E_{\text{onset}}$ (V)	0.60	0.50	0.59
HOMO (eV)	5.29	5.19	5.28
LUMO (eV)	3.47	3.32	3.41
Band gap (eV)	1.82	1.87	1.87

In order to compare the HOMO LUMO levels of the new pentacene derivatives with TIPS-pentacene it has been calculated under the same conditions. The small difference compared with literature values arises from the different experiment techniques<sup>[58]</sup>.

The addition of the silylethynyl groups to the 6,13 positions of pentacene decrease the band gap of the materials due to a exceptionally low LUMO level. A conclusive explanation for this effect is still unknown but it has been widely observed<sup>[58]</sup>.

In the case of these new materials it has been observed that TMTES-pentacene has higher in energy HOMO and LUMO levels than TIPS-pentacene and TMTIPS-pentacene. When comparing TIPS-pentacene with TMTIPS-pentacene we observe that the addition of the electron donating methyl groups has increase the energy of both HOMO and LUMO. These results are consistent with previous studies that observe increase in the HOMO LUMO levels as a result of addition of electron donating groups to the pentacene core.

Gold was the metal used as source and drain electrodes in all the thin film transistors fabricated for this thesis. The energy level of the HOMO for all these materials is within the limits of gold ohmic contacts ( $5.1 \pm 0.3$  eV) and

consequently the injection of charges from the electrodes into these semiconducting materials is favoured.

### **3.4 Thermal analysis of TMTES-pentacene and TMTIPS-pentacene**

Thermal analysis of TIPS-pentacene and the new pentacene derivatives TMTES-pentacene and TMTIPS-pentacene, including thermal gravimetric analysis (TGA) and differential scanning calorimetry (DSC) were carried out. TGA provided information of the decomposition temperature of the materials. This was the limiting temperature up to which DSC were performed. The melting points for the three materials are 256-257 °C for TIPS-pentacene, 260-262 °C for TMTIPS-pentacene and 257-259 °C for TMTES-pentacene.

TIPS-pentacene sample showed a 20 % weight loss from room temperature to 100°C believed to be due to entrained water absorbed in the material. To overcome this problem the samples were pre-dried in a vacuum oven at 50 °C over night. The range of temperatures at which all samples fully decompose is from 310 to 340 °C, Figure 3.6. This gives us an indication to the limit temperature to which the DSC study of the materials can be carried out.

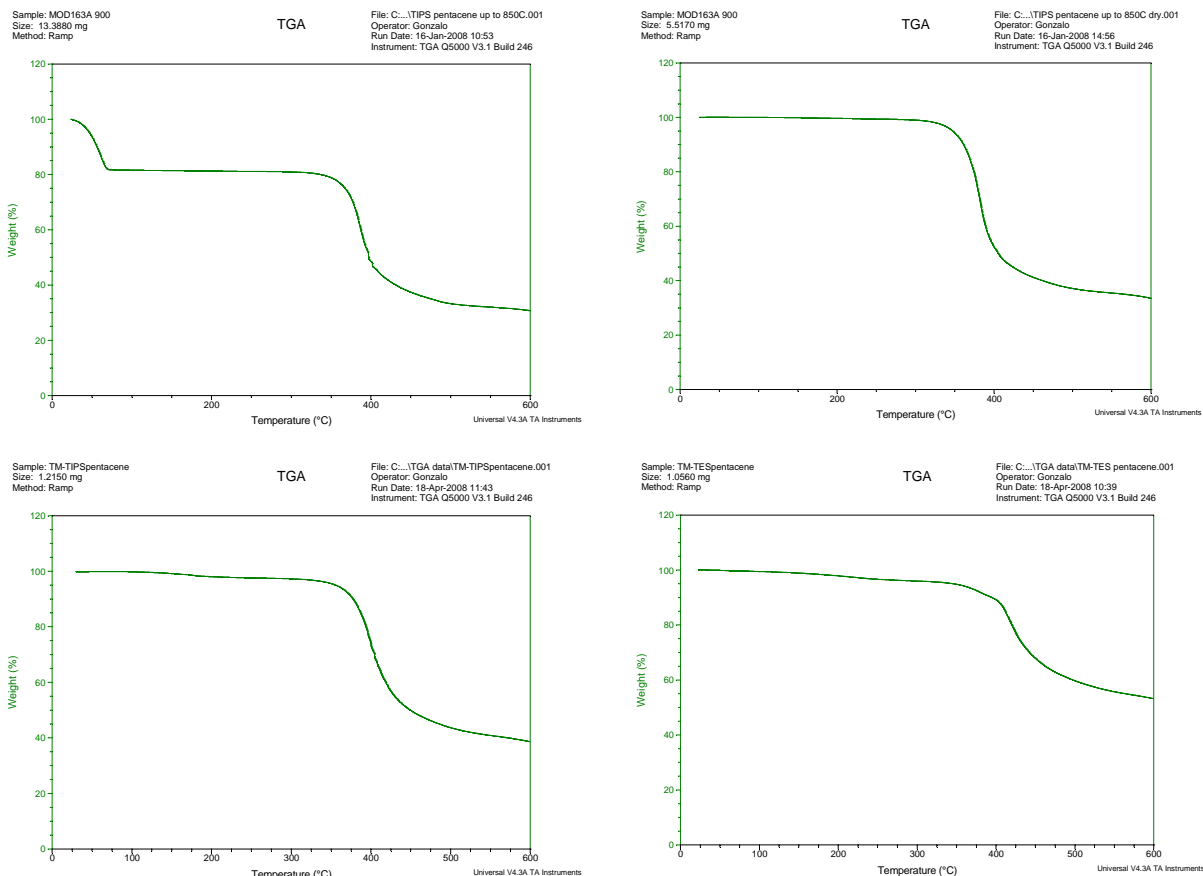


**Figure 3.6** From left to right, top to bottom thermal gravimetric analysis of TIPS-pentacene before drying, dry TIPS-pentacene, dry TMTIPS-pentacene and dry TMTES-pentacene. The samples were run at 5 °C/min heating rate under nitrogen atmosphere.

Previous differential scanning calorimetry studies carried out by Anthony et al. on TIPS-pentacene showed a reversible phase transition observed at 124 °C<sup>[31]</sup>, Figure 3.7. This transition was reversible so long as the decomposition temperature of the material was not reached. The exothermic degradation of TIPS-pentacene takes place at 266 °C just a few degrees above the melting point of the material, which is 261 °C. The exothermic degradation is believed to be due to Diels-Alder reaction taking place between the alkyne triple bond and the pentacene backbone.

The reversible transition observed in TIPS-pentacene at 124 °C is due to a distortion in the crystallographic cell. The driving force for this distortion is believed to be the increase of freedom of the TIPS groups as the temperature is increased.

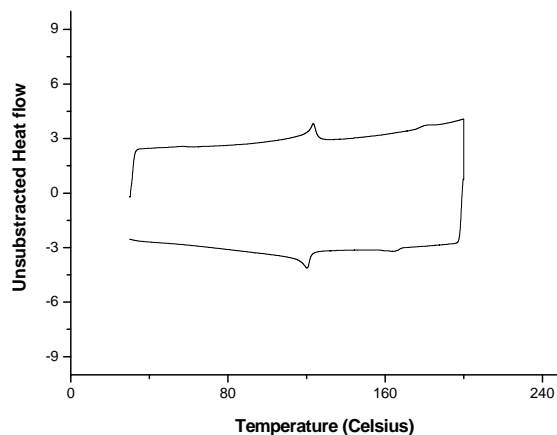


**Figure 3.7 DSC of TIPS-pentacene up to 200°C at a heating rate of 5 °C/min showing a reversible phase transition at 124 °C.**

The DSCs of TMTES-pentacene and TMTIPS-pentacene are shown in, Figures 3.8. In the case of TMTIPS-pentacene a reversible phase transition at 183 °C was observed. Further study towards the understanding of this transition needs to be carried out. However, due to the similarity with the mother molecule, TIPS-pentacene, a comparable process, including a distortion of the crystallographic cell due to and increase of the conformational freedom of the TIPS groups might be taking place.

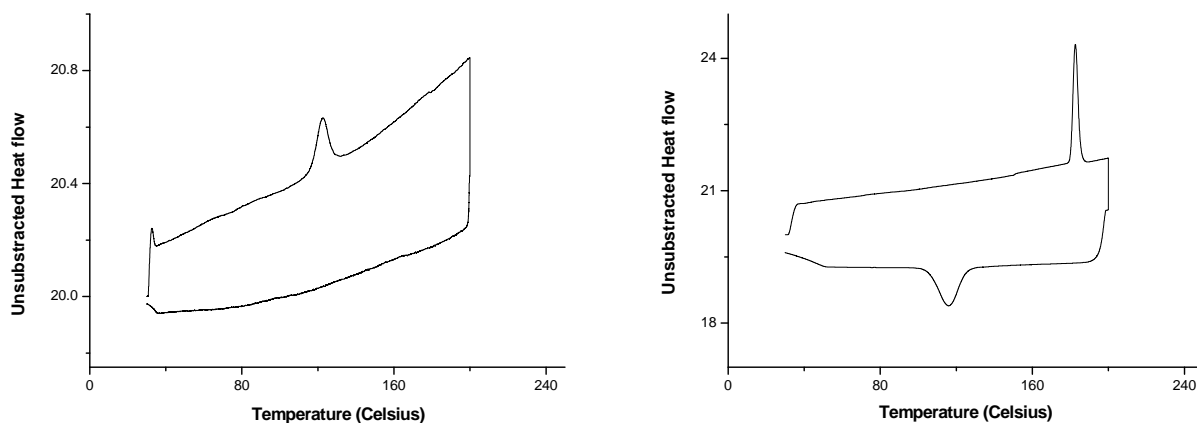


**Figure 3.8 DSC of TMTES-pentacene (left hand side) and TMTIPS-pentacene (right hand side) at 5 °C/min Heating rate.**

The TMTES-pentacene behaviour is completely different. A non-reversible transition was observed at 122 °C. To verify the non-reversibility of the transition a second thermal cycle using the same sample was carried out and in this second cycle no transitions were observed. The <sup>1</sup>H NMR analysis of the sample did not show any difference respect to the original material and consequently a rearrangement of the molecules in the solid state, as in the case of TIPS-pentacene, is believed to be the explanation. The larger vibrational freedom of the ethyl groups in comparison to the TIPS group could have a deeper impact in the disruption of the crystallographic structure. Another possibility could be that the kinetics driving the cooling down process are too slow as for the calorimeter to measure it at the measured cooling rates and as a consequence no sing of the phase transition in the cooling down side of the graph is observed<sup>[80]</sup>. In this case, the stable form created at high temperatures can exist at room temperature as a metastable form. The lack of time did not allowed us do all the desired experiment to achieve a full understanding of the phenomena. Among these remaining experiments are hot stage optical microscopy and hot stage X-ray diffraction.

Despite the similarity, the two new pentacene derivatives show different behaviour in thermal analysis. The reversibility in the phase transitions observed for TMTIPS-



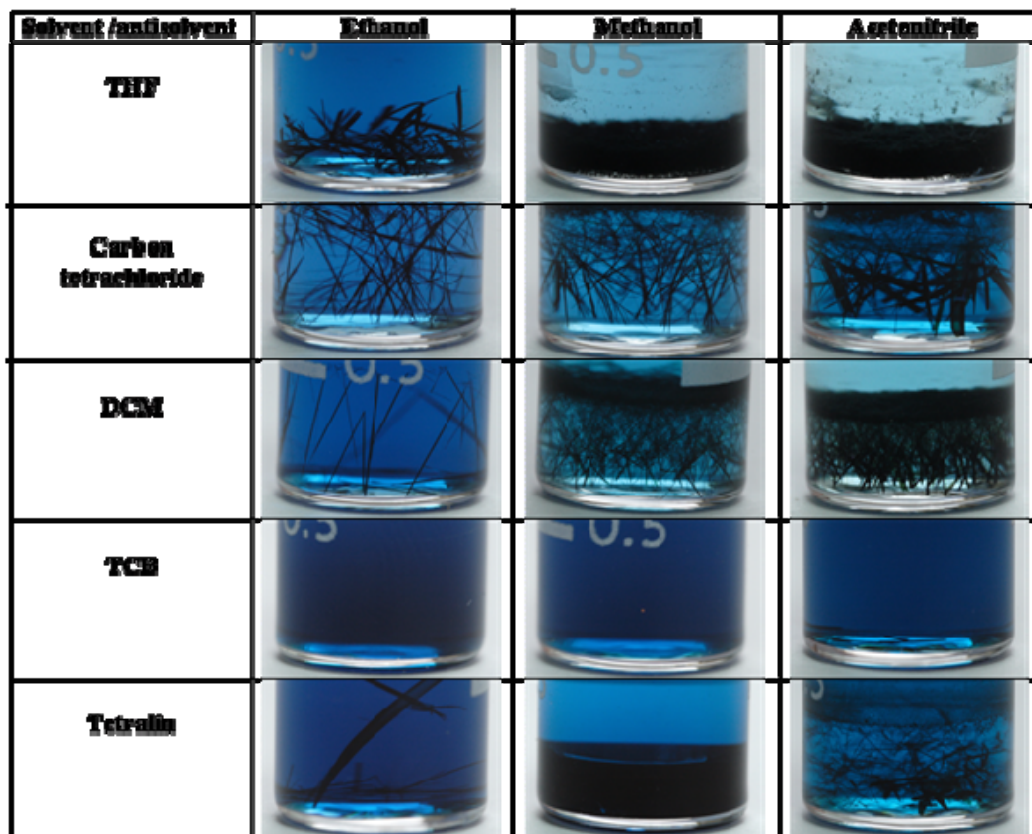
pentacene could in somehow be comparable to the one observed for TIPS-pentacene. TMTES-pentacene undergoes no reversible phase transition at 122 °C, possibly due to internal rearrangement of the molecules in the crystal as in the case of the two other materials. However, the studies carried out so far, even when reproducible, are not conclusive and further study needs to be carried out for a fully understanding the behaviour of the material.

### **3.5 Crystal structure of TMTES-pentacene and TMTIPS-pentacene**

Different methods were investigated to grow single crystals of TMTES-pentacene and TMTIPS-pentacene suitable for X-rays crystallography. Evaporation, using solvents of low and high boiling point (Toluene, 1,2,3,4-tetrahydronaphthalene (Tetralin), tetrahydrofuran and dichloromethane), under open atmosphere and under a solvent saturated atmosphere in an attempt to promote slower evaporation rates did not yield the desired crystals.

The method providing the suitable crystals was crystallisation by slow diffusion. This method consisted in dissolving a certain amount of materials in the minimum amount of a high density solvent required to achieve full dilution. Then, the same volume of a lighter solvent, in which the materials are not soluble in (anti-solvent), was added carefully on top, avoiding mixing of both solvents. The samples were left overnight and the solvents slowly start diffusing into each other. This promotes crystallisation due to a decrease in the solubility of the solvent towards the material. Pictures of all the samples used for slow diffusion method are shown in Table 3.2.

**Table 3.2 Slow diffusion TMTES-pentacene samples after overnight resting. The solvents used were Tetrahydrofuran (THF), carbon tetrachloride, dichloromethane (DCM), trichlorobenzene (TCB) and Tetralin. The anti-solvents used were ethanol, methanol and acetonitrile.**



The study of the single crystal structure of the new derivatives gives key insight into understanding saturated hole mobility. Both TMTIPS-pentacene and TMTES-pentacene show P-1 symmetry which is the space group with the least symmetry. The only symmetry operation is the molecule itself and as a triclinic structure it shows  $a \neq b \neq c$  and that  $\alpha \neq \beta \neq \gamma$ . The crystallographic structures were submitted to the Cambridge Crystallographic Data Centre being the reference numbers: CCDC 717661 for TMTES-pentacene and CCDC 717662 for TMTIPS-pentacene. It calls the attention that a group with such a low symmetry possesses, as we will see, such good semiconducting properties. Something that can help us to understand these positive results is the fact that these materials pack in the highly desirable 2D slip

stack structure which allows, as presented in the introduction, charge transport in 2 dimensions through the crystal. Being the average distance measured between the pentacene backbones of 3.52 Å, 3.47 Å and 3.43 Å for TMTIPS-pentacene, TIPS-pentacene<sup>[34]</sup>, and TMTES-pentacene respectively.

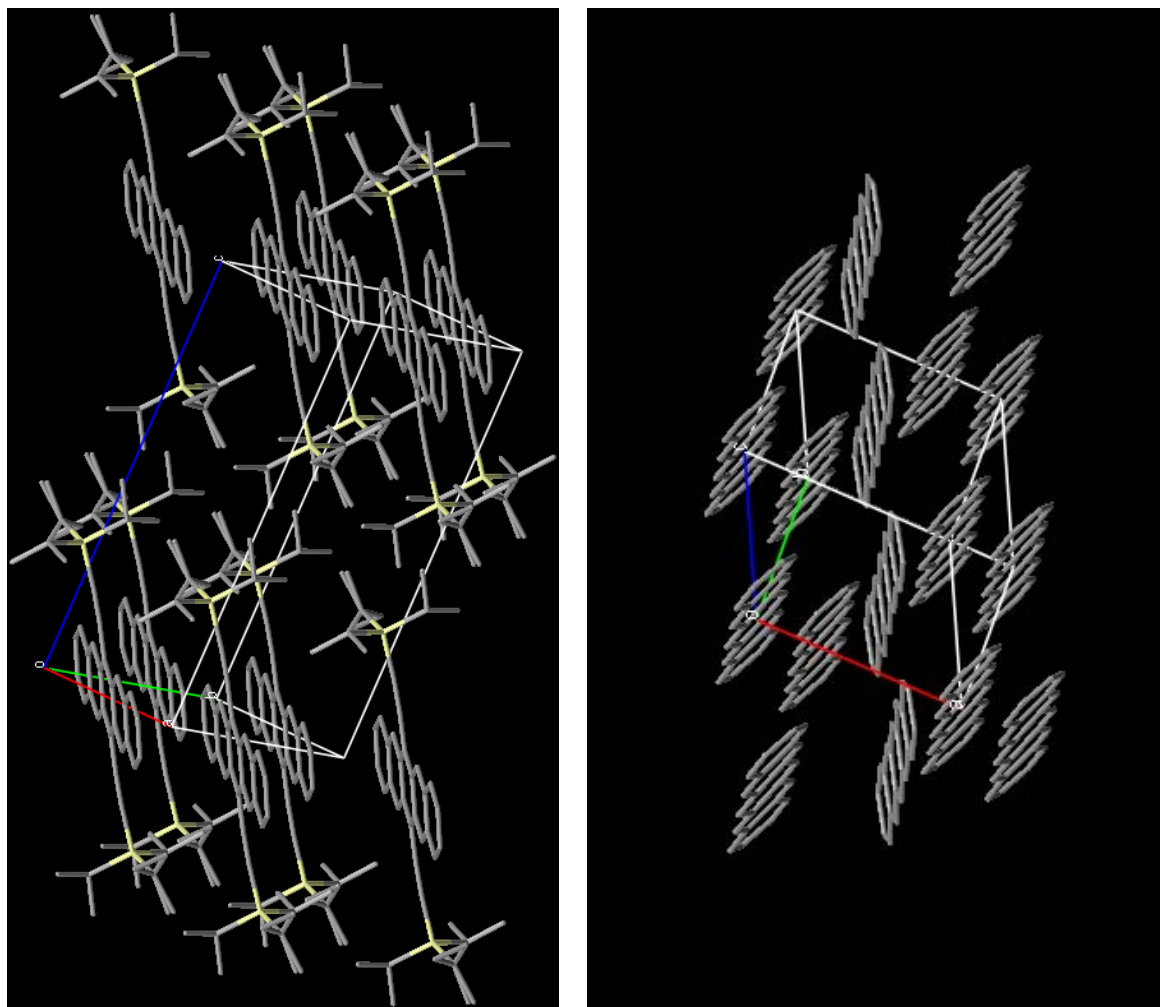


**Figure 3.9** Crystal lattice for TIPS-pentacene (left hand side) and pentacene (right hand side).

There is a significant difference in the area of the pentacene backbone<sup>[25a]</sup> which is overlapped in TMTES-pentacene and TMTIPS-pentacene. Being similar for TMTIPS-pentacene and TIPS-pentacene and being much larger for TMTES-pentacene. In Figure 3.10 are shown the crystal lattices for TMTIPS-pentacene and

TMTES-pentacene. Although the overlapping is visually obvious, it needs further investigation in orbital modelling to indicate if an increase in the overlapping is beneficial for the mobility of carriers<sup>[81]</sup>.

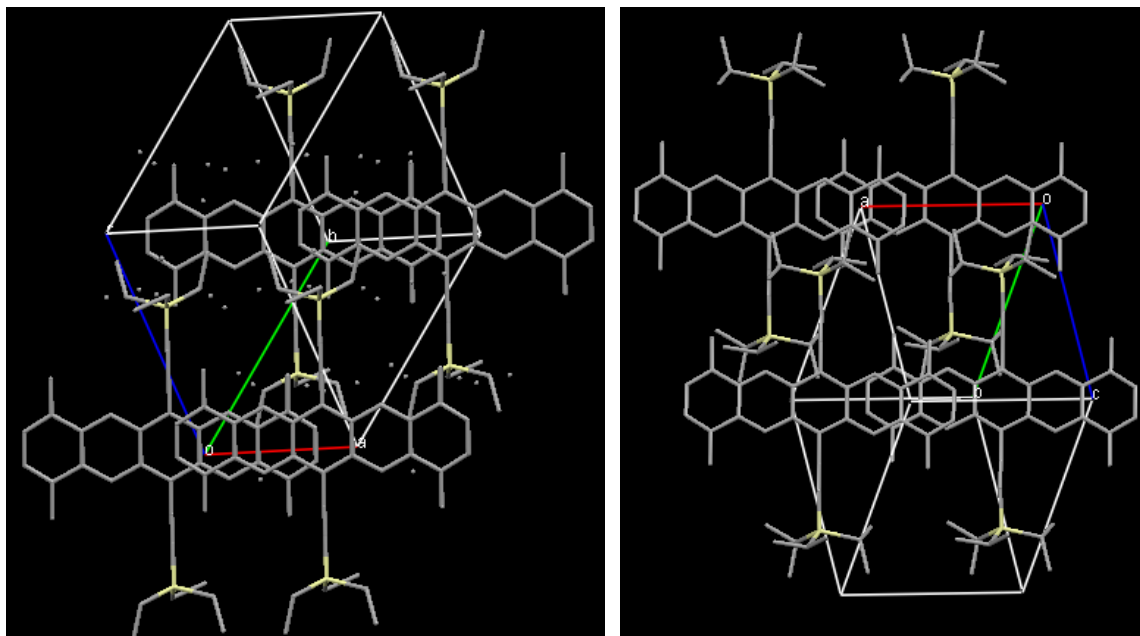


**Figure 3.10** Crystal lattice for TMTES-pentacene (left hand side) and TMTIPS-pentacene (right hand side).

The increase in the overlapped area is not only along the long axis of the pentacene core but also along the short axis of the molecule backbone. We believe that this enhancement in the  $\pi$ - $\pi$  stacking and the closer packing of the molecules, measured for TMTES-pentacene, will have a deep influence in the hole mobility and in the film formation properties of these materials<sup>[9a]</sup>.

### **3.6 Thin Film deposition of TMTES-pentacene and TMTIPS-pentacene**

Among the many factors that have an influence in the electronic performance of solution processable materials are: the deposition technique, the film processing

conditions, the nature of the solvent, the formulation of the solution and the substrate surface energy. Therefore, it is important to define the sample preparation process for our materials. The solutions were drop cast on OTS treated silica wafer from a solution 0.5 % w/w in toluene. When TMTES-pentacene was deposited almost continuous coverage of the substrate was observed. However, under the same conditions, TMTIPS-pentacene only wets the substrate partially and it was impossible to achieve continuous films, Figure 3.11.

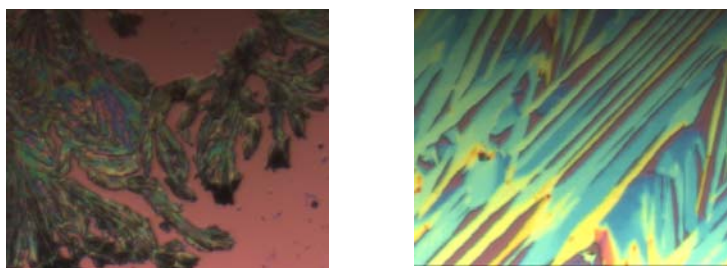


**Figure 3.11 Optical micrographs (250 x 400 micron) of TMTIPS-pentacene (left hand side) and TMTES-pentacene (right hand side), drop cast onto OTS treated silica from a solution of 0.5 %w/w in toluene.**

Atomic force microscopy (AFM) image (tapping mode) of a thin film of TMTES-pentacene (deposited by drop casting from a  $10^{-4}$  M solution in HPLC grade toluene onto a hydrophilic silica wafer) reveals atomic steps of about 1.64 nm, which is about the length of the molecule from ethyl to ethyl group, Figure 3.12. This indicates that the molecules pack almost vertically to the substrate (approximate tilt angle  $\alpha=77.5^\circ$ ) in an atomic layer. This result is comparable to that observed for the reference material TIPS-pentacene<sup>[75, 82]</sup>.

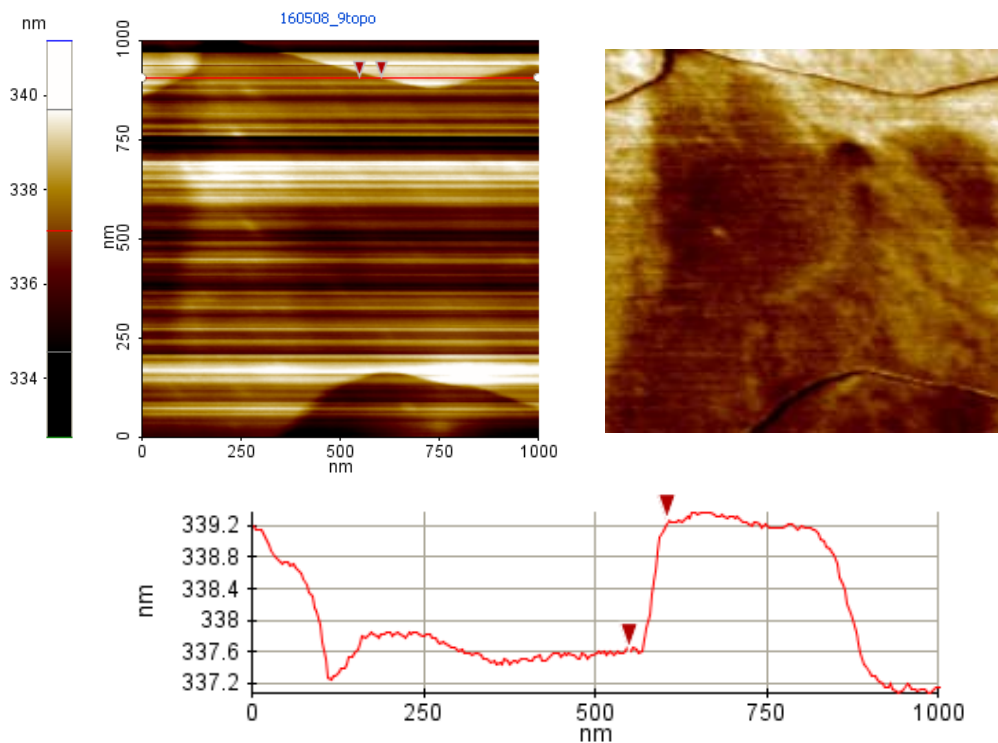


**Figure 3.12 Observation by atomic force microscopy in dynamic mode of a terraced film of TMTES-pentacene. The topographic scan (left hand side) and the dynamic mode amplitude image (right hand side) gives an enhanced viewing of the atomic step.**

The length of the molecule was calculated from the single crystal x-ray data (Mercury was the software used for the calculations) and the tilt angle was calculated using basic trigonometric calculations considering the length of the molecule (1.68 nm) and the molecular step measured by AFM (1.64 nm).

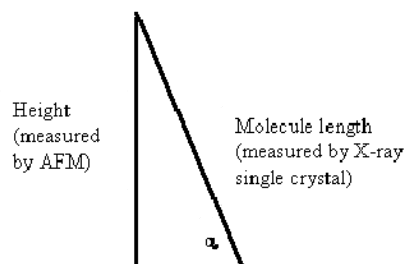


**Figure 3.13 Diagram explaining the calculations of the tilt angle from the height obtained from AFM and the molecular length obtained by X-ray single crystallography.**

X-ray powder diffraction (XRD) of TMTES-pentacene and TMTIPS-pentacene drop cast from a 1 % w/w tetralin solution on OTS treated silicon substrates and dried at room temperature was carried out, Figure 3.14.

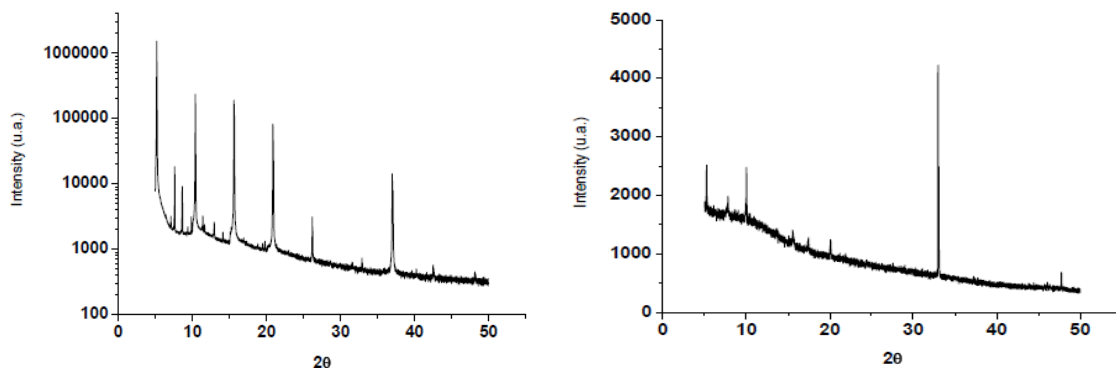


**Figure 3.14 Out-of-plane XRD patterns (0,0,P) of TMTES-pentacene (left hand side) and TMTIPS-pentacene (right hand side) on OTS treated silicon substrates using a Cu  $K_{\alpha}$  source at 0.15405980 nm.**

Only in the case of TMTES-pentacene we did an estimation of the XRD diffraction pattern calculating manually possible  $2\theta$  angles from a vertically standing molecular disposition on the substrate. The estimation was made using Bragg's law.

$$n\lambda = 2d \sin \theta \quad 3.5$$

Where  $n$  is an integer,  $\lambda$  is the wavelength of the incident wave,  $d$  is the inter-planar distance in the molecular lattice and  $\theta$  is the angle between the incident wave and the scattered one. To calculate the different  $2\theta$  signals we have used the wavelength of the Cu  $K_{\alpha}$  X-ray source ( 0.15405980 nm) and as distance ( $d$ ) we have considered the length of the TMTES-pentacene molecule calculated from the single crystal data (1.68 nm).

The results, Table 3.3, compared with the experimental data help to support the idea that TMTES-pentacene packs almost vertically to the substrate with an approximate tilt angle  $\alpha = 77.5^{\circ}$ .

**Table 3.3 Out-of-plane X-rays diffraction  $2\theta$  values observed and calculated for TMTES-pentacene.**

(0,0,P)	$2\theta$ ° calculated	$2\theta$ ° Observed
(0,0,1)	5.26	5.20
(0,0,2)	10.52	10.41
(0,0,3)	15.80	15.62
(0,0,4)	21.14	20.89
(0,0,5)	26.50	26.20

### **3.7 Determination of saturated hole mobility of TMTES-pentacene and TMTIPS-pentacene**

Gold was chosen as the material for the electrodes. The reason was that the work function of gold is 5.1 eV which is energetically very close to the HOMO of our materials, making it possible for an easy movement of carriers between the electrodes and the material and as such we should have ohmic contact.

Bottom-gate, top contact organic field effect transistors (OFET) devices, Figure 3.13, were fabricated on octadecyltrichlorosilane (OTS) treated heavily n-doped silicon wafers comprising a 3000 Å thermally grown gate oxide layer. The material was drop cast from a 0.5 % w/w solution in toluene at room temperature. To secure complete solvent evaporation the substrates were allowed to dry under ambient atmosphere at room temperature in an open laboratory. No post thermal annealing was employed. All the devices were characterised at room temperature under normal atmosphere and in the dark.



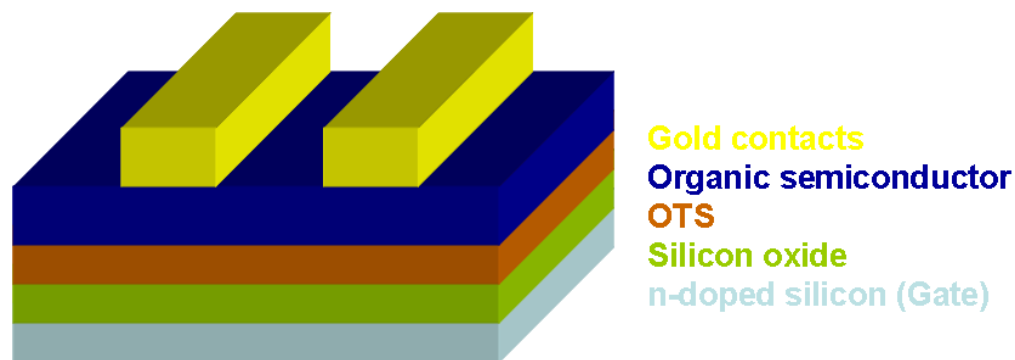


**Figure 3.15 Bottom gate top contact organic thin film transistor structures.**

Improved film formation was observed for TMTES-pentacene when the silicon oxide insulator layer was treated with octadecyltrichlorosilane (OTS). OTS is a compound that forms continuous and homogeneous self assembled monolayers attached to the silicon oxide dielectric. This hydrophobic layer improves the growing and orientation of certain materials<sup>[36]</sup>. It improves the dipolar disorder appearing from a inhomogeneous insulator layer<sup>[83]</sup> and avoids the presence of OH groups that appear at the surface of the silicon oxide layer. This OH groups could act like traps in the accumulation layer, which is perhaps the most important part of the device, decreasing so the transistor performance. Figure 3.16 shows the mechanism through which OTS attaches to the silicon oxide surface.

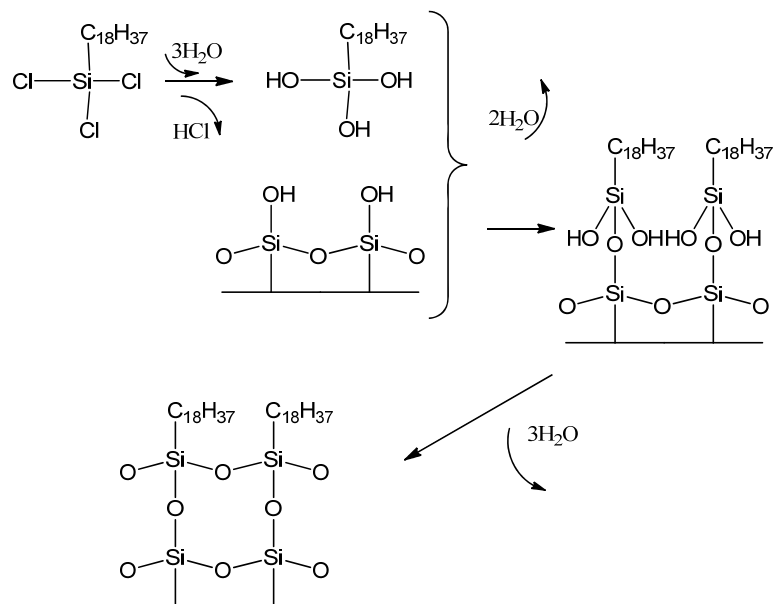


**Figure 3.16 Mechanism of coating of OTS on silica surface<sup>[84]</sup>.**

Under these conditions the average saturated hole mobility of TIPS-pentacene measured is  $3.7 \times 10^{-3} \text{ cm}^2/\text{Vs}$  and on/off ratios of  $10^6$ , Figure 3.17. The low mobilities of TIPS-pentacene measured here compared to the results in literature ( $1.8 \text{ cm}^2/\text{Vs}$ ) arises from the different processing conditions<sup>[45]</sup>. Among these conditions is the treatment of the gold electrodes with pentafluorobenzenethiol to improve the electrode interface or the difference in the semiconductor deposition method<sup>[45, 48]</sup>. The method used for calculation of the saturated mobilities is described in detail in Chapter 6.

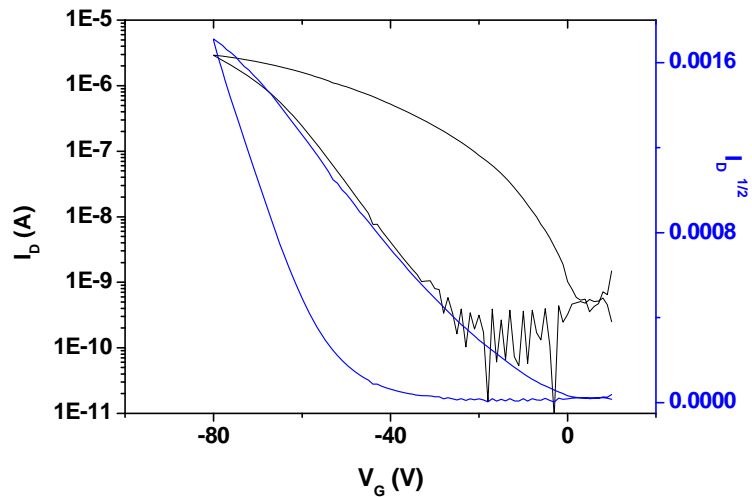


**Figure 3.17 Transfer Characteristics for an OTFT made using TIPS-pentacene.**

The results obtained using TMTIPS-pentacene are less than those obtained for TIPS-pentacene. We believe, that this can be explained due to the difficulty in achieving continuous films under these conditions. On/off ratios of  $10^3$  and maximum saturated hole mobility of  $4 \times 10^{-4} \text{ cm}^2/\text{Vs}$  were measured. Transfer characteristics are presented in Figure 3.18.

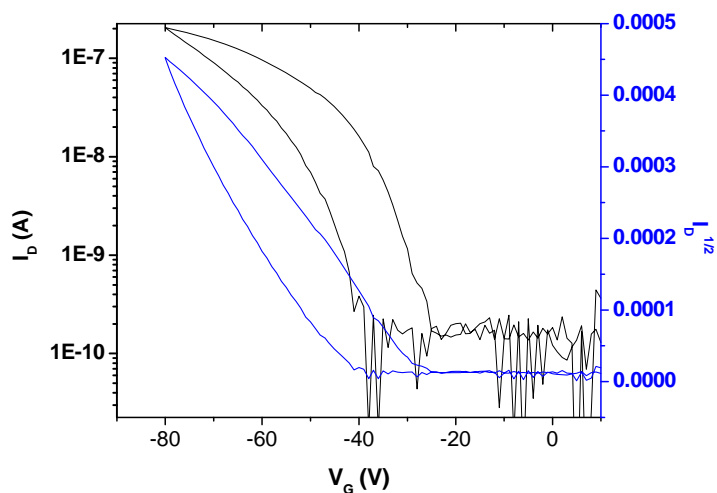


**Figure 3.18 Transfer Characteristics for an OTFT made using TMTIPS-pentacene.**

However, under the same conditions, the results obtained for TMTES-pentacene were superior with saturated hole mobility of  $1.3 \text{ cm}^2/\text{Vs}$  and reaching maximum mobilities of  $2.5 \text{ cm}^2/\text{Vs}$ , Figure 3.19. The range of mobilities went from  $0.6 \text{ cm}^2/\text{Vs}$  to  $2.5 \text{ cm}^2/\text{Vs}$  with a standard deviation of  $0.4 \text{ cm}^2/\text{Vs}$ . Table 3.4 summarises the results obtained for all the materials.

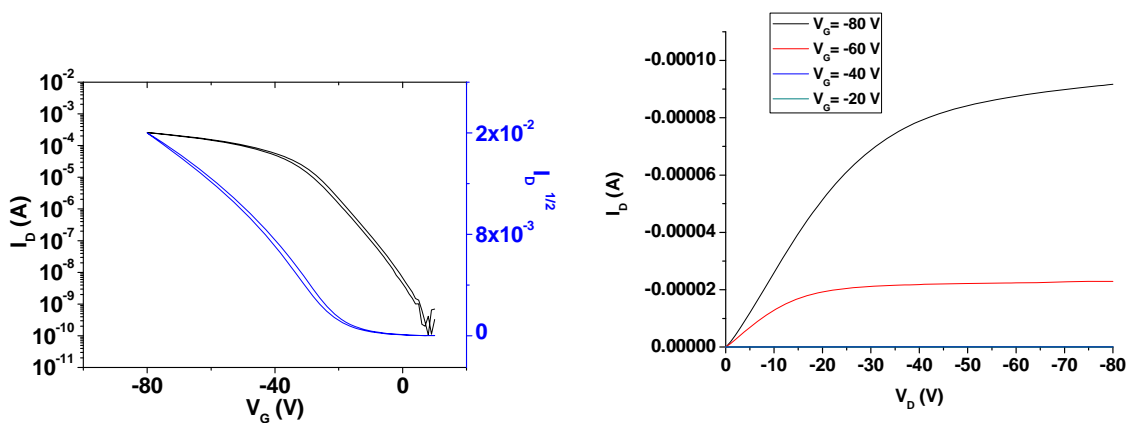


**Figure 3.19 Transfer (left hand side) and output (right hand side) characteristics for an OFET using TMTES-pentacene.**

**Table 3.4. Table compiling the OTFT result. The average mobility was calculated from the data obtained from 9 devices which were fabricated for each substrate.**

	Average $\mu$	$\mu_{\max}$	On/off ratio	$V_{\text{TH}}$	Standard deviation
TIPS-pentacene	$3.7 \times 10^{-3} \text{ cm}^2/\text{Vs}$	$5 \times 10^{-3} \text{ cm}^2/\text{Vs}$	$10^6$	-1 V	$0.6 \times 10^{-3} \text{ cm}^2/\text{Vs}$
TMTIPS-pentacene	$1 \times 10^{-4} \text{ cm}^2/\text{Vs}$	$4 \times 10^{-4} \text{ cm}^2/\text{Vs}$	$10^3$	-23 V	$1.3 \times 10^{-4} \text{ cm}^2/\text{Vs}$
TMTES-pentacene	$1.3 \text{ cm}^2/\text{Vs}$	$2.5 \text{ cm}^2/\text{Vs}$	$10^7$	-10 V	$0.4 \text{ cm}^2/\text{Vs}$

Apart from the large increase in the mobility, there are some details that can be commented by looking at the graphs. The hysteresis observed in the transfer characteristic for TIPS-pentacene and TMTIPS-pentacene almost disappears in the TMTES-pentacene characteristics. We believe that this is due to the nature of the crystal. The closer packing of the TMTES-pentacene molecules makes more difficult the appearance of defects. In addition, TMTES-pentacene is “OTSphilic” and it forms molecular continuous films, Figure 3.11. In contrast TIPS-pentacene and TMTIPS-pentacene do not cover the surface of the transistor substrate fully. This lack of homogeneity forms grain boundaries which have a critical effect in the mobility of carriers and in the apparition of hysteresis.

Normally hysteresis is due to grain boundaries, induced for the presence of traps principally in the interface semiconductor-dielectric or influenced by a phenomenon of oxygen doping inherent of the semiconducting material<sup>[85]</sup>. It has been reported that the crystal size of TIPS-pentacene together with the concentration of grain boundaries in the channel of the thin film transistors have a massive influence in the apparition of hysteresis in the transfer characteristics<sup>[86]</sup>. Using deposition method that promotes the increase of the crystal size in organic semiconducting thin films

might improve the performance of these materials in organic electronic applications.

The output characteristics, Figure 3.18, showed, as predicted from the calculations of the molecular orbital levels, ohmic contacts between the material and the gold electrodes. At high  $V_G$  the output exhibit full saturation. When gate was unbiased no residual offset current was recorded (it was minor than 0.1nA and can be consider as negligible). This is an indicative of the high purity of the materials and the absence of leaks.

### **3.8 Summary and Conclusions**

To conclude, we have shown that 1,4,8,11-tetramethyl-6,13-triethylsilylethynyl pentacene (**4**) can make excellent OFETs, with high mobilities and on/off ratios when solution processed in air with improved device to device reproducibility as a consequence of the extended  $\pi$ - $\pi$  overlap and closer packing. With optimization of formulation and device architecture it is believed that this new family of compounds will enable all solution processed devices with high performance and excellent reproducibility to be fabricated.

## **4 Physical and electronic characterization of low molar mass semiconductor-insulator blends**

This chapter combines results already published, with summary comments on how the state of the art has developed since completion of the experimental part of this thesis.

Organic field effect transistors from ambient solution processed low molar mass semiconductor-insulator blends<sup>[87]</sup>. Madec, Marie-Beatrice; Crouch, David; Rincon Llorente, Gonzalo; Whittle, Tracie J.; Geoghegan, Mark; Yeates, Stephen George. *Journal of Materials Chemistry* (2008), 18(27), 3230-3236.

A New family of High Mobility Solution Processable Polyacenes<sup>[88]</sup>. Rincon-LLOrente, Gonzalo; Madec, Marie Beatrice, Crouch, David; Pritchard, Robin; Yeates, Stephen; *Mater. Res. Soc. Symp. Proc. Vol. Date 2009*, 1114E (Organic and Hybrid Materials for Large-Area Functional Systems), No pp. given, Paper #: 1114-G06-05.

Organic Semiconductor-Polymer Insulator Blends: a Morphological Study of the Guest-Host Interactions<sup>[89]</sup>. Marie-Beatrice Madec,, David J. Crouch, Gonzalo Rincon-Llorente, Tracey Whittle, Mark Geoghegan, Stephen G. Yeates, e-J. *Surf. Sci. Nanotech.* (2009). Vol. 7.

## 4.1 Introduction

Organic electronic devices can exhibit impressive levels of performance. For example hole carrier mobilities ( $\mu_{\text{FET}}$ ) for vacuum deposited pentacene of  $5 \text{ cm}^2/\text{Vs}$  have been reported<sup>[90]</sup>, whilst for single crystal pentacene and rubrene values of  $7 \text{ cm}^2/\text{Vs}$  and  $15 \text{ cm}^2/\text{Vs}$  have been observed<sup>[44],[46]</sup>. However it is unclear whether vacuum evaporation will offer sufficient technological and commercial advantages whilst the growth and manipulation of molecular crystals does not offer a low cost facile manufacturing process<sup>[91]</sup>. There has been significant recent progress in the development of solution processable polycrystalline oligomeric and polymeric semiconductors but it remains a challenge to combine the generally good processing characteristics with the high crystalline order required to obtain high values of  $\mu_{\text{FET}}$ <sup>[81]</sup>. Whilst localized high

crystalline order in thin films has been demonstrated extending this across large areas and a large number of different discrete devices is still problematic.

Recent studies focusing on solution blending of organic semiconductors with organic insulating polymers such as polystyrene have been reported. These polymers were chosen for their low permittivity dielectric constant ( $\epsilon$ ) which limits the reduction in  $\mu_{\text{FET}}$  arising from dipolar disorder<sup>[92],[15, 93]</sup>. The advantages of such an approach are seen as improved formulation latitude for printing, improved cost effectiveness and greater control over morphology of the organic semiconductor active layer. Initial studies on amorphous poly(triarylamine)s (PTAA) blended with polystyrene gave OFETs having retained mobility even down to 50 wt-% of PTAA with reduced device hysteresis<sup>[93]</sup>.

More recently hypereutectic blends of rubrene with ultra high molecular weight amorphous polystyrene and a glass inducing phenyl-substituted oligoacene have been reported<sup>[94]</sup>. When cast from solution the blends are amorphous but when annealed at temperatures  $>180^{\circ}\text{C}$  controlled crystallization of rubrene occurs with mobilities of  $0.7\text{ cm}^2/\text{Vs}$  and On/Off ratios  $\geq 10^6$  being obtained. Additionally, when regioregular poly(3-hexylthiophene) (P3HT) is blended with amorphous polystyrene and cast and dried at  $125^{\circ}\text{C}$  it shows good mobility down to 50 wt-% P3HT<sup>[95]</sup>. However when semi-crystalline polystyrene and high density polyethylene (HDPE) are used mobility is retained down to 10 wt-% and 1 wt-% P3HT respectively when cast and dried at  $125^{\circ}\text{C}$ . The use of crystalline-crystalline semiconducting-insulator blends is therefore a useful strategy for yielding higher performing cost effective materials with improved environmental and mechanical properties.

Here we investigate the blending of two component blends comprising semicrystalline TIPS-pentacene<sup>[94],[50],[54],[31],[75]</sup> and selected amorphous and semi-crystalline side chain aromatic low permittivity dielectric materials.

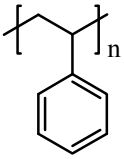
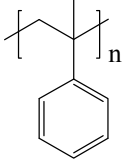
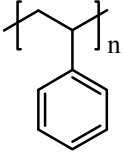
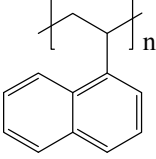


## 4.2 Blends containing TIPS-pentacene and side-chain aromatic polymers

### 4.2.1 Materials

Selected amorphous and semi-crystalline side chain aromatic polymers, Table 4.1, were chosen because they are low permittivity dielectric materials and are soluble in the same range of solvents as TIPS-pentacene, Table 4.2.

**Table 4.1 Structure of side-chain aromatic polymers used in this study.**

Amorphous polymers	Polystyrene (PS) 	Poly- $\alpha$ -methylstyrene (PAMS) 
Semicrystalline polymers	Isotactic Polystyrene (iPS) 	Isotactic Poly(1-vinyl naphthalene) (iPVN) 

**Table 4.2 Physical properties of low permittivity insulator polymer binders.**

Polymeric Binder	Crystalline Structure	$M_n$ (g/mol)	$T_g$ ( $^{\circ}\text{C}$ )	$T_m$ ( $^{\circ}\text{C}$ )	$\epsilon$ at 1 KHz (low frequency permittivity)
PS	Amorphous	350000	100	-	2.5
PAMS	Amorphous	1300	74	-	2.6
iPS	Semicrystalline	400000	100	212	2.6
iPVN	Semicrystalline	100000	162	360	2.6

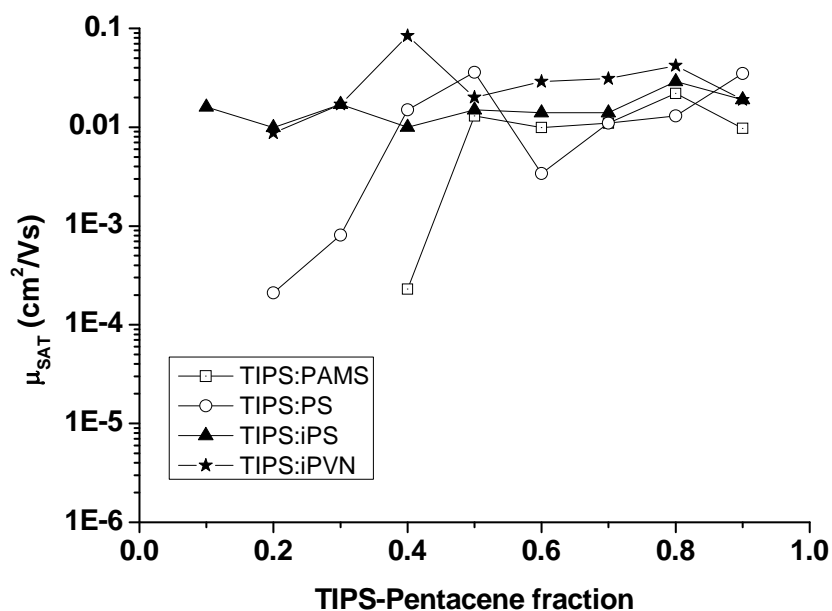
1,2,3,4-Tetrahydronaphtalene (tetralin) was chosen for the study as solubility studies show it to be a good solvent for all components and its high boiling point (210 °C) make it suitable for future micro-deposition studies.

#### **4.2.2 Solution processing**

TIPS-pentacene–insulator solution blends were prepared as follows. Stock solutions (1% w/w in tetralin) of TIPS-pentacene and polymer binder were prepared. TIPS-pentacene stock solution was filtered using a 0.45  $\mu\text{m}$  PTFE filter. Polymer binder solutions were left unfiltered. Blends were prepared fresh prior to device fabrication. The total mass content was kept constant at 1% w/w, with the weight fraction of TIPS-pentacene being varied from 0.1 to 0.9.

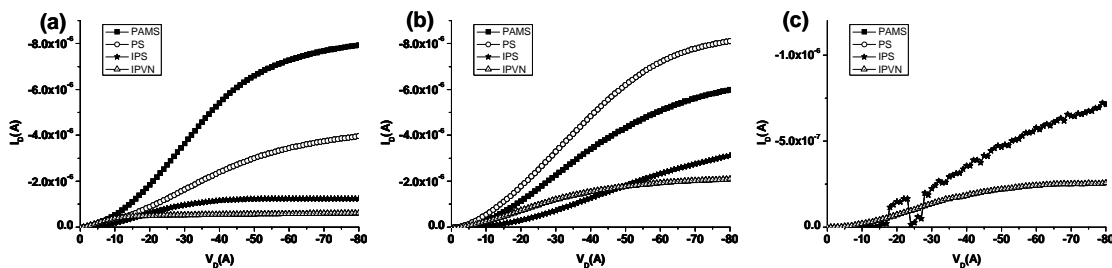
#### **4.2.3 OFET performance of TIPS-pentacene–insulator blends.**

Figure 4.1 shows the evolution of the saturated hole mobility with increasing weight fraction of TIPS-pentacene in each of the polymeric binders. We observe that for all blends having a TIPS-pentacene weight fraction  $\geq 0.5$  the saturated hole mobility is  $\geq 0.01 \text{ cm}^2/\text{Vs}$  and  $I_{\text{on}}/I_{\text{off}} > 10^4$  compared with  $\sim 10^{-3} \text{ cm}^2/\text{Vs}$  for pure TIPS-pentacene under the same conditions. At weight fractions  $< 0.5$  TIPS-pentacene the saturated hole mobility and  $I_{\text{on}}/I_{\text{off}}$  are strongly dependent upon the nature of the polymeric binder falling off rapidly when it is amorphous,  $< 10^{-6} \text{ cm}^2/\text{Vs}$  at 0.2 in PAMS, but being retained at weight fraction of TIPS-pentacene  $\leq 0.2$  when it is crystalline.



**Figure 4.1** Maximum saturated hole mobility of TIPS-Pentacene–insulator blends as a function of weight fraction of TIPS-pentacene for PAMS, PS, iPS and iPVN.

From the output characteristics in Figure 4.2, we observe that the drain current saturates completely only when semi-crystalline binders, iPS and iPVN, are used. However, the FET current density for comparable applied voltages is much smaller than when the binder is amorphous.



**Figure 4.2** Output characteristics in the saturated regime ( $V_G = -80V$ ) for TIPS-pentacene–insulator blends at (a) 0.8, (b) 0.5 and (c) 0.2 weight fraction TIPS-pentacene.

All devices show differing levels of anticlockwise hysteresis in the  $I_d/V_g$  curves which is reproducible upon cycling of the device, Figure 4.3.

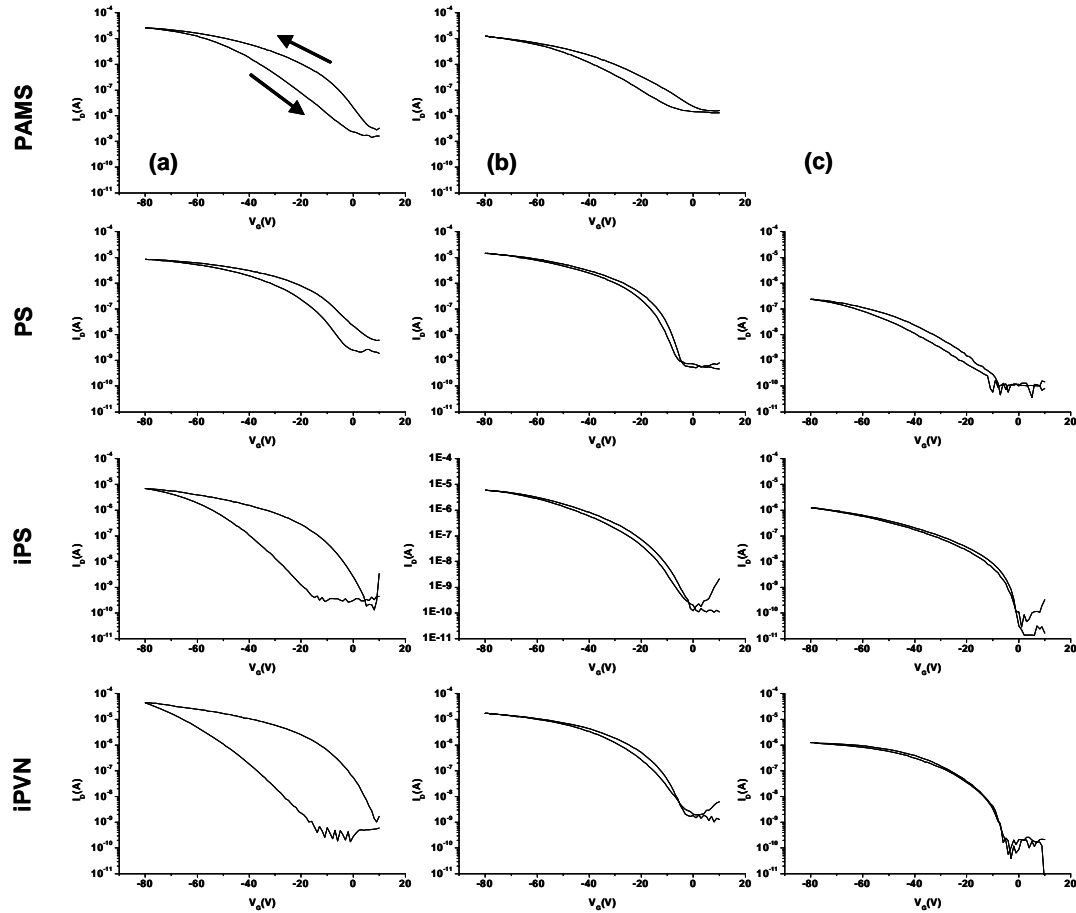


**Figure 4.3** Transfer characteristics in the saturated regime ( $V_{sd} = -80V$ ) for TIPS-pentacene–insulator blends at (a) 0.8, (b) 0.5 and (c) 0.2 weight fraction TIPS-pentacene.

The observation of hysteresis in organic devices can arise for many reasons amongst which are high energy trap states at the dielectric interface<sup>[96]</sup>, inherent semiconductor doping and dynamic processes of trapping de-trapping of the injected charges<sup>[97]</sup>, or the presence of grain boundaries. Mechanisms involving slow polarization of the dielectric and charge injection within it by the gate can be eliminated as this gives rise to clockwise hysteresis<sup>[85]</sup>. Therefore we have a phenomenon which maybe attributed to

intrinsic dynamic doping of the TIPS-pentacene. Upon decreasing the weight fraction of TIPS-pentacene hysteresis is found to reduce in all binders, with the lowest concentration of TIPS-pentacene in iPS showing a characteristic which virtually hysteresis-free. To improve further interfacial energy states, an OTS self assembled monolayer (SAM) covalently bonded to the silica surface was used. More than the topographical smoothing effect, OTS SAM is well known to create a uniformly oriented dipole moment at the interface with the dielectric<sup>[98]</sup>. Whilst this monolayer can shift the threshold voltage of the device<sup>[99]</sup>, it does not reduce either the on/off voltage or the sub-threshold slope, which are characteristic of the inherent quality of the organic semiconductor.

By using blends based upon low  $\epsilon$  dielectric polymer binders the detrimental effect of the additional interfaces created within the active layer can be offset<sup>[15]</sup>. With other factors being equal (air moisture, substrate quality, adhesion of semi-conducting film to the OTS treated substrate) we propose that the gradual disappearance of the hysteresis in the case of TIPS-pentacene - crystalline blends is due to the improved crystallisation of TIPS-pentacene at the OTS interface as previously reported for P3HT<sup>[95]</sup>

#### **4.2.4 Morphology of TIPS-pentacene–insulator blends.**

Since we are unable to monitor the kinetics of the drop cast process in detail, information on the film formation and morphology development processes have to be inferred from the finally observed non-equilibrium structures. Hence our analysis of film morphology is restricted to the “frozen-in” phase structure after drop cast coating.

The evolution of morphology within TIPS-pentacene–insulator blends as a function of TIPS-pentacene is different for amorphous and semi-crystalline polymer binders. Scanning force microscopy (SFM) contact mode images of the top surface for TIPS-pentacene-PAMS and TIPS-pentacene-iPS illustrate this behaviour as shown in Figure 4.4.

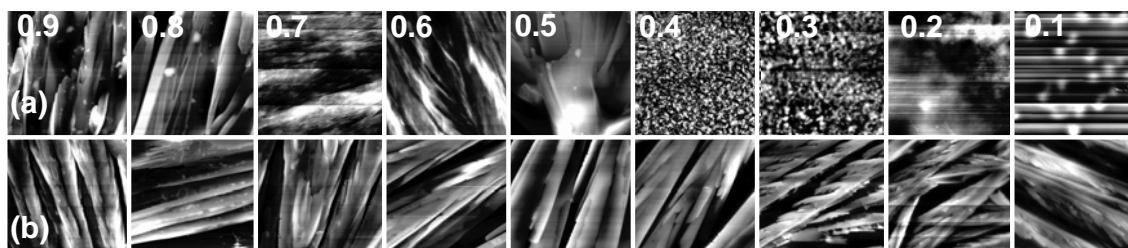


**Figure 4.4 Evolution of film morphology in thin films of TIPS-pentacene blended with (a) PAMS and (b) iPS as a function of TIPS-pentacene weight fraction (SFM contact mode, 20x20 $\mu\text{m}$ ).**

A general qualitative observation from contact mode SFM in Figure 4.4a is that upon dilution with amorphous binder the crystalline structure of TIPS-pentacene is progressively disrupted, with the crystals losing definition and showing smoother edges. The loss of TIPS-pentacene crystalline structure is confirmed by the loss in XRD peak intensity as shown in Figure 4.5.

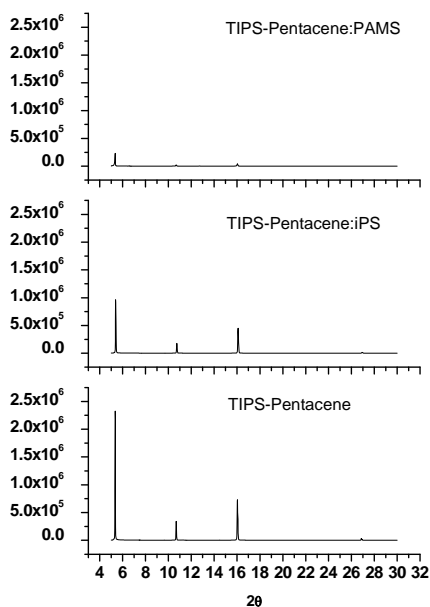


**Figure 4.5 X-Ray Diffraction patterns (from top to bottom) of TIPS-pentacene–PAMS, TIPS-pentacene–iPS and TIPS-pentacene. Blends were containing 0.8 weight fraction of TIPS-pentacene**

For fractions of TIPS-pentacene  $< 0.5$  the long lamellar structure disappears giving rise to crystalline islands of TIPS-pentacene dispersed in amorphous binder, consistent with very low saturated hole mobility. In the case of crystalline binder, Figure 4.4b and Figure 4.5, the crystalline structure of TIPS-pentacene remains essentially unchanged even at high weight fraction of binder. We notice that for low TIPS-pentacene fraction, the crystal is highly branched indicative of slow growth. The electrical consequence of the absence of complete phase segregation between the organic semiconductor and the insulator host can be compared to the damaging effect of dislocations within the organic crystal<sup>[99]</sup>. Each imperfection in the crystal results in a loss of symmetry in the cell implying the generation of localized quasi stationary traps levels within the forbidden energy band. This phenomenon increases with the fraction of the host. Eventually, the concentration of traps reaches a level that can not be overcome by the maximum polarization applied to the gate. The recorded value of saturated mobility as well as the on/off ratio decrease until they are not discernable in the analyzer white noise.

Compositional mapping of the surface was performed, using Fourier transform infrared spectroscopy (FTIR) centred on the stretching band in TIPS-pentacene<sup>[54]</sup> at  $2130\text{ cm}^{-1}$  (Figure 4.6). The films used for this study were prepared by drop casting the blend solutions on OTS treated silicon oxide substrates. Bottom surfaces were obtained by removing the dried films from the OTS treated wafer using double sided adhesive tape. When mixed with PAMS, we observe crystalline TIPS-pentacene both segregated towards the air interface and dispersed within the bulk film with no evidence of segregation towards the active interface of the device. When mixed with amorphous polystyrene the crystalline TIPS-pentacene morphology is consistent with a simple blend, and the concentration at both interfaces being consistent with the volume fraction of TIPS-pentacene present. When mixed with crystalline binder the crystalline structure of TIPS-pentacene is still observed even at high dilution and is clearly present at both interfaces.

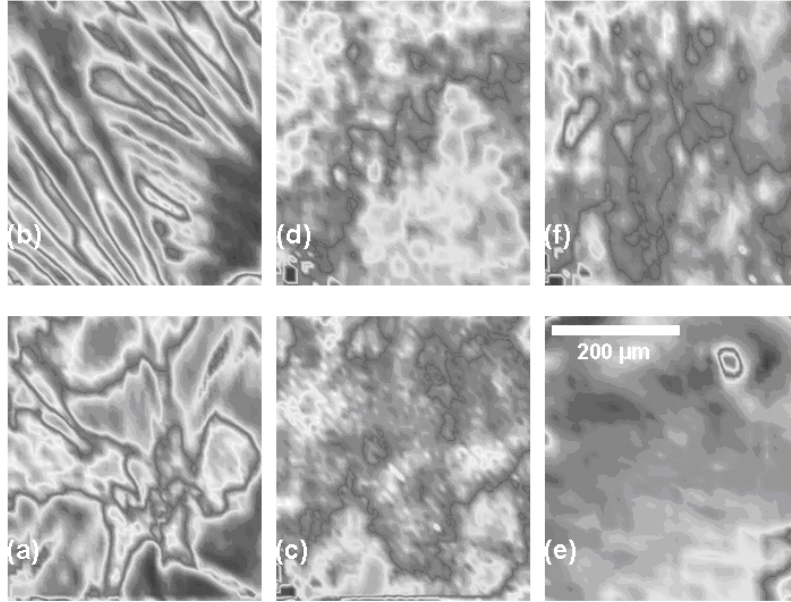


**Figure 4.6 Infrared spectroscopic imaging of TIPS-pentacene–insulator blends at TIPS-pentacene weight fraction = 0.1: (a) TIPS:iPS bottom surface, (b) TIPS:iPS top interface, (c) TIPS:PS bottom surface, (d) TIPS:PS top interface, (e) TIPS:PAMS bottom surface, (f) TIPS:PAMS top interface. The absorbance image is focused on the stretch peak at  $2130\text{cm}^{-1}$  band consequently the contrast in the images represent the areas where TIPS-pentacene is present.**

The effect of selective solvent etching of TIPS-pentacene with hexane<sup>[100]</sup> from the dried films was followed using contact mode SFM (Figure 4.7). Although not exactly on the same spot, average roughness data were obtained from the SFM image software (Table 4.3, Figure 4.8). When blended with amorphous binder we observe the crystalline structure of TIPS-pentacene at high weight fraction and the polarized light micrograph shows that the orientation within the crystal is twisted, indicative of dislocation<sup>[101]</sup>.



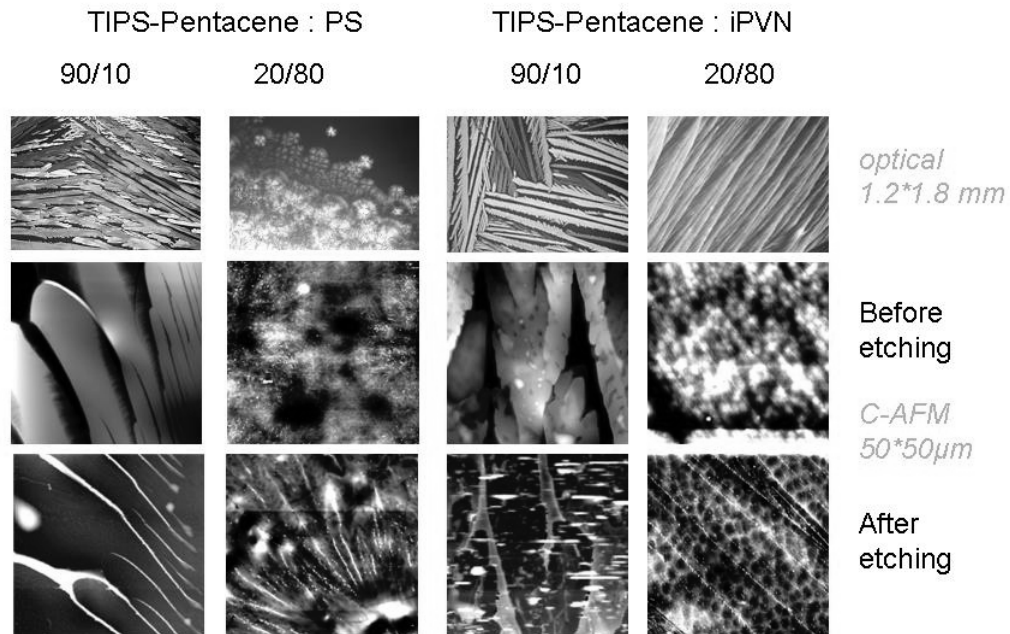


**Figure 4.7** Optical images before etching and AFM topographic images of TIPS-pentacene–insulator blends for 0.9 and 0.2 weight fraction TIPS-pentacene before and after solvent etching. The contrast in the images represent crystals of TIPS-pentacene.

**Table 4.3** Average surface roughness from AFM of TIPS-pentacene–insulator blends before and after selective solvent etching.

Binder	TIPS-pentacene weight fraction	Average roughness (nm)	
		Before etching	After etching
PS	0.2	2	20
PS	0.9	80	80
iPVN	0.2	3	5
iPVN	0.9	120	120

At high dilution we observe crystalline islands of TIPS-pentacene. Upon solvent etching, all TIPS-pentacene is removed and the underlying topography is consistent with that of a non-vertically stratified blend. When blended with crystalline binder we

observe that the crystalline structure of TIPS-pentacene persists down to 0.1 weight fraction, with polarized light micrographs showing few defects. Upon solvent etching the image is consistent with removal of a TIPS-pentacene surface layer with residual spikes of crystalline binder protruding from the surface.

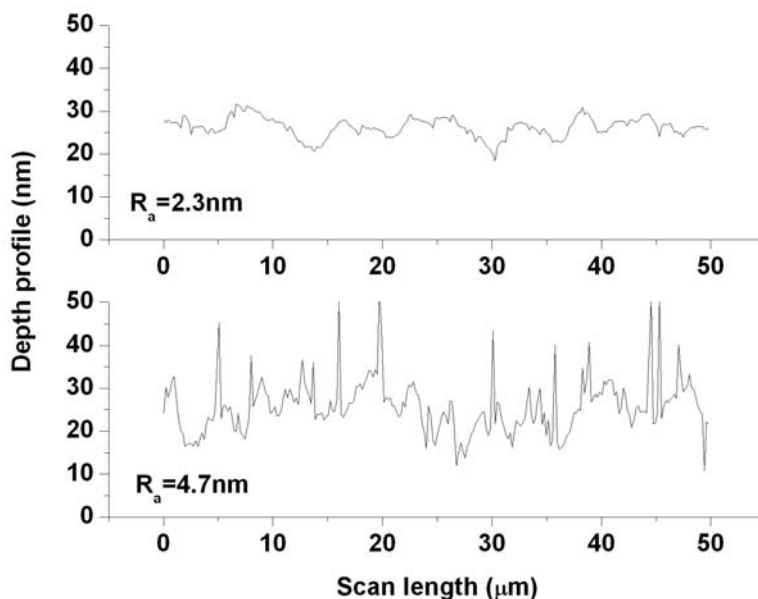


**Figure 4.8** Line profile of TIPS-pentacene-iPVN (0.2 weight fraction TIPS-pentacene) before (top) and after (bottom) selective chemical etching.

X-ray photoelectron spectroscopy is a surface analysis technique used to determine the compositional analysis of surfaces. By irradiating a material with x-rays and studying the ionisation and the kinetic energy of the emitted electrons it is possible to know the composition of a surface.

The XPS experiments in this thesis were carried out at The University of Sheffield and they were carried out by Tracie J. Whittle and Mark Geoghegan. Samples were prepared as previously describe, by drop casting on OTS treated silicon oxide substrates, and they were degassed overnight in a vacuum oven prior analysis.

In the XPS data, the presence of shake-up satellites on the high binding energy side of the main core level corresponds to the competitive phenomenon of the ejection of a

photoelectron and promotion of an occupied – unoccupied ( $\pi$ - $\pi^*$ ) transition within an isolated benzene ring or other localised conjugated part of the molecule<sup>[102]</sup>. We focused our observation on the high resolution C1s spectra in the shake-up region as shown in Figure 4.9. The area of the shake-up satellite can reach up to 10% of the general C1s peak and for PAMS, PS and iPS is observed at binding energies of 291.5eV and 295.5 eV<sup>[103]</sup>. The intensity of the shake-up satellite for the binder is independent of whether it is amorphous or crystalline. When blended with TIPS-pentacene the carbon shake-up satellite of the amorphous binder disappears indicating that the conjugation length has increased significantly. We ascribe this to evidence of TIPS-pentacene–binder interaction within the solid film. When blended with TIPS-pentacene the carbon shake-up satellite of the crystalline binder is not affected indicating no interaction between the two.

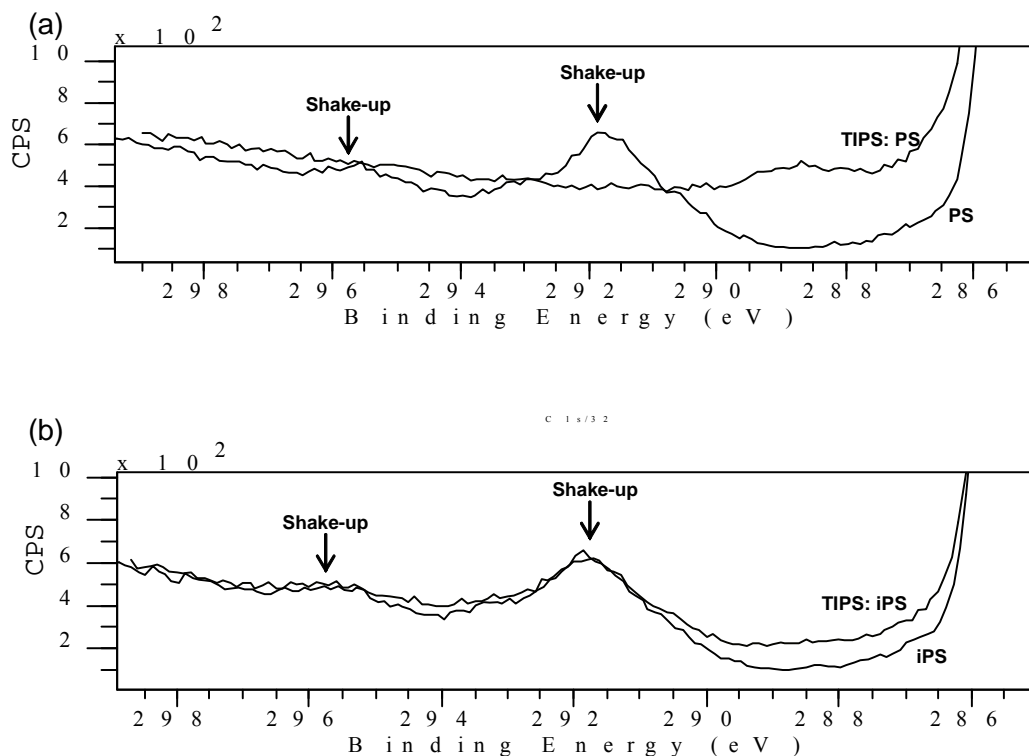


**Figure 4.9 Comparison of high resolution XPS C1s spectra for TIPS-pentacene–insulator blend for 0.5 weight fraction TIPS-pentacene (a) PS and (b) iPS.**

The electronic performance of TIPS-pentacene–insulator binder blends is highly dependent upon the crystalline morphology of TIPS-pentacene within the film. The development of morphology within the film is the result of a ‘double-percolation’-like mechanism where liquid-liquid phase separation at the early stages of drying is followed by segregation within the solidifying film caused by crystallization of one or both of the components<sup>[104]</sup>.

In the case of amorphous binder there is evidence for strong interaction between TIPS-pentacene and binder in the solidified film arising from the drying process. In the early stages of film drying liquid-liquid phase separation of amorphous low molecular weight PAMS and TIPS-pentacene is not as strong on simple entropic grounds as when a polymeric binder is used. Consequently the crystallization of TIPS-pentacene is strongly influenced by PAMS and the morphology is consistent with a simple blend. At decreasing TIPS-pentacene weight fractions down to 0.5 we observe increasingly dislocated large crystals. Below 50 wt-% TIPS-pentacene, these appear as dispersed small crystallites within a continuous PAMS matrix. Due to the strong interaction between TIPS-pentacene and PAMS we see no evidence of segregation towards the active interface. When amorphous high molecular weight PS is used the driving force for liquid-liquid phase separation is greater but again there is no evidence of phase separation at the active interface. Since there is no stratification towards the active interface saturated hole mobility falls away rapidly below 50 wt-% TIPS-pentacene.

In the case of high molecular weight crystalline binders such as iPS and iPVN we observe stratification to both interfaces of crystalline TIPS-pentacene even down to low weight fraction of active material. We believe this stratification is a consequence of TIPS-pentacene crystallizing first from solution with segregation being driven by enthalpic interactions arising from subsequent binder crystallization<sup>[94]</sup>. Stratification of TIPS-pentacene to the active interface gives rise to retention of saturated hole mobility even down to 10 wt-%. Due to the small observable crystal size we have a higher density of grain boundaries with selective solvent etching suggesting the presence of crystalline binder at some of these, and are the probable cause of the low current

density. These grain boundaries give rise to low current density observed in the output characteristics acting as deep charge trapping levels giving rise to extra resistive effects.

### 4.3 Blends containing TMTES-pentacene and i-polyvinyl naphthalene

The study was also extended to look at the effect of blending TMTES-pentacene with isotactic poly1-vinylnaphthalene (iPVN) at 1 wt-% total solids in tetralin and drop casting from solution at RT on OTS treated SiO<sub>2</sub> wafers, Figure 4.10.

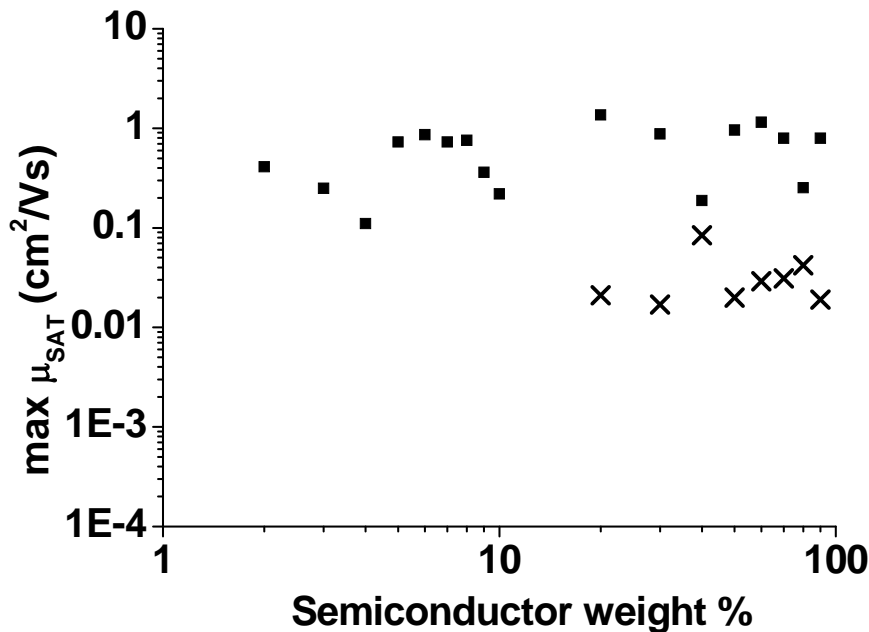


**Figure 4.10** Maximum saturated hole mobility as a function of the weight concentration of compound TMTES-pentacene (■) and TIPS-pentacene (×) when blended with iPVN drop cast on OTS from tetralin solution at RT.

Comparing with TIPS-pentacene we see that TMTES-pentacene retains its high mobility even when blended at < 10 weight-%. Powder diffraction XRD on films of TMTES-pentacene blended with iPVN when drop cast on OTS treated glass from tetralin solution clearly show retention of the (001) peak of TMTES-pentacene down to a

concentration 1 wt-%, Figure 4.11. Down to 10wt-% of TMTES-pentacene in the blend we see no reduction in (001) peak intensity below which we see a steady fall off.

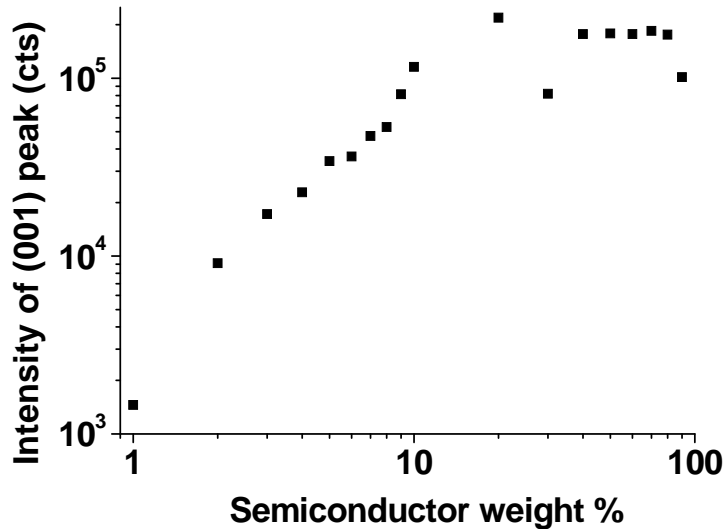


**Figure 4.11 Evolution of the (001) peak intensity of the powder diffraction XRD pattern of TMTES-pentacene as a function of weight concentration when blended with isotactic iPVN drop cast on OTS treated glass from tetralin solution at RT.**

## 4.4 Conclusions

Two component blending of semicrystalline TIPS-pentacene and TMTES-pentacene with selected amorphous and semi-crystalline low permittivity insulating binders at room temperature under vacuum from a good solvent has been studied. Characterisation of the intensity of the shake-up satellites in XPS for PS and iPS in the two component blends has proved an exceptionally powerful tool in determining thin film morphology. When amorphous insulating binders are used there is strong evidence of interaction between binder and active material. This gives rise to twisted TIPS-pentacene crystals with dislocations but there is no evidence of its stratification towards the active interface. Hence we observe high offset current at high drain voltage characteristic of interfacial trapping states or of a depleted region at the interface. When a crystalline

binder is used which crystallizes more slowly from solution than TIPS-pentacene or TMTES-pentacene we observe stratification of the organic semiconductor to both interfaces and retention of saturated hole mobility even down to 10 wt-%. With this approach, it should be possible to formulate low-cost organic semiconductors whose solution and solid state properties can be fine-tuned by careful binder selection without the need to design all of the necessary functionality into the one organic semiconductor molecule.

Recent literature focused in blends containing crystalline TIPS-pentacene and commodity polymers have confirmed, by means of time of flight secondary ion mass spectrometry (TOF-SIMS) combined with local cesium ion sputtering (LCIS), stratification of the semiconductor towards the film interfaces<sup>[105]</sup>. This vertical nanophase separation not only improves the crystallisation of the semiconductor in the channel region of the thin film transistor but increases the thermal stability of the device.

The segregation observed in the films formed by the blend is deeply influenced by the surface energy of the substrates. Being highly polar substrates the ones achieving better performances<sup>[106]</sup> due to the relative non polar nature of the TIPS-pentacene- polymer solution nature.

Other recent results published by Anthony describe the behaviour of TIPS-pentacene and 2,8-difluoro-5,11-bis(triethylsilylethynyl) anthradithiophene (diF-TESADT) when blended with a semiconducting polymer, poly(trialrylamine)<sup>[35, 42, 106]</sup> (PTAA). The same stratification effect was observed when PTAA was used and improved device performance was observed when compared with the insulating poly- $\alpha$ -methylstyrene.

## **5 Aggregation studies of anthracene derivatives and their interactions with single walled carbon nanotubes (SWNTs)**



## 5.1 Introduction to Single wall carbon nanotubes (SWNTs)

Since the discovery of carbon nanotubes by Iijima<sup>[107]</sup> in 1991 a great interest towards them as poly-functional materials has been awoken<sup>[108]</sup>. Two types of structures were reported, single and multi walled carbon nanotubes, each of them with their own chemical and physical properties. In the scope of this project are the electronic properties of single walled carbon nanotubes<sup>[109]</sup>. Therefore, multi walled carbon nanotubes are not discussed here.

Structurally single walled carbon nanotubes consist of a graphite sheet rolled up to form a tube. SWNTs are ~0.9-2 nm in diameter and ~1-100  $\mu\text{m}$  long. Both ends of the tube are capped with hemi-spheres of aromatic rings (fullerene like).

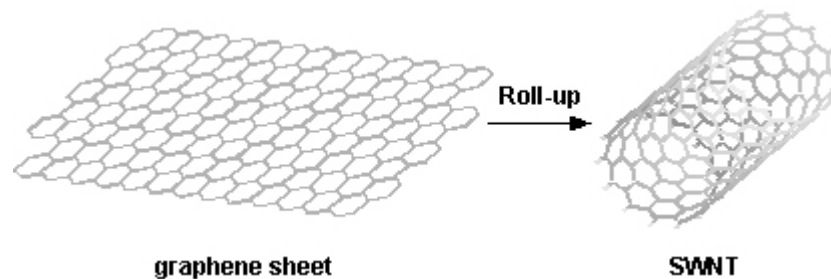


**Figure 5.1 Basic structure of single wall carbon nanotubes<sup>[110]</sup>.**

There are many ways of rolling up a graphite sheet. The chiral angle is the main parameter to differentiate them, Figure 5.2. The chiral angle,  $\theta$ , is defined as the angle of the hexagon helix around the nanotubes axis. It is related to the chiral vector that follows the equation  $C = na_1 + ma_2$ , where  $(n,m)$  are the integers. When  $n=m$  they are called armchair tubes, when  $(n,0)$  they are called zig-zag tubes. Otherwise when  $n \neq m$  they are called chiral nanotubes<sup>[111]</sup>.

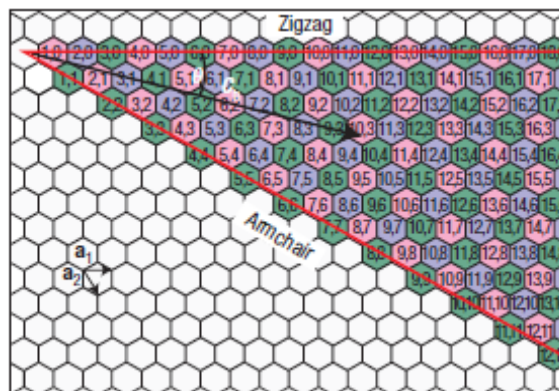


**Figure 5.2 Scheme representing chiral vector and angle<sup>[112]</sup>.**

The chiral angle is a key parameter for determining the electronic properties of the nanotube since nanotubes will be metallic or semiconducting depending on it and on the tube diameter. Armchair nanotubes are always metallic, zig-zag nanotubes can be either metallic or semiconducting depending on the diameter.

Our interest is in the electronic properties of SWNTs as a consequence only these ones will be discussed here. The problem with SWNTs is that as soon as they are synthesised they form bundles due to Van der Waal forces taking place between the aromatic rings on their structures<sup>[111]</sup>. When bundled, metallic and semiconducting nanotubes are together and it is a difficult process to separate them. In a bundle the properties of each type of nanotube are hindered by the others and the desired individual properties of single wall carbon nanotubes cannot be exploited.

The aim of this part of the thesis was to develop a method to separate semiconducting from metallic nanotubes. There have been many attempts to achieve a method capable to disperse nanotubes<sup>[113]</sup>. Some of them considered not only the dispersion in solution but the separation of nanotubes by classes. However, good separation and ease of processability for use in organic electronic devices is still a long way off. Here we present a review of important achievements towards SWNTs separation.

At the moment, there are two well differentiated chemical approaches used for the separation of nanotubes. Both of them consist in attaching chemical moieties on the

nanotube surface<sup>[114]</sup>. The first one is based in covalent functionalisations. These methods consist of covalent attachment of the molecules to the surface of the nanotube<sup>[115]</sup>. These molecules act as spacers preventing the nanotubes to bind together. The main problem with this approach is that the covalent attachment of chemical compounds to the nanotube structure disrupts the conjugation of the system and this changes their desired electronic properties.

The second approach makes use of the conjugated nature of the nanotubes and suggests separation by deposition of aromatic molecules on the surface of the nanotube by  $\pi$ - $\pi$  stacking<sup>[116]</sup>. As in previous case these molecules attached to the nanotube surface will act as spacers avoiding the bundle formation. This second method avoids the disruption of the conjugation in the nanotube surface.

This part of the thesis is focused in the electronic properties of the nanotubes. Therefore, only non-covalent dispersing methods that attend at the separation of nanotubes by electronic classes will be discussed here.

### **5.1.1 Non-covalent SWNTs functionalisation**

As previously said the non-covalent functionalisation does not affect the electronic properties of the nanotubes since the  $sp^2$  carbon structure remains unaffected. These methods are based on the deposition of polyaromatic groups around the surface of the nanotube. In literature this approach has been carried out with different kind of materials including poly nuclear aromatic compounds<sup>[116b]</sup>, biomolecules<sup>[117]</sup> and conjugated polymers<sup>[118]</sup>. Below, an introduction to the most important ones is discussed.

### 5.1.1.1 Non covalent SWNTs functionalisation using biomolecules

Different methods involving biomolecules have been reported. Single stranded Deoxyribonucleic acid (DNA) can individualize the SWNTs by  $\pi$ -stacking of the bases around the nanotube maintaining the sugar-phosphate structure to the outer side<sup>[116a, 119]</sup>, Figure 5.3. The DNA-SWNT blend can in addition be separated by different electronic structures by ion-exchange chromatography. However, the separation does not seem to be perfect as it is nanotube length and diameter dependant. Long nanotubes or with diameter larger than 1.4 nm are still an issue and remain to be separated<sup>[120]</sup>.

It has been also reported individualisation through the use of 1-pyrenebutanoic acid succinimidyl ester<sup>[117]</sup> which links the aromatic group on the surface of the tube, Figure 5.3. The succinimidyl groups can react then with other materials leaving the door opened to specific substitution.

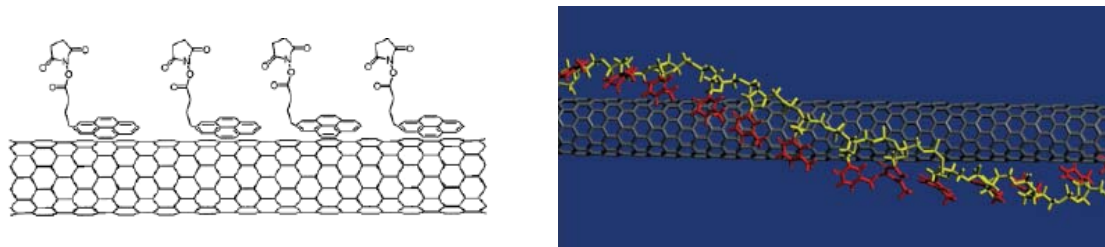


**Figure 5.3 Non covalent functionalisation using 1-pyrenebutanoic acid succinimidyl ester (left hand side) and single stranded DNA (right hand side)<sup>[116a, 117]</sup>.**

The importance of this method resides in the fact that small molecules can be attached and immobilised on the surface of the nanotubes. These small molecules could be functionalised with a large variety of chemical moieties and in this way the carbon nanotubes can be functionalised with all kind of substituents without affecting their electronic nature.

### 5.1.1.2 Non covalent SWNTs functionalisation using polymers

The presence of aromatic rings in the structure of semiconducting polymers makes them ideal candidates to disperse single wall carbon nanotubes via non covalent interactions. Many different blends containing SWNTs and semiconducting polymers have been reported<sup>[121]</sup>. Polymers such as poly((m-phenylenevinylene)-co[(2,5-dioctyloxy-p-phenylene) vinylene]) (PmPV), Figure 5.4, lead to a good dispersion of the nanotubes. Organic light emitting diodes (OLEDs) devices using blends of PmPV-SWNTs as electron transport layer have been constructed and improved brightness have been reported<sup>[121b]</sup>. STM images of the PmPV-SWNTs blend showed that the polymer wraps around the structure of individual carbon nanotubes<sup>[122]</sup> avoiding the formation of bundles.

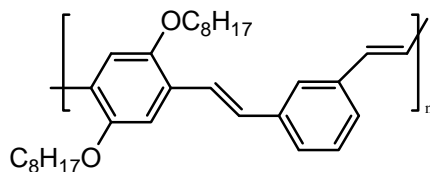


**Figure 5.4 Structure of PmPV.**

Polymers such as poly(aryleneethynylene)s (PPEs) present other distributions towards the nanotubes resting on their surface and extending the alkyl chains around the nanotube structure<sup>[123]</sup>. Addition of ionic groups at the end of the alkyl chains could yield formation of small ropes or even individual nanotubes.

Polymers have proven their ability as dispersing agents of single wall carbon nanotubes. It still remains an issue the separation and purification of nanotubes attending at their electronic behaviour. Until the full achievement of this challenge the possible applications of the nanotubes will be hindered.

### 5.1.1.3 Non covalent SWNTs functionalisation using small poly-aromatic materials

An interesting method towards the dispersion of SWNTs is that describing the interaction between SWNTs and small polyaromatic molecules (organic dyes). The structure of the small molecules will determine onto which type of SWNTs they can be absorbed. This allows selective nanotube dispersion by careful selection of the small molecules architecture. A study of the molecular orbitals interactions taking place between some small aromatic molecules and the surface of the nanotubes has been carried out<sup>[124]</sup>. This study gives an idea of which small molecules will selectively be absorb onto which nanotubes.

Theresa G. Hedderman and co-workers at the Dublin Institute of Technology<sup>[125]</sup> have been developing a detailed study focused on the nanotube dispersing abilities of two small molecules, anthracene and terphenyl. In their experiments, a range of different concentrations solutions of SWNTs with the dyes (1:1 w/w) in toluene were prepared. The interaction between SWNTs and the dyes was studied by spectroscopic methods. They observed a change in the intensity of the fluorescence of the dyes solutions after addition of the nanotubes. They propose that this change takes place due to a decrease in the concentration of dyes in solution as they get absorbed in the nanotube surface. In the case of terphenyl a red shift is also observed, it is believed to be related to an enhancement on the conjugation once the molecule becomes planar on the surface of the nanotube. These results are supported by the presence of new peaks in the Raman spectra of the blends.

Anthracene and terphenyl were chosen due to their perfect match onto the armchair and zig-zag nanotubes respectively. Taking into account that all the armchair tubes are metallic and  $\frac{2}{3}$  of the zig-zag tubes are semiconducting, a possible separation by electronic properties could be achieved, Figure 5.5.

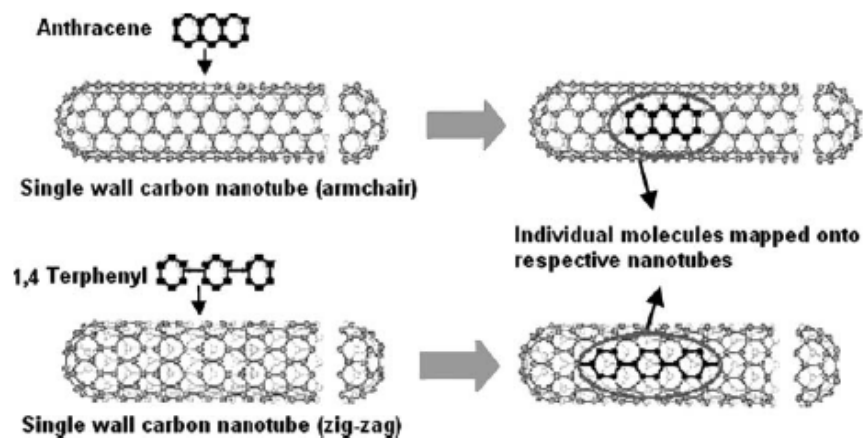


**Figure 5.5 Selective interactions of anthracene and terphenyl with armchair and zig-zag nanotubes respectively<sup>[126]</sup>.**

This method provides partially enriched suspensions of metallic or semiconducting nanotubes dispersion depending on the selected small molecule used as dispersant. The results are highly concentration dependent and in all cases only partial separation was observed.

Up to this day, a method providing solution dispersion as well as defined separation by electronic properties has not been found. In order to take advantage of all the electronic properties brought by carbon nanotubes an improved method is fundamental.

## 5.2 Single walled carbon nanotubes aims

As a precursor to understanding how substituted acenes may disperse single wall carbon nanotubes it is important to realise how they behave in solution<sup>[125]</sup> and particularly how they aggregate as a function of concentration, temperature, solvent and structure. We believe that this understanding of the aggregation process in solution is also important regarding the formation of crystals. This can be link to the crystallisation processes taking place in the channel of a thin film transistor when the materials are alone or in blends.

The aim of this part of the thesis was to study the aggregation behaviour in solution of the 9,10 disubstituted anthracene derivatives presented in Figure 5.6 and then study their possible application as single wall carbon nanotube dispersants.

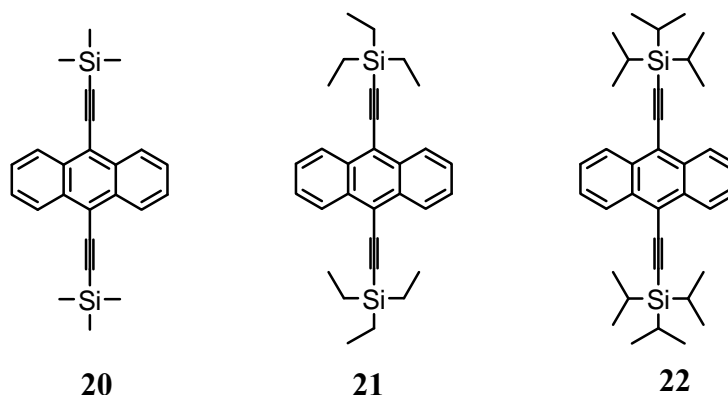


**Figure 5.6 Anthracene derivatives used for the aggregation and SWNTs dispersion studies .**

### **5.3 Aggregation studies of 9,10-disubstituted anthracene derivatives**

The dispersion of single wall carbon nanotubes was studied in accordance with the method proposed by Hedderman et al<sup>[125]</sup>. They used anthracene and terphenyl as non covalent dispersing agents. This non covalent method was chosen to avoid disruption in the electronic structures of the nanotubes, as described in the introduction section.

Fluorescence spectroscopy was the tool used to measure the interaction between the dyes and the nanotubes. In their study, they sonicated a series of mixtures at different concentrations of small dyes with carbon nanotubes. Then, they allowed the solutions to precipitate and studied the fluorescence of the supernatant liquid. Study of the fluorescence was made before and after the addition of nanotubes, since it was made to see if any difference could be observed.



As they postulated in their study, anthracene attaches selectively onto armchair nanotubes and ter-phenyl does it onto zigzag ones. It is also known that armchair nanotubes are all metallic and the 2/3 of the zigzag ones are semiconducting. Our interest is on semiconducting nanotubes and their application on thin film transistors. For that reason we have tried to disperse the metallic nanotubes and end up with a precipitate rich on semiconducting carbon nanotubes. In order to achieve that aim we have focused our study on dispersions based on anthracene and anthracene derivatives.

In order to measure the interaction between nanotubes and the small molecules a deep study of the fluorescence of the materials and the fluorescence of the materials-SWNT blend was carried out. The study of the fluorescence of the materials depending on concentration gave us information about the aggregation of the molecules in solution and the study of the fluorescence of the blends gave us information on the interaction dispersant-nanotube. A brief summary on fluorescence spectroscopy is presented here for a better understanding of the results.

### **5.3.1 Fluorescence spectroscopy**

At room temperature the molecules are in the ground electronic state. Absorption of light (energy,  $h\nu$ ) promotes some of the electrons to a higher state of energy called excited state. All of these electronic states are divided in vibrational sublevels. This can be clearly observed in a Jablonski diagram, Figure 5.7.

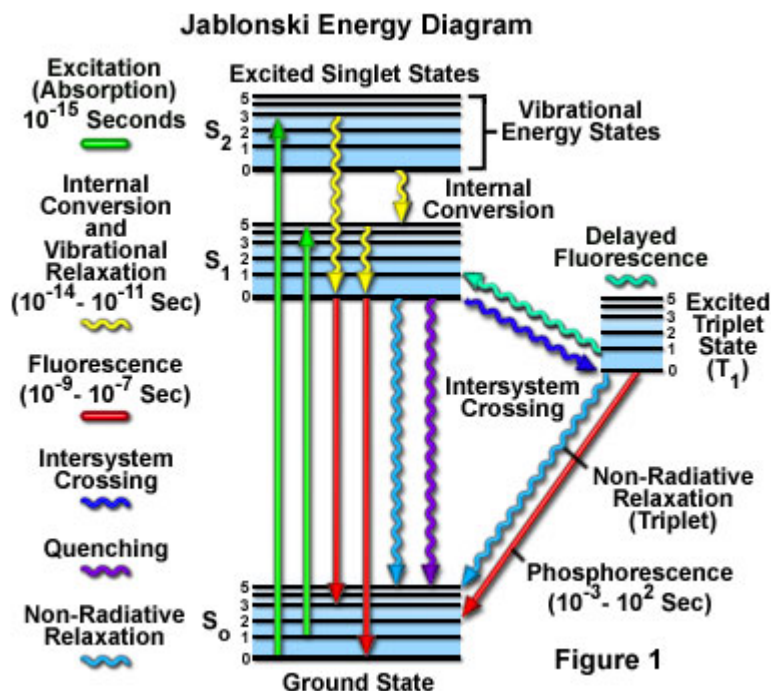


**Figure 5.7 Jablonski Diagram**<sup>[127]</sup>.

After the promotion of one of the electrons to an excited state there will be a rapid loss of the vibrational energy, known as internal conversion, taking the electron to the lowest vibrational sublevel of the excited state. At that point the electron returns to any of the vibrational sublevels of the ground state emitting energy in form of fluorescence<sup>[128]</sup>.

### 5.3.2 Aggregation studies for anthracene and its derivatives

The absorption (UV-vis) and emission (fluorescence) spectra for a  $10^{-4}$ M anthracene solution in toluene are shown in Figure 5.8. From the absorption spectra can be calculated the energy required to promote one electron from the ground state to the different excited states, Equation 5.1.

$$E = h \cdot \frac{c}{\lambda} \quad 5.1$$

Where  $E$  is the energy of the transition,  $h$  is the Planck's constant,  $c$  is the speed of light and  $\lambda$  is the wavelength. The maximums at 389, 375, and 356 nm represent the transition for one electron going to the first, second and third excited states respectively. The energy required (absorbed) to promote one electron from the lowest vibrational sublevel of the ground state to the lowest vibrational sublevel of the first excited level is equal to the energy that this electron releases in form of fluorescence when it is coming back to the lowest vibrational state of the ground state. For that reason, the peak with lowest energy in the absorption diagram corresponds with the peak of higher energy in the fluorescence diagram. Normally a small difference in wavelength is observed between those two peaks. In the case of anthracene this difference is 5 nm. When the emission peak is shifted towards higher wavelength the effect is called Stokes shift. If the emission peak is shifted towards lowers wavelength it is called anti-Stokes shift.

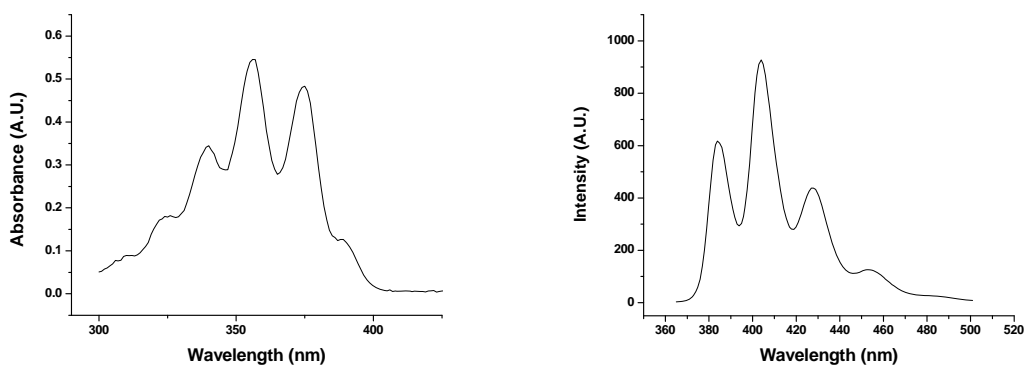


**Figure 5.8 Absorption (left hand side) and fluorescence (right hand side) spectrum of a  $10^{-4}$  M solution of anthracene in toluene.**

Fluorescence spectrum of anthracene at different concentrations, Figure 5.9.

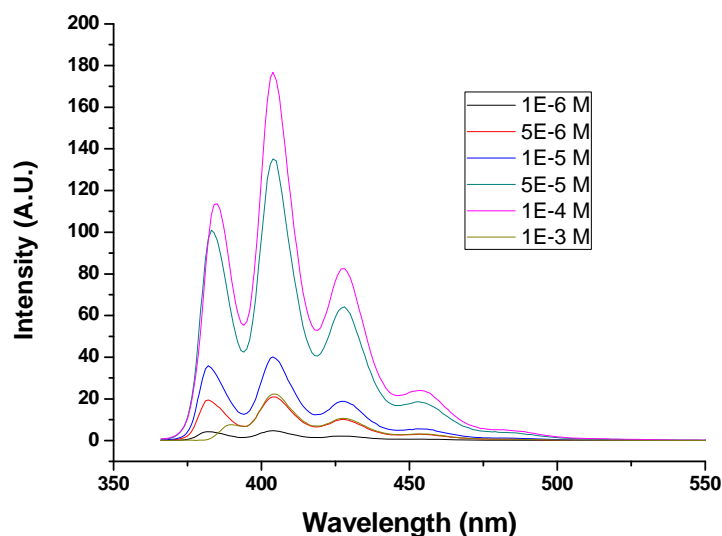


**Figure 5.9** Fluorescence intensity of anthracene at different concentrations in toluene.

The part of the molecule responsible for the fluorescence in anthracene and its derivatives is very rigid. In a rigid system there is no loss of energy due to change of configuration. That is why the absorption and emission bands are well defined and several peaks are observed in the spectra of this kind of compounds. In order to be able to plot a graph showing maximum of intensity vs. concentration we must choose one of the peaks. A shift was observed in the first peak (lower wavelength). This peak is concentration dependent. To avoid the interference of this effect and in accordance with Hedderman's papers<sup>[116b, 125]</sup>, the second peak was the one chosen for our study. Then, we plotted a graph showing the maximum intensity of the fluorescence vs. the concentration. The following common facts were observed for all the studied molecules:

- 1- Intensity of fluorescence almost zero at very low concentration.
- 2- Increase in the intensity until a maximum is reached as the concentration is increased

3- After the maximum the fluorescence decreases to zero as the concentration is increased.

The results obtained for anthracene are presented below, Figure 5.10. This curve can be understood by looking at the behaviour of the molecules in solution.

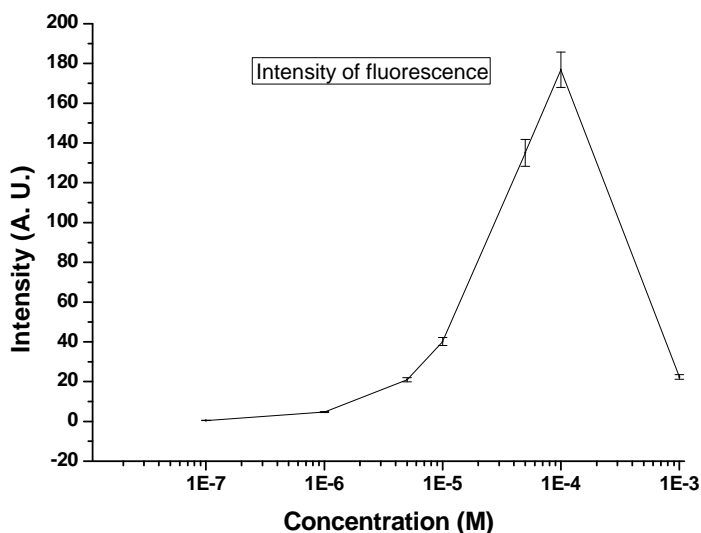


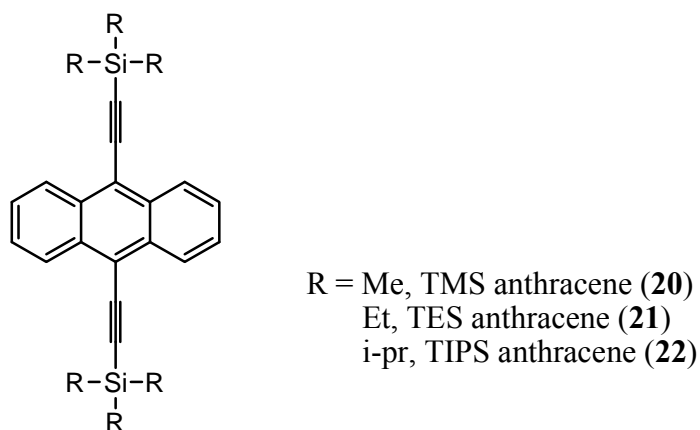
**Figure 5.10 Intensity of the fluorescence vs. concentration for anthracene.**

At low concentrations  $10^{-7}$  M -  $10^{-6}$  M there is not material enough as for the instrument to detect any fluorescence. From  $10^{-6}$  M to  $10^{-4}$  M increase in the fluorescence is observed. This fluorescence corresponds to an increase of the free molecules in solution. The increment of free molecules in solution corresponds to the increment of molecules that can experience radiative decay.

The maximum is reached at  $\sim 10^{-4}$  M. This point indicates the concentration at which the molecules begin to form aggregates<sup>[125]</sup>. Between  $10^{-4}$  M and  $10^{-3}$  M decrease of the intensity is observed. This quenching in the fluorescence can be explained as a result of the formation of aggregates of the molecules in solution. As the concentration is increased, small aggregates of material begin to form. These aggregated quench the fluorescence and there is competition between the radiative

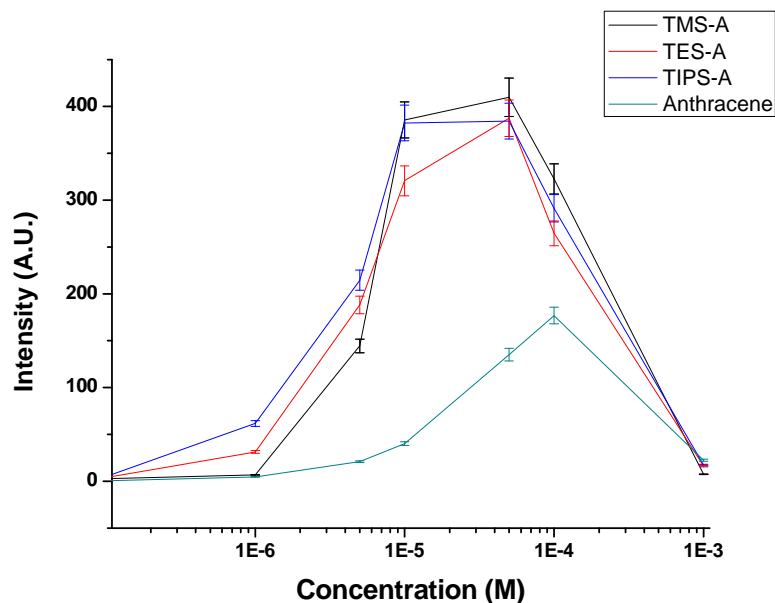
decay (fluorescence) and the non-radiative recombinations. It will be easier for the electrons to move through the orbitals of the neighbouring molecules than coming back to their ground electronic states. These electrons would induce a non radiative phenomenon that could be explained as intermolecular energy transfers<sup>[129]</sup>. At concentrations higher than  $10^{-3}$  M the fluorescence is zero. Increasing the number of molecules in the system promotes the formation of aggregates, all the emission process would be quenched by the formation of these aggregates, reducing as a result the fluorescence to zero.

The study carried out for anthracene was extended to the new 9,10-disubstituted anthracene derivatives, Figure 5.11



**Figure 5.11 Anthracene derivatives.**

The first consideration by looking at the derivatives was that the addition of solubilising groups would shift the maximum on the Figure 5.10 towards the right. In other words, if the molecules were more soluble, it could be possible to have more molecules in solution before the aggregation process takes place. However, the results obtained were quite different from that observation. The maximums for all the derivatives instead of being shifted towards the higher concentrations were shifted towards lower concentrations, Figure 5.12.



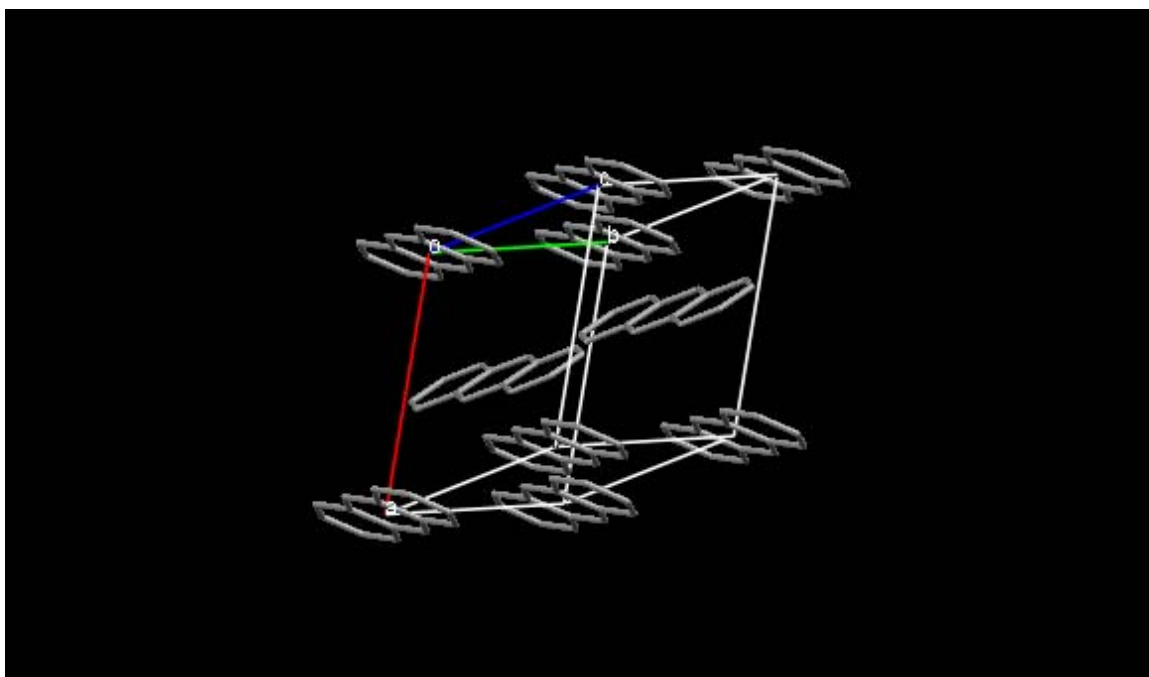
**Figure 5.12 Intensity of the fluorescence vs. concentration comparison.**

Table 5.1 shows at which concentration each material is showing the maximum fluorescence.

**Table 5.1 Concentrations at which fluorescence intensity is maximised for each anthracene derivative.**

	Concentration (M)
<b>Anthracene</b>	$\sim 1 \times 10^{-4}$ M
<b>TMS-Anthracene</b>	$\sim 5 \times 10^{-5}$ M
<b>TES-Anthracene</b>	$\sim 5 \times 10^{-5}$ M
<b>TIPS-Anthracene</b>	$\sim 5 \times 10^{-5}$ M

We believe, that this phenomena result from the fact that the formation of aggregates is favoured in the case of anthracene derivatives. The reason for this preference is not fully understood but we suggest that it could be related to the way in which the molecules pack together<sup>[130]</sup>. The crystallographic cell for anthracene shows that anthracene packs in a herringbone structure, Figure 5.13.



**Figure 5.13** Crystallographic cell for anthracene.

Whereas the crystallographic structure of the derivatives show a preferred edge to face distribution, Figure 5.14.

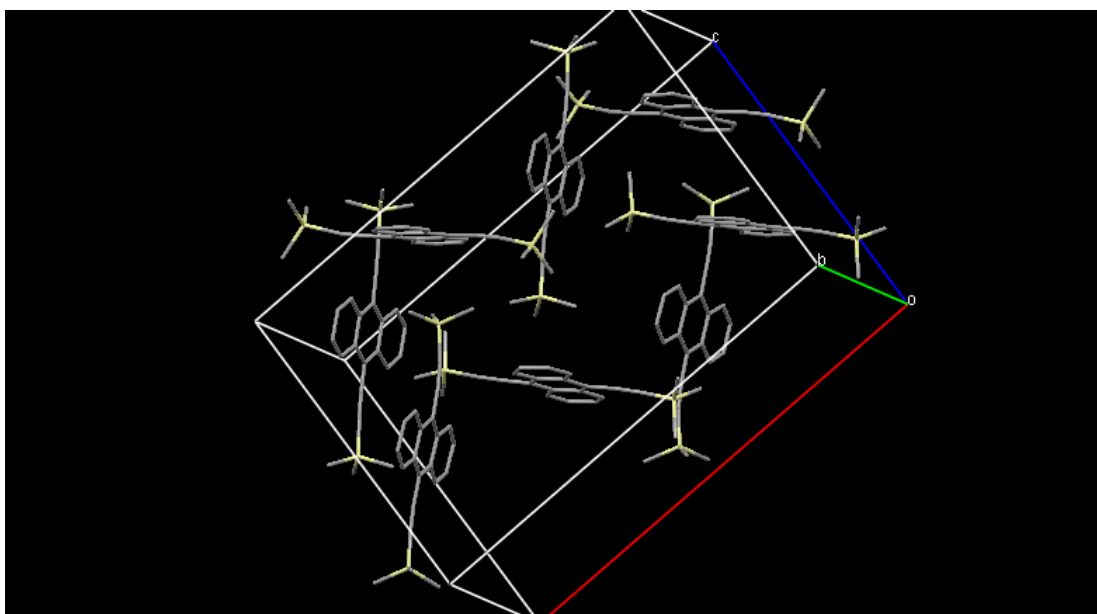


**Figure 5.14** Crystallographic structure for TMS-anthracene.



The addition of the silylethynyl groups has a dramatic influence in the packing of the molecules. It acts in the way in which the molecules form aggregates and as a consequence in the solubility of the material.

## **5.4 Dispersion of SWNTs using anthracene derivatives**

The second part of the experiment was focused on the ability of these new anthracene derivatives to disperse single walled carbon nanotubes. Previous papers<sup>[116b, 125]</sup> report a better degree of dispersions when working at concentrations below the aggregation point. In particular they claim that the best results observed for anthracene were at  $1 \times 10^{-7}$  M. The range of concentrations used for the study of the new anthracene derivatives was from  $1 \times 10^{-7}$  M to  $5 \times 10^{-5}$  M which is the aggregation limit for the new derivatives.

At this range of concentration, the higher the concentration was, the higher the intensity of the fluorescence was observed. When the nanotubes were added to the solution a quench on the fluorescence was observed. This quench can be explained as a decrease in the number of free molecules in solution. The molecules lay over the nanotubes attracted by the interaction which takes place between the  $\pi$  electrons of the aromatic cores in the dyes and the  $\pi$  electrons of the carbon nanotubes. Therefore, the electrons of the molecules attached to the nanotubes do not produce a radiative decay.

Sonication of the nanotubes was needed in order to unbundle them. Different sonication times were applied (30 seconds, 1 minute and 5 minutes) to the samples. Only after 5 minutes sonication quenching in the fluorescence was observed. 5 minutes sonication was set as the limit due to two factors. The first one was that longer sonication times could have some influence on the nanotubes (disrupt of the structure). The second one was due to the heat produced during the sonication process. High temperatures induce evaporation of the solvent and therefore change in

the concentration of the solution. The change in the concentration would show a dramatic effect in the fluorescence as expected.

The results obtained after 5 minutes sonication of the blends of anthracene and its derivatives with the single wall carbon nanotubes are plotted in Figure 5.15.

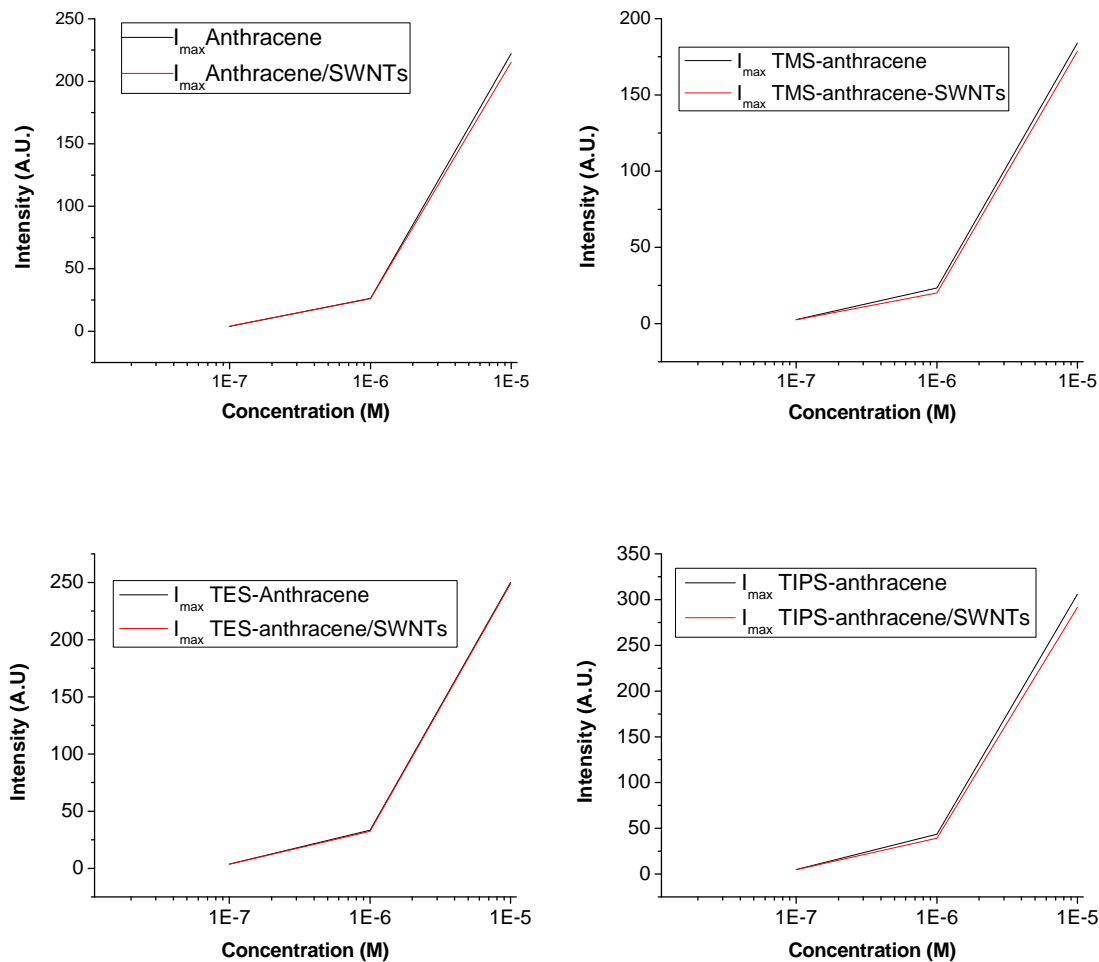


**Figure 5.15** Graphs showing the fluorescence intensity of anthracene and its derivatives at different concentrations and the intensity of the blends with SWNTs.

Quenching in the fluorescence is observed for all the different dispersants. Fluorescence spectroscopy does not provide quantitative results of how many

molecules are bond to the nanotubes. However, from the data obtained on the previous graphs it was possible to determine the percentage of the quenching and hence at which concentration is more effective each dispersing agent. The percentages were calculated for each individual point and the results were plotted in Figure 5.16.

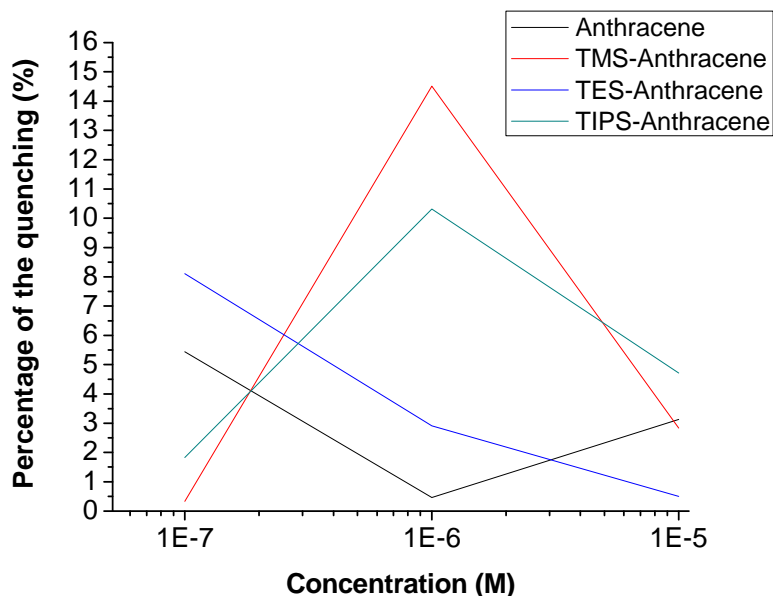


**Figure 5.16 Percentages quenching of the fluorescence intensity for each derivative at different concentrations after the addition of the nanotubes.**

From Figure 5.16 the following information can be obtained. There are derivatives which show a larger percentage of quenching in the fluorescence than anthracene and at higher concentrations. This is not sufficient information as to claim that we can achieve better dispersion of the nanotubes with the new molecules because we do not know the relative fluorescence for each individual molecule and we can not compare the results obtained for different molecules. However, this could imply two different things: the first one is that the quench of the fluorescence is larger in the new derivatives due to a larger decrease in the concentration of the molecules in solution. In this case a larger number of individual molecules have been absorbed at the surface of the SWNTs and a better dispersion could be achieved. The second possibility would be that longer quench in fluorescence is not due to a larger decrease of the

concentration of the molecules in solution but to the relative intensity of each derivative in solution. If this is the case, the amount of anthracene derivative molecules absorbed on the surface of the nanotubes could be smaller and this would lead to worst dispersion.

The discussion of the data obtained above shows clearly that the results presented here are not conclusive and further study towards the understanding of the relative fluorescence of each individual derivative is needed before a full statement of the facts studied here could be pronounced. The results in the single wall carbon nanotubes experiments of the thesis were not encouraging enough as to proceed with a full study of the samples. The quench in the fluorescence observed after the addition of the nanotubes was minimum and in all cases the values measured were within the limits of the errors in the experiments. In addition the results presented here are based only in one experiment; consequently, further study is required to measure the reproducibility and to be able to validate the results.

Towards understanding the anthracene derivative-SWNT blend further experiments are required. Raman spectroscopy is a key technique needed to understand the nanotube-dye interaction and it will also provide information about the dye selective functionalisation of nanotubes. Imaging techniques such as atomic force microscopy (AFM) or scanning tunnelling microscopy (STM) could provide information about the level of debundling of nanotubes.

In this chapter we have studied, using spectroscopic methods, the aggregation behaviour of 9,10 disubstituted anthracene derivatives in solution as a function of the concentration. A similar study should be carried out using the pentacene derivatives family as it can provide essential information in the crystallisation process which as we have seen previously in chapters 3 and 4 is fundamental for the good operation of organic electronic devices.

To conclude, a preliminary study of the ability of these anthracene derivatives as SWNTs dispersants is presented. The poor results obtained did not encourage us as to

proceed towards a full study of the samples. Consequently, in this thesis, we focused mainly in the TIPS-pentacene derivatives which provided excellent results and which are presented here as the main body of the thesis.

## 6 Experimental Chapter

## 6.1 Materials

All the reagents and solvents were obtained from Aldrich, Fluka, Fisher Scientific, Alfa Aesar and BDH laboratory reagents. They were used without further purification unless otherwise specified. Super purified HiPco single walled carbon nanotubes were obtained from Carbon Technologies Inc. Toluene (Fisher Scientific) was distilled over sodium before used. THF (Fisher Scientific) was distilled over sodium and benzophenone.

## 6.2 Synthetic characterisation techniques

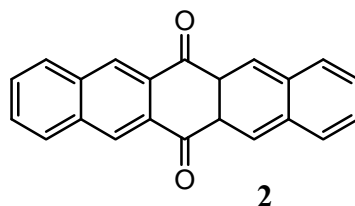
- $^1\text{H}$  NMR spectra were obtained using a Varian Bruker AMX 300 (300MHz) and a Bruker AMX 500 (500MHz) spectrometer. Chemical shifts are given on the  $\delta$ -scale in parts per million (ppm) units. Coupling constants (J) are given in Hz. The abbreviations used in the NMR splitting patterns were: singlet (s), doublet (d), triplet (t), quartet (q), double doublets (dd) and multiplet (m).
- Infrared (IR) absorption spectra were measured using an ATI Mattson Genesis series Fourier transform infrared (FTIR) spectrometer. Powder samples were prepared using a ground KBr (matrix) (1:5 sample/matrix) placed on an agate mortar and ground until homogeneity was achieved. Samples were pressed to form pellets.
- Electron Impact/Chemical Ionisation (EI /CI) mass spectrometry were carried out using a Fison VG Trio 2000 EI/CI spectrometer.
- Accurate mass measurements were obtained using a Thermo Finnigan MAT95XP spectrometer.

- Atmospheric pressure chemical ionisation (APCI) mass spectrometry and Electrospray were obtained using a Micromass Platform II
- Matrix assisted laser desorption/ionisation (MALDI-ToF) mass spectrometry were carried out using a Micromass ToF Spec 2E spectrometer.
- Elemental analysis data were obtained using a Carlo Erba Instrument EA1108 Elemental analyzer.
- Ultraviolet/Visible spectroscopies (UV/vis) were recorded using a UV-Vis-NIR Spectrometer Varian Cary 5000. Solution measurements were made using 10x10 mm quartz cuvettes.
- Fluorescence spectra were obtained using a fluorescence spectrophotometer Varian Cary Eclipse. Using the same cuvettes as above.



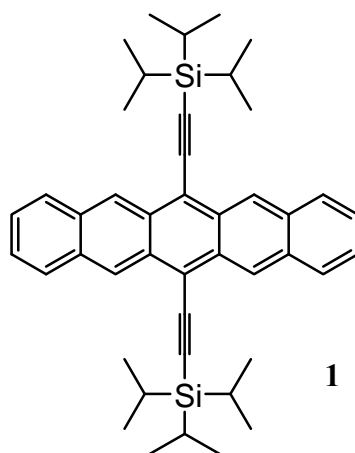
## 6.3 Synthesis

### 6.3.1 Synthesis of 6,13-pentacenequinone (2) <sup>[131]</sup>



0.58 g of phthalaldehyde (4.3 mmol) was dissolved in ethanol (EtOH) (50ml) in a 250 ml round bottomed flask. 0.25 g of 1,4-cyclohexanedione (2.2 mmol) was then added to the mixture. Upon the addition of 15% KOH solution (few millilitres), precipitate began to form immediately. The mixture was then stirred for 1 hour and then filtered to yield 0.51g (1.64 mmol, 75% yield, Mpt. 270-272 °C) of the desired product. Mass spectrum (EI/CI): 309 (100%), 252 (15%). Elemental analysis (calc.) found: C (85.70), 85.38, H (3.92) 3.79. IR( $\nu_{\max}/\text{cm}^{-1}$ ): 2921, 2928, 1676, 1652, 1600, 1450, 1446, 1394, 1309, 1213.

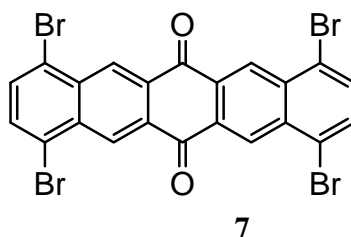
### 6.3.2 Synthesis of 6,13-bis(triisopropylsilylethynyl)pentacene (TIPS-Pentacene) (1) <sup>[60]</sup>.



Under an atmosphere of nitrogen 5.06 ml of butyllithium (8.1 mmol, 1.6 M solution in hexanes) was added dropwise to a solution of 1.477 g of triisopropylsilyl acetylene (8.1 mmol) in 10 ml of dry THF at 0 °C. The mixture was kept at 0 °C for half an hour. It was transferred to a solution of 1g of 6,13-pentacenequinone (3.24 mmol) in 10ml dry THF at 0 °C. The reaction was allowed to warm up to room temperature and stirred overnight.

The mixture was quenched with 3 ml of 10% HCl aqueous solution and then subjected to a chloroform-water work up. The blue crude was dissolved in 10 ml of acetone and then a solution of tin (II) chloride dihydrate (1.8276 g, 8.1 mmol) in 50% acetic acid (10 ml) was added drop wise. The mixture was stirred at room temperature for 24 hours. The resulting blue product was filtered. The solid was then dissolved in hexane, washed with water and saturated sodium bicarbonate solution, and then dried over magnesium sulphate. The hexane solution was then poured onto a silica plug, which is flushed with hexane. No further purification was carried out. 1.41 g of the desired product was obtained (2.21 mmol, ~70% yield, Mtp. 256-257 °C ). <sup>1</sup>H NMR (300 MHz, CDCl<sub>3</sub>): δ= 9.34 (s, 4H), 8.01 (dd, J= 6.6 and 3.2 Hz, 4H), 7.45 (dd, J= 6.6 and 3.1 Hz, 4H), 1.42 (m, 42H). Mass spectrum (APCI): 638 (100%), 639 (88%), 640 (52%). Elemental analysis (calc.) found: C (82.69) 82.14, H (8.51) 8.72. IR( $\nu_{\max}/\text{cm}^{-1}$ ): 2940, 2938, 2120, 1383, 1252, 1003, 925.

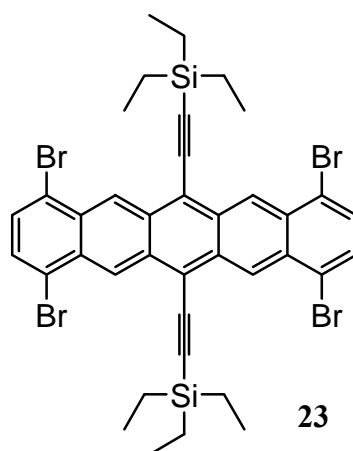
### 6.3.3 Synthesis of 1,4,8,11-tetrabromo-6,13-pentacenequinone (7)



N,N-Dimethylacetamide (40 ml) was placed in a dry 100 ml round bottomed flask. The solvent was purged with nitrogen for ten minutes. The reactants, 2.4 g of 2,5-

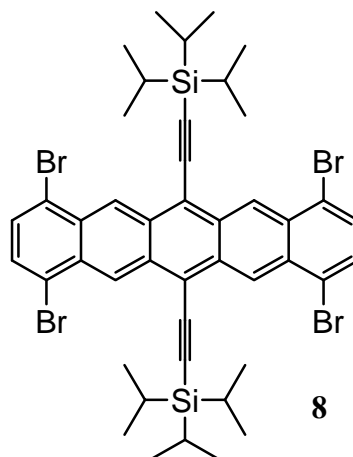
dibromo-1,6-bis(bromomethyl) benzene (5.68 mmol), 0.31 g of benzoquinone (2.84 mmol), 4.25 g of sodium iodide (28.4 mmol), were added and the reaction was allowed to stir for 48 hours at 90 °C. The crude was allowed to cool down filtered and washed with acetone and water. The solid was dissolved in chloroform and filtered to yield 0.3 g of a brownish powder (0.48 mmol, 17% yield, Mtp. 285-287 °C). Mass spectra (MALDI): 624 (100 %), 623 (88 %), 625 (80 %), 626 (73 %), 622 (65 %), 621 (57 %), 627 (58 %), 633 (40 %). Elemental analysis (calc.) found: C (42.35) 42.03, H (1.29) 1.36, Br (51.23) 50.99.

#### 6.3.4 Attempted synthesis of 1,4,8,11-tetrabromo-6,13-bis(triethylsilylethynyl) pentacene (23)



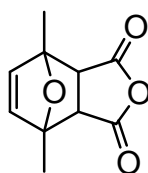
The procedure followed was the same as the one used in the synthesis of TIPS pentacene. The quantities of the reactants added were 0.4 g of 1,4,8,11-tetrabromo-6,13-pentacenequinone (0.64 mmol), 0.22 g of triethylsilyl acetylene (1.6 mmol) and 1 ml of butyllithium (1.6 mmol, solution 1.6 M in hexanes). However, the reaction was not successful, at the end of the work up only the mono-substituted species was obtained. <sup>1</sup>H NMR of the mono-substituted species obtained after the work up. <sup>1</sup>H NMR (300 MHz, CDCl<sub>3</sub>): δ= 9.23 (d, j= 4.69 Hz, 4H), 7.81 (dd, J=8.1 and 17.6 Hz, 4H), 3.19 (s, 1H), 1.15 (t, j=7.8 Hz, 9H), 0.82 (q, j=7.9 Hz, 6H).

### 6.3.5 Attempted synthesis of 1,4,8,11-tetrabromo-6,13-bis(triisopropylsilylethynyl) pentacene (8)



Again same procedure as for the synthesis of TIPS-pentacene was used. Quantity of reactants added 0.3 g of 1,4,8,11-tetrabromo-6,13-pentacenequinone (0.48 mmol), 0.22 g of triisopropylsilyl acetylene (1.2 mmol) and 0.75 ml of butyllithium (1.2 mmol, solution 1.6 M in hexanes). The reaction was not successful at the end of the work up as mono-substituted compound was obtained.  $^1\text{H}$  NMR of the mono-substituted species  $^1\text{H}$  NMR (300 MHz,  $\text{CDCl}_3$ ):  $\delta$ = 9.21 (d,  $j$ = 7.9 Hz, 4H), 7.79 (dd,  $j$ =8.1 and 19.8 Hz, 4H), 3.32 (s, 1H), 1.23 (m, 42H)

### 6.3.6 Synthesis of 1,4-dimethyl-7-oxabicyclo[2,2,1]hept-5-ene-2,3-dicarboxylic anhydride (11) <sup>[132]</sup>

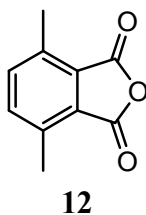


**11**

To a stirred suspension of 22.55 g of maleic anhydride (230 mmol) in diethyl ether (40 ml) was added 22 g of 2,5-dimethylfuran (230 mmol) at room temperature. The

mixture was stirred overnight. The resulting crystals were filtered off and washed with anhydrous diethyl ether. The mother liquid was concentrated under vacuum and the second crop of crystals was combined with those obtained previously. 27 g of the aimed product was obtained (140 mmol, ~60% yield. Mtp. 60-62 °C ). <sup>1</sup>H NMR (300 MHz, CDCl<sub>3</sub>): δ= 6.39(s, 2H), 3.20 (s, 2H), 1.81(s, 6H). IR (ν<sub>max</sub>/cm<sup>-1</sup>): 3600, 3090, 2992, 1856, 1775, 1586, 1446, 1392, 1242, 1214, 1083, 900, 832. The starting material did not transform into the final product in its totality. A mixture of the starting materials and the product was achieved (70:30 product:reactants). The molecule was taken to the next step without further purification.

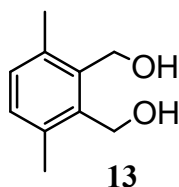
### 6.3.7 Synthesis of 3,6-dimethylphthalic anhydride (12) <sup>[132]</sup>



The enoxide starting material (20 g, 100 mmol) was added in small portions to 200 ml of concentrated H<sub>2</sub>SO<sub>4</sub> cooled at -6 °C. The mixture was stirred vigorously and the temperature was not allowed to rise above 0 °C. After all the enoxide was added the mixture become orange in colour and the temperature was allowed to rise slowly to 10°C before being poured slowly into crushed ice (1 Kg). The resulting white crystals were collected on a Buchner funnel and washed with ice water. The crystals were then dissolved in a solution of NaOH (15 g) in water (150 ml). Glacial acetic acid (25 ml) was added and the solution was filtered to remove all the insoluble materials. The solution was then acidified with HCl (36%) until a precipitate was formed. The resulting precipitate was collected and washed with water until the washing were neutral. The precipitate was added to toluene and azeotropic distillation carried out to remove most of the water. The toluene solution was filtered while hot and the solvent was removed under vacuum. 8.65 g of the desired compound were obtained (49

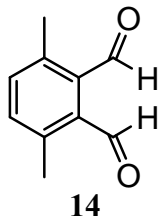
mmol, ~50% yield, Mpt. 143-144 °C). <sup>1</sup>H NMR (300 MHz, CDCl<sub>3</sub>): δ= 7.44 (s, 2H), 2.61(s, 6H). Mass spectrum: (EI) 176 (58%), 148 (43%), 132 (18%), 131 (18%), 103 (100%), 91 (32%), 76 (36%). IR (ν<sub>max</sub>/cm<sup>-1</sup>): 3030, 2929, 1844, 17775, 1569, 1497, 1386, 1349, 1241, 1186, 1022, 911, 890, 748.

### 6.3.8 Synthesis of 3,6-dimethylphthalyl alcohol (13) <sup>[66]</sup>



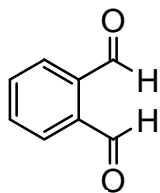
To 50 ml of dry THF 1.14 g of LiAlH<sub>4</sub> (30 mmol) were added. The addition was carried out with stirring under a static atmosphere of N<sub>2</sub>. Then a solution containing 4 g of 3,6-dimethylphthalic anhydride (22.7 mmol) in 40 ml of dry THF was added drop wise for a period of 45 minutes. After the addition was complete the resulting mixture was refluxed overnight. The mixture was then cooled to 0 °C and treated sequentially with 2 ml of water, 2 ml of 15% aqueous solution of sodium hydroxide and 4 ml of water. The granular solid was filtered and the filter cake was washed with ether. The solid was washed several times checking the washing with TLC until all the material was recovered. The combined filtrate was then dried of solvent and the resulting yellow oil which solidified upon standing was recrystallised from ethyl acetate/petroleum ether to give 2.69 g of pure 3,6-dimethylphthalyl alcohol (16.2 mmol, 70% yield, Mpt 69-70°C). <sup>1</sup>H NMR (300 MHz, CDCl<sub>3</sub>): δ= 7.09 (s, 2H), 4.80 (s, 4H), 2.84 (s, 2H), 2.41 (s, 6H). Mass spectrum: (EI): 189 (100%), 356 (20%). Elemental analysis (calc.) found: C (72.26) 72.43, H (8.49) 8.93. IR (ν<sub>max</sub>/cm<sup>-1</sup>): 3290, 2956, 2920, 1746, 1484, 1456, 1243, 992, 810.

### 6.3.9 Attempted synthesis of 3,6-dimethylphthaldialdehyde (Swern oxidation) (14) <sup>[67]</sup>



To a dry 3-necked round-bottomed flask equipped with a N<sub>2</sub> inlet and a dropping funnel, was added a solution of oxalyl chloride (5 g, 40.0 mmol) in dry DCM (50 ml) under an atmosphere of N<sub>2</sub>. The stirred solution was cooled down to -78 °C and a solution of dry DMSO (3.52 g, 45.0 mmol) in dry DCM (12 ml) was added drop wise. The solution was stirred for few minutes and a solution of 3,6-dimethylphthalyl alcohol (2.5 g, 15.0 mmol) in DCM and DMSO (2.5 ml of each solvent) was added drop wise. The reaction was allowed to continue for one hour and then 50 ml of triethylamine was slowly added at -78 °C. The reaction mixture was allowed to stir for 15 minutes and then slowly warmed to room temperature. Ice cooled water was added to the reaction mixture and the aqueous layer extracted with DCM (2x50 ml). The organic layer was dried with magnesium sulphate and removal of the solvent yielded the crude material, which was purified by column chromatography (10:90 ethyl acetate:hexane). From the column was obtained a mixture of 3,6-dimethylphthaldialdehyde and 4,7-dimethyl-1(3H)-isobenzofuranone. The yield obtained was less than 10% and the final product was not clean. As a conclusion an alternative method needs to be found. Characterisation data for 4,7-dimethyl-1(3H)-isobenzofuranone: <sup>1</sup>H NMR (300 MHz, CDCl<sub>3</sub>): δ= 7.15 (dd, 2H), 5.13 (s, 2H), 2.58 (s, 3H), 2.22 (s, 2H). Mass spectrum: (GC/MS): 162 (62%), 133 (100%), 105 (39%), 77 (22%), 63 (11%), 51 (14%).

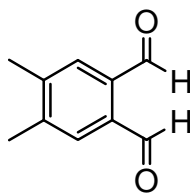
### 6.3.9.1 Synthesis of phthaldialdehyde (16)



16

The same procedure used for the attempted synthesis of 3,6-dimethylphthaldialdehyde using the Swern oxidation method was tried for 1,2-benzenedimethanol. The quantity of reactants used was 0.91 g of 1,2-Benzenedimethanol (6.6 mmol), 1.85 g of oxalyl chloride (14.6 mmol), 1.54 ml of dimethylsulfoxide (19.8 mmol). 0.49 g of the dialdehyde was achieved (3.6 mmol, 56% yield, Mtp 54-55°C). <sup>1</sup>H NMR (300 MHz, CDCl<sub>3</sub>): δ= 10.59 (s, 2H), 8.04 (dd, j= 2.2 and 3.3Hz, 2H), 7.83 (dd, j=2.3 and 3.4Hz, 2H).

### 6.3.9.2 Synthesis of 4,5-dimethylphthaldialdehyde (17)

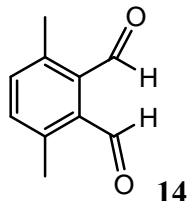


17

The same procedure used for the attempted synthesis of 3,6-dimethylphthaldialdehyde using the Swern oxidation method was tried for 4,5-dimethylphthalyl alcohol. The quantities of reactants used was 1 g of 4,5-dimethylbenzene-1,2-dimethanol (6.0 mmol), 2.03 g of oxalyl chloride (16.0 mmol), 1.41 g of dimethylsulfoxide (18.0 mmol), 0.69 g of the dialdehyde was obtained (4.2 mmol, 70% yield, Mtp 55-56 °C). <sup>1</sup>H NMR (300 MHz, CDCl<sub>3</sub>): δ= 10.23 (s, 2H), 7.75 (s, 2H), 2.48 (s, 6H).

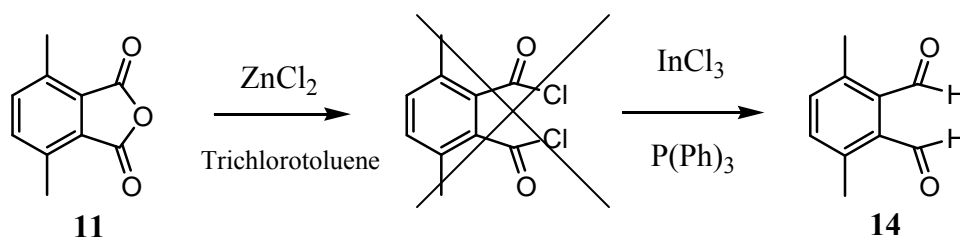


### 6.3.10 Attempted synthesis of 3,6-dimethylphthalaldehyde (Pyridinium chlorochromate) (14)



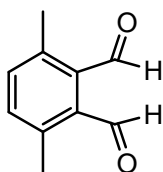
To a mixture of PCC (2.3g, 10.8 mmol) and magnesium sulphate (1.15 g, 9.5 mmol) in dry DCM (20 ml) was added 3,6-dimethylphthalyl alcohol (0.3 g, 1.8 mmol) at 0 °C. The reaction mixture was stirred for 4 hours at room temperature. DCM was evaporated and to the residue, diethyl ether was added. The slurry was stirred and filtered through a silica plug. The filtrate was washed 3 times with Et<sub>2</sub>O and few drops of water were added. Then, the filtrate cake was concentrated under vacuum to yield the product. The reaction was not successful. The reaction was repeated without magnesium sulphate to obtain the same final product. The product achieved was 4,7-dimethyl-1(3H)-isobenzofuranone this product was confirmed with NMR and mass spectroscopy. <sup>1</sup>H NMR (300 MHz, CDCl<sub>3</sub>): δ= 7.15 (dd, 2H), 5.13 (s, 2H), 2.58 (s, 3H), 2.22 (s, 2H). Mass spectrum: (GC/MS): 162 (62%), 133 (100%), 105 (39%), 77 (22%), 63 (11%), 51 (14%).

### 6.3.11 Attempted synthesis of 3,6-dimethylphthalaldehyde (14) <sup>[69-70]</sup>



A mixture of 2 g of 3,6-dimethylphthalic anhydride (11.4 mmol), 2.22 g of trichlorotoluene (11.4 mmol) and 0.15 g of zinc chloride (1.14 mmol) was heated in an oil bath at 50 °C overnight. Distillation of the reaction mixture should yield the desired material. However, the final product was not achieved and therefore this method was also discarded. <sup>1</sup>H NMR showed no data of the product. However, signals at 7.45 ppm and 2.60 ppm showed evidence of the starting material (3,6-dimethylphthalic anhydride) and signals at 7.85 ppm and 7.35 ppm showed evidence of trichlorotoluene.

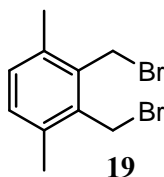
### 6.3.12 Attempted synthesis of 3,6-dimethylphthalaldehyde (14)



14

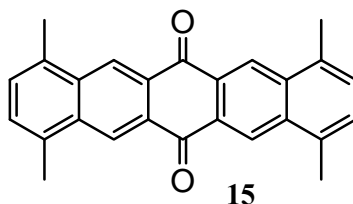
To a pre-dried 25 ml round bottomed flask 0.5 ml of dry DCM and 0.3 g of anhydride (1.7 mmol) were added. The solution was cooled to -78°C and 4.08 ml of diisobutylaluminium (DIBAL) (4.08 mmol, 1 M solution in hexanes) was added drop-wise to the reaction. The reaction was allowed to stir at room temperature for two hours. To the resulting solution dry DCM (2 ml) and methanol (0.3 ml) were added. The reaction began to boil and after few seconds become very thick. To this slurry 1 g of silica and 0.1 g of tartaric acid were added. After few minutes the mixture became liquid again. The mixture was allowed to stir overnight, filtered and the filter cake was washed with DCM. <sup>1</sup>H NMR showed a fraction of the starting material (3,6-dimethylphthalic anhydride) with the characteristic peaks at 7.45 ppm and 2.60 ppm and the formation of 4,7-dimethyl-1(3H)-isobenzofuranone with the signals at 7.35 ppm and 7.32 ppm.

### 6.3.13 Synthesis of 3,6-dimethyl-1,2-bis(bromomethyl)benzene (19)<sup>[66]</sup>



To a stirred solution of 3,6-dimethylphthalyl alcohol (3 g, 18.0 mmol) in 50 ml of dry toluene, under a static pressure of nitrogen, was added drop-wise a solution containing 9.72 g of phosphorus tribromide (36.0 mmol) in 12.5 ml of dry toluene. After the addition was completed, the mixture was stirred at room temperature for 1 hour and then for an additional hour at 40 °C. The mixture was then poured onto ice (60 g). After the ice was melted the mixture was extracted with 1:1 diethyl ether/toluene (3x20 ml). The combined organic layers were washed with a saturated solution of NaCl (2x25 ml) and dried over magnesium sulphate. Filtration and removal of the solvent under vacuum gave 4.90 g of white powder (16.8 mmol, 95% yield, Mtp. 101-103°C). <sup>1</sup>H NMR (500 MHz, CDCl<sub>3</sub>): δ= 7.08 (s, 2H), 4.69 (s, 4H), 2.41 (s, 6H). Mass spectroscopy (accurate mass): 292 (2%), 211 (36%), 132 (100%), 115 (35%), 91 (26%), 51 (19%). Elemental analysis (calc.) found: C (41.13) 41.58, H (4.14) 4.00, Br (54.73) 53.04. IR( $\nu_{\max}$ /cm<sup>-1</sup>): 2924, 1480, 1443, 1222, 1999, 1167.

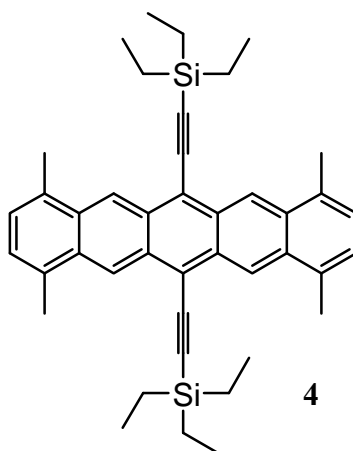
### 6.3.14 Synthesis of 1,4,8,11-tetramethyl-6,13-pentacenequinone (15)



To an oven dried round bottomed flask, cooled under nitrogen, were added 50 ml of dimethylacetamide. The solvent was degassed for 30 minutes with nitrogen. 4.5 g of 3,6-dimethyl-1,2-bis(bromomethyl)benzene (15.4 mmol) was added to the flask with

vigorous stirring, followed by p-benzoquinone (0.81 g, 7.5 mmol) and 11.46 g of sodium iodide (76 mmol). The mixture was then closed and stirred at 90 °C for 48 H. The mixture was then filtered and the yellow-brown solid washed with acetone and water. Oven dried (40 °C, under vacuum) to yield 0.60 g of the product (1.65 mmol, 22% yield, Mtp 271-272°C). Mass spectra (EI/CI): 390 (17%), 364 (100%), 313 (12%), 170 (8%). Elemental Analysis (calc.) found: C(85.69) 85.52, H (5.53) 5.91. IR( $\nu_{\max}/\text{cm}^{-1}$ ): 2917, 1672, 1657, 1604, 1456, 1387, 1300, 1208.

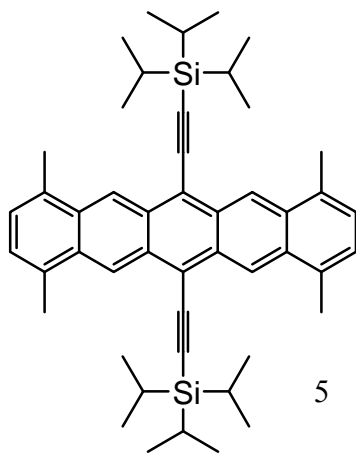
### 6.3.15 Synthesis of 1,4,8,11-tetramethyl-6,13-bis(triethylsilylethynyl)pentacene (TMTES-pentacene) (4)



Under an atmosphere of nitrogen 1.5 ml of n-buthyllithium (2.4 mmol) was added drop-wise to a solution containing 0.34 g of triethylsilyl acetylene (2.4 mmol) in dry THF (5 ml) at 0 °C. The mixture was kept at 0 °C for 40 minutes before it was transferred to a solution of 0.35 g of 1,4,8,11-tetramethyl-6,13-pentacenequinone (0.96 mmol) in THF (5 ml) at 0 °C. The mixture was allowed to warm up to room temperature and stirred overnight. The reaction was quenched with 1.5 ml of 10% HCl aqueous solution and then subjected to a  $\text{CHCl}_3/\text{H}_2\text{O}$  work up. The solvent was removed and the resulting blue-green material was collected by filtration.

The solid crude was dissolved in 5 ml of acetone and then a solution of tin (II) chloride dihydrated (0.43 g, 1.92 mmol) in 50% acetic acid aqueous solution (5 ml) was added drop-wise. The mixture was stirred at room temperature for 24 hours. The resulting crude product was filtered. The solid was then dissolved in DCM, washed with water and sodium bicarbonate solution and the dried over magnesium sulphate. The solvent was removed under vacuum. The material was purified using a silica plug. Hexane was used as eluent. 0.29 g were obtained (4.7 mmol, 50% yield, Mtp 257-259 °C).  $^1\text{H}$  NMR (300 MHz,  $\text{CDCl}_3$ ):  $\delta$ = 9.43 (s, 4H), 7.18 (s, 4H), 2.85 (s, 12H), 1.32 (t, 18H), 0.96 (q, 12H). Mass spectroscopy (APCI): 610.3 (100%). Elemental analysis (calc.) found: C (82.56%) 81.82%, H (8.25%) 8.47%. IR( $\nu_{\text{max}}/\text{cm}^{-1}$ ): 2952, 2127, 1455, 1369.

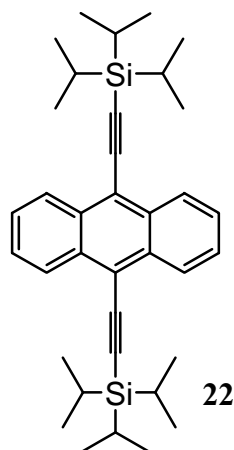
### 6.3.16 Synthesis of 1,4,8,11-tetramethyl-6,13-bis(triisopropylsilyl ethynyl) pentacene (TMTIPS-pentacene) (5)



The same procedure as the one used for the synthesis of TMTES was followed to synthesise TMTIPS. The quantities of reactants used were 1 g of 1,4,8,12-tetramethyl-6,13-pentacenequinone (2.7 mmol), 4.2 ml of butyllithium (6.75 mmol, 1.6M in hexanes), 1.23 g of triisopropylsilylacetylene (6.75 mmol). It was achieved 1.03 g of pure material (1.48 mmol, ~55% yield, Mtp 260-262°C).  $^1\text{H}$  NMR (300 MHz,

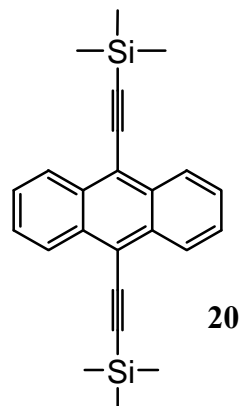
CDCl<sub>3</sub>):  $\delta$ = 9.39 (s, 4H), 7.10 (s, 4H), 2.76 (s, 12H), 1.32 (m, 42H). Mass spectroscopy (APCI): 695.5 (100%), 696.8 (24%), 697.7 (11%). Elemental analysis (calc.) found: C (82.93) 82.65, H (8.99) 9.56. IR( $\nu_{\max}/\text{cm}^{-1}$ ): 2942, 2850, 2121, 1420, 1366, 1080.

### 6.3.17 Synthesis of 9,10-bis(triisopropylsilylethynyl) anthracene (22)



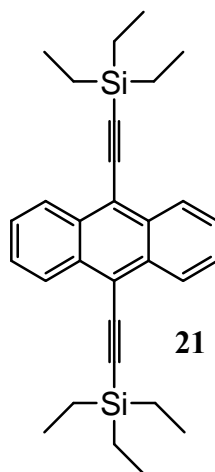
The addition of the protecting groups was carried out using the method described in the synthesis of TIPS-pentacene. The purification of the crude was made by pouring the crude onto a silica plug, which was flushed with hexane. No further purification was carried out. The amounts of reactants were 3.55 g of triisopropylsilyl acetylene (19.5 mmol), 12.2 ml of butyllithium (19.5 mmol solution 1.6 M in hexanes), 1.62 g of 9,10-anthraquinone (7.8 mmol). 2.72 g of the desired product were obtained (5.0 mmol, ~65% yield, Mtp 234-235 °C). <sup>1</sup>H NMR (300 MHz, CDCl<sub>3</sub>):  $\delta$ = 8.67 (dd, J= 3.2 and 6.6Hz, 4H), 7.64 (dd, J=3.2 and 6.6Hz, 4H), 1.31 (m, 42H). Mass spectrum (APCI): 539 (100%). Elemental analysis (calc) found: C (80.29) 79.88, H (9.29) 9.71. IR ( $\nu_{\max}/\text{cm}^{-1}$ ): 3059, 2939, 2862, 2120, 1621, 1459, 1375, 1043, 799.

### 6.3.18 Synthesis of 9,10-bis(trimethylsilylethynyl) anthracene (20)



The same procedure was followed for the synthesis of trimethyl derivative. The amount of the reactants were 1 g of 9,10-anthraquinone ( 4.75 mmol), 7.4 ml of butyllithium (11.8 mmol, 1.6 M in hexanes), 1.16 g of trimethylsilyl acetylene (11.8 mmol). 1.05 g of pure material was achieved (2.8 mmol, 60% yield, Mtp 228-229 °C).  $^1\text{H}$  NMR (300MHz,  $\text{CDCl}_3$ ):  $\delta$ = 8.50 (dd,  $J$ =3.2 and 6.6Hz, 4H). 7.54 (dd,  $J$ =3.4 and 6.7Hz, 4H), 0.36 (s, 18H). Mass spectrum (EI): 370 (25%), 355 (11%). Elemental Analysis (calc) found: C (77.77) 78.26, H (7.07) 6.94. IR ( $\nu_{\text{max}}/\text{cm}^{-1}$ ): 3059, 2957, 2123, 1767, 1376, 1246, 1049, 845.

### 6.3.19 Synthesis of 9,10-bis(triethylesilylethynyl) anthracene (21)



Same procedure was used for the synthesis of the triethyl derivative. The amount of starting materials was 1 g of 9,10-anthraquinone ( 4.75 mmol), 7.4 ml of butyllithium (11.8 mmol, 1.6 M in hexanes), 1.65 g triethylsilyl acetylene (11.8 mmol). 1.33 g was achieved (2.9 mmol, 61% yield, Mtp 230-232 °C). <sup>1</sup>H NMR (300MHz, CDCl<sub>3</sub>): δ= 8.59 (dd, J= 3.2 and 6.6Hz, 4H), 7.58 (dd, J= 3.2 and 6.6Hz, 4H), 1.17 (t, J= 7.9Hz, 18H). 0.83 (q, j=7.9Hz, 12H). Mass spectrum (APCI): 454 (100%), 374 (8%). Elemental Analysis (calc) found: C (79.23) 77.61, H (8.42) 8.65. IR (ν<sub>max</sub>/cm<sup>-1</sup>): 3056, 2953, 2872, 2123, 1619, 1374, 1233, 1017, 974, 801, 718.

## 6.4 Materials Characterisation techniques

- Scanning force microscopy (SFM) was carried out using an AFM XE 100 (PSIA Inc, Seoul, Korea). The images were obtained in contact mode using a 1 Hz and a constant force of 21.4 nN. A soft commercial silicon cantilever was used. It had a nominal spring constant of ~0.6 Nm<sup>-1</sup> and the back of it was coated with aluminium to increase the signal feedback.
- X-rays Powder diffractions were performed using a Philips Xpert station with a Cu K<sub>α</sub> source at 0.15405980 nm. The Samples were prepared by drop casting different solution on OTS treated silicon oxide substrates.
- Fournier transform infrared spectroscopy (FTIR) Near surface reflective mode infrared images were taken of the top and bottom film surfaces using a Biorad Stingray Infrared Spectrometer which is an infrared/optical microscope coupled to a FTS600 bench FTIR spectrometer. The 64x64 detector array records 4096 separate FTIR spectra over a 400x400 μm area, which leads to a spatial resolution of 39 μm<sup>2</sup> per pixel. The spectra were recorded between 4000 to 850 cm<sup>-1</sup> with infrared absorbance bands labelled to produce a 2D false colour image.



- X-ray photoelectron spectroscopy (XPS) was measured using a Kratos Axis Ultra Spectrometer. Monochromated Al K $\alpha$  at a power of 150 W was used to acquire the spectra under a secondary vacuum of  $1 \times 10^{-6}$  Pa. All samples were left overnight to degas in a vacuum oven at room temperature prior analysis. Data were first recorded using a pass energy of 160 eV over 4 minutes whilst high resolution C1s and Si2p scans were recorded at a pass energy of 20 eV over 10 minutes. Data were analysed using CasaXPs software and quantification was realized using the default Kratos RSF (relative sensitivity factor) library. All spectra were charge corrected according to the value of aliphatic carbons C1s at 285 eV. High resolution peaks were fitted using a Gaussian-Lorentzian model. FWHM was kept below 1.7 eV except for fitting the shake-up profile on the narrow carbon peak.
- Thermo gravimetric analyses (TGA) were obtained using a TGA Q5000 IR from TA instruments. Aluminium pans (high temperature resistant) were used. The range of temperatures was from room temperature up to 800 °C and the scan rate was 5 °C/m.
- Differential scanning Calorimetry (DSC) was measured using a Diamond DSC from Perkin Elmer. The samples were loaded using aluminium sample pans (40  $\mu$ l, 0.15 mm) with holed aluminium covers (0.05 mm). The heating and cooling rates were 5°C/m. The covers were holed to allow the release of pressure inside the pans when high temperatures are reached. Both, pans and covers were acquired from Perkin Elmer.
- Cyclic Voltametry (CV) were measured in thin film (solid state). The results were compared with those obtained for ferrocene (HOMO is 4.8 eV) in the same conditions in order to obtain the HOMO levels of the measured compounds. The instrument used to carry out the measurements was a BASI C3 stand cell used with an Epsilon electrochemical instrument. Samples were

drop cast (DCM solution 1 mg/ml) over platinum foil (working electrode). The films were allowed to dry for 1 hour in a solvent saturated atmosphere. The counter electrode was a platinum wire and silver nitrate was used as the reference electrode. Tetrabutylammonium hexafluorophosphate (0.1 M) in acetonitrile was used as electrolyte. The oxidation scans were from -200 mV to 1500 mV measured at 100 mV/s. The loop cycle was repeated three times.

## **6.5 Organic field effect transistors device fabrication and characterisation**

All the devices in this thesis have been prepared using bottom gate top contact configuration. Substrates were heavily n-doped silicon wafer, which acted as the gate, covered with a 300nm layer of thermally grown silicon oxide. Hydrophilic substrates were prepared by dipping the substrate in piranha solution for 1 min followed by a good rinse with deionised water and acetone. Hydrophobic substrates were prepared by treating them with Octadecyltrichlorosilane (OTS).

OTS treatment: In order to clean the substrates, they were sonicated in different solvents: deionised water, acetone and methanol (15 minutes each). Then they were submerged in a 1M solution of OTS in toluene for 20 minutes maintained at 60°C. Rinsed with acetone hexane and ethanol (electronic grade) and allowed to dry on a hot plate for two hours at 120°C (open atmosphere).

Solutions of the organic semiconductor (range of concentrations, pure material and blends) were drop cast on the substrate and dried in a vacuum oven at room temperature. No post thermal annealing was employed. Gold source and drain channel electrodes, 60  $\mu\text{m}$  width and 2 mm long were thermally evaporated, at  $10^{-6}$  mBar at a rate of 0.1 nm/s for the first 10 nm and then 0.3 nm/s until a layer thickness of 50 nm was obtained, yielding 9 transistors per substrate. DC characteristics of the devices were obtained using an E5270B 8 Slot precision measurement frame from

Agilent Technology coupled to a 3 Agilent E5287A atto level High Resolution Module. Contacts were made using Karl Süss PH100 manual microprobes. Output characteristics were obtained at a constant gate voltage  $V_G = -80$  V and transfer characteristics at a constant drain voltage  $V_{SD} = -80$  V. From the slope of the square root of the drain intensity characteristic, we were able to calculate the saturated hole mobility ( $\mu_{FET}$ ) and the threshold voltage, according to Equation 6.1.

$$I_D = \frac{\mu_{FET} W C_i}{2L} (V_G - V_{TH})^2 \quad 6.1$$

where  $W$  is the width of the channel (2 mm),  $L$  the length of the channel (60  $\mu\text{m}$ ),  $C_i$  is the equivalent capacitance of the dielectric intercepting the channel and  $V_{TH}$  the threshold voltage. Measurements were performed in air, in the dark under normal atmospheric pressure.

### 6.5.1 Solution preparation

In the case of pristine materials 0.5 % w/w solution of TIPS-pentacene, TMTIPS-pentacene and TMTES-pentacene in toluene were prepared. Organic semiconductor-polymer blends were prepared as follows. Stock solution (1 % w/w in tetralin) of organic semiconductor and polymer binder were prepared. Organic semiconductor solutions were filtered using a 0.45  $\mu\text{m}$  PTFE filter. Polymer binder solutions were left unfiltered. Blends were prepared freshly prior device fabrication. The total mass content was kept at 1 % w/w, with weight fractions of organic semiconductor being varied from 0.1 to 0.9. In the case of TMTES-pentacene ten times less concentrated solutions were also prepared. These solutions were directly drop cast on the thin film transistor substrates.

## 6.6 TMTES-pentacene and TMTIPS-pentacene crystallisation

X-rays crystallography requires suitable single crystals to be capable of measuring the structure of the material. Solvent evaporation using different solvents (toluene, tetralin, tetrahydrofuran and dichloromethane) was not a successful crystallisation method. Experiments were repeated under a solvent saturated atmosphere to promote slower evaporation without success in the crystallisation. The crystals were grown using the diffusion method. In extremely clean 1ml vials, 1mg of the material was diluted in the minimum amount of solvent as possible. To this solution was added very carefully a second solvent in which the material is not soluble (anti-solvent) but which is miscible with the previous solvent. 5 solvents were used with 3 different anti-solvents. Therefore 15 different systems were tried in order to grow crystals. The samples were left overnight for the solvents to mix together. After this period the crystals crash down. The solvents and anti-solvent used are shown in the Table 6.2

**Tabla 6.1 Table showing the solvents and antisolvents used for the slow diffusion crystallisation method.**

<b>Solvents</b>	DCM	Chloroform	Carbon Tetrachloride	Tetralin	Trichlorobenzene
<b>Anti-Solvents</b>	Ethanol	Methanol		Acetonitrile	

## 6.7 Aggregation studies of anthracene and its derivatives

A  $1 \times 10^{-3}$  M solution of each of the anthracene derivatives in toluene was prepared. From this stock solution, by dilution, were prepared 5 samples of the following concentrations:  $1 \times 10^{-4}$  M,  $5 \times 10^{-5}$  M,  $1 \times 10^{-5}$  M,  $5 \times 10^{-6}$  M and  $1 \times 10^{-6}$  M. UV/vis and fluorescence spectroscopy were measured for all of them. The fluorescence parameters are detailed in the following Table 6.3.

**Tabla 6.2 Fluorescence set up parameters**

	Excitation	Start	Stop	Excitation slit	Emission slit
Anthracene	356	366	600	2.5	2.5
TMS-A	414	424	600	2.5	2.5
TES-A	414	424	600	2.5	2.5
TIPS-A	415	425	600	2.5	2.5

## 6.8 Anthracene derivatives-SWNTs interaction

$1 \times 10^{-4}$  M solutions of each anthracene derivative were prepared. From this solution by dilution,  $1 \times 10^{-5}$  M,  $1 \times 10^{-6}$  M and  $1 \times 10^{-7}$  M were made. UV/vis and fluorescence were recorded for all of them being the fluorescence parameters those described in Table 6.3.

From the previously prepared  $1 \times 10^{-4}$  M solution a new  $1 \times 10^{-5}$  M solution was prepared and to this one SWNTs were added in 1:1 w/w ratio. This solution containing SWNTs was sonicated for 30 seconds using a tip sonicator (Misonix S3000 Ultrasonic Processor) at 33W. After sonication, homogeneous dispersion was achieved. And from this solution  $1 \times 10^{-6}$  M and  $1 \times 10^{-7}$  M solutions were prepared. The solutions were left to settle down for 24 hours, after which, the supernatant was carefully pipetted out to a clean vial. Again the samples were allowed to rest for 24 hours and again the upper layer was separated. UV/vis and fluorescence spectroscopy were measured. The experiment was repeated allowing different sonication times (1 and 5 minutes).

## **7 Conclusions and further work**

In this thesis we have presented the synthesis and electronic characterisations of a new family of 1,4,8,11-tetramethyl-6,13-disubstituted pentacene derivatives. Excellent thin film transistor performance using TMTES-pentacene has been measured. Maximum hole mobility of  $2.4 \text{ cm}^2/\text{Vs}$  has been obtained comparable to amorphous silicon.

The improvement brought by blending TIPS-pentacene and TMTES-pentacene with low dielectric constant side chain aromatic polymers and how formulation can have a critical role in device performance is discussed. Among the improvements brought by blends are the disappearance of hysteresis in the transfer characteristics, encapsulation of the sensitive semiconductor material, reduction in the amount of organic semiconductor required for quality film formation and improvement in the mobility enhanced by better crystallisation of the organic semiconductor at the OSC-insulator interface in the TFT channel. This improved crystallisation is believed to be due to the vertical phase separation observed when blending these pentacene derivatives with semicrystalline polymers.

Blend formulation is a challenging process as it is influenced by several factors including: solute concentration, blend ratio, temperature, and deposition technique. Formulation optimisation can improve considerably the performance of these pentacene derivatives as a consequence it should be considered for further work.

Other important factor that should be considered towards improving the TFT performance is the fabrication process. All the electronic characterisation and TFT processes presented in this thesis were carried out under ambient conditions using drop casting. We believe that these results can be largely improved by using clean room facilities under inert atmospheres. It will be interesting to investigate the use of inkjet printing where thin film devices can be more readily fabricated and where the drying kinetics will be subtly different.

Crystallisation is a key process that must be considered when aiming for enhanced electronic transport in organic semiconducting materials. The study of the aggregation processes taking place in solution as a function of the concentration can be seen as a precursor of the crystallisation processes. Here we have presented the aggregation study of a family of 9,10-disubstituted anthracene derivatives. We believe that a full study of the aggregation processes taking place within pentacene derivatives would help understanding these materials and would provide helpful information in terms of film formation properties and blends formulation.

Preliminary studies of the use of anthracene derivatives to disperse SWNT have been presented. From this initial study we can only suggest that there is an interaction between the nanotubes and the anthracene derivatives as can be observed in the fluorescence spectrum. However, additional experiments, including Raman spectroscopy and imaging techniques, should be carried out for a full understanding of the results.



## 8 References

- [1] a)M. A. M. Leenen, V. Arning, H. Thiem, J. Steiger, R. Anselmann, *physica status solidi (a)* **2009**, *206*, 588; b)G. Schmidt, H. Kempa, U. Fuegmann, T. Fischer, M. Bartzsch, T. Zillger, K. Preissler, U. Hahn, A. Huebler, *Vol. 6336* (Eds.: B. Zhenan, J. G. David), SPIE, **2006**, p. 633610.
- [2] J. Zaumseil, H. Sirringhaus, *Chemical Reviews* **2007**, *107*, 1296.
- [3] a)Y. Yamashita, *Science and technology of advanced materials* **2009**, *10*, no pp. given; b)Y.-L. Loo, *AIChE Journal* **2007**, *53*, 1066; c)S. Allard, M. Forster, B. Souharce, H. Thiem, U. Scherf, *Angewandte Chemie International Edition* **2008**, *47*, 4070.
- [4] M. Thelakkat, J. Hagen, D. Haarer, H. W. Schmidt, *Synthetic Metals* **1999**, *102*, 1125.
- [5] N. Gomathi, V. K. Prasad, S. Neogi, *Journal of Applied Polymer Science* **2009**, *111*, 1917.
- [6] Z. Bao, A. Dodabalapur, A. J. Lovinger, *Applied Physics Letters* **1996**, *69*, 4108.
- [7] John E. Anthony, *Angewandte Chemie International Edition* **2008**, *47*, 452.
- [8] S.-W. Park, J. M. Hwang, J.-M. Choi, D. K. Hwang, M. S. Oh, J. H. Kim, S. Im, *Applied Physics Letters* **2007**, *90*, 153512.
- [9] a)C. R. Newman, C. D. Frisbie, D. A. da Silva Filho, J.-L. Bredas, P. C. Ewbank, K. R. Mann, *Chemistry of Materials* **2004**, *16*, 4436; b)G. Horowitz, *Advanced Materials* **1998**, *10*, 365; c)H. Sirringhaus, *Proceedings of the IEEE* **2009**, *97*, 1570.
- [10] C. D. Dimitrakopoulos, P. R. L. Malenfant, *Advanced Materials* **2002**, *14*, 99.
- [11] C. R. Kagan, P. Andry, *Thin-film transistors*, Taylor & Francis Inc., **2003**.
- [12] M. E. Roberts, S. C. B. Mannsfeld, R. M. Stoltenberg, Z. Bao, *Organic Electronics* **2009**, *10*, 377.
- [13] A. Facchetti, M.-H. Yoon, T. J. Marks, *Advanced Materials* **2005**, *17*, 1705.
- [14] S. Steudel, S. D. Vusser, S. D. Jonge, D. Janssen, S. Verlaak, J. Genoe, P. Heremans, *Applied Physics Letters* **2004**, *85*, 4400.
- [15] J. Veres, S. Ogier, S. W. Leeming, D. C. Cupertino, S. M. Khaffaf, *Advanced Functional Materials* **2003**, *13*, 199.

- [16] Y. Shen, A. R. Hosseini, M. H. Wong, G. G. Malliaras, *ChemPhysChem* **2004**, 5, 16.
- [17] R. C. Ropp, *Solid state chemistry*, Elsevire Science, **2003**.
- [18] C. K. Chiang, C. R. Fincher, Y. W. Park, A. J. Heeger, H. Shirakawa, E. J. Louis, S. C. Gau, A. G. MacDiarmid, *Physical Review Letters* **1977**, 39, 1098.
- [19] F. Ebisawa, T. Kurokawa, S. Nara, *Journal of applied physics* **1983**, 54, 3255.
- [20] W. Brutting, *Physics of organic semiconductors*, Wiley-VCH, **2006**.
- [21] J. D. Wright, *Molecular Crystals*, Cambridge University Press, **1995**.
- [22] J. Maunoury, University of Manchester (Manchester), **2006**.
- [23] M. P. Boone, Y. Dienes, T. Baumgartner, *Arkivoc Journal* **2009**, V, 90.
- [24] A. M. Leszek, University of Sheffield (Sheffield), **2005**.
- [25] a)M. D. Curtis, J. Cao, J. W. Kampf, *Journal of the American Chemical Society* **2004**, 126, 4318; b)J. E. Anthony, *Angewandte Chemie International Edition* **2008**, 47, 452.
- [26] J. Cornil, D. Beljonne, J.-P. Calbert, J.-L. Brédas, *Advanced Materials* **2001**, 13, 1053.
- [27] H. Sirringhaus, P. J. Brown, R. H. Friend, M. M. Nielsen, K. Bechgaard, B. M. W. Langeveld-Voss, A. J. H. Spiering, R. A. J. Janssen, E. W. Meijer, P. Herwig, D. M. de Leeuw, *Nature* **1999**, 401, 685.
- [28] D. Jerome, K. Bechgaard, *Nature* **2001**, 410, 162.
- [29] Z. Bao, J. Locking, *Organic field-effect transistors*, Taylor & Francis Ltd., **2007**.
- [30] S. A. DiBenedetto, A. Facchetti, M. A. Ratner, T. J. Marks, *Advanced Materials* **2009**, 21, 1407.
- [31] J. Chen, J. Anthony, D. C. Martin, *The Journal of Physical Chemistry B* **2006**, 110, 16397.
- [32] O. D. Jurchescu, M. Popinciuc, B. J. van Wees, T. T. M. Palstra, *Advanced Materials* **2007**, 19, 688.
- [33] Z. Bao, in *Polymers for Microelectronics and Nanoelectronics*, American Chemical Society, Washington, DC, **2004**, pp. 1.

- [34] J. E. Anthony, J. S. Brooks, D. L. Eaton, S. R. Parkin, *Journal of the American Chemical Society* **2001**, *123*, 9482.
- [35] R. Hamilton, J. Smith, S. Ogier, M. Heeney, J. E. Anthony, I. McCulloch, J. Veres, D. D. C. Bradley, T. D. Anthopoulos, *Advanced Materials* **2009**, *21*, 1166.
- [36] S. C. Lim, S. H. Kim, J. H. Lee, M. K. Kim, D. J. Kim, T. Zyung, *Synthetic Metals* **2005**, *148*, 75.
- [37] M. L. Chabiny, Y.-L. Loo, *Polymer Reviews* **2006**, *46*, 1
- [38] A. Bolognesi, M. Catellani, A. Musco, R. Pontellini, *Synthetic Metals* **1993**, *55*, 1255.
- [39] M. Jaiswal, R. Menon, *Polymer International* **2006**, *55*, 1371.
- [40] K. S. Novoselov, A. K. Geim, S. V. Morozov, D. Jiang, Y. Zhang, S. V. Dubonos, I. V. Grigorieva, A. A. Firsov, *Science* **2004**, *306*, 666.
- [41] M. Thelakkat, H.-W. Schmidt, *Advanced Materials* **1998**, *10*, 219.
- [42] J. Smith, R. Hamilton, M. Heeney, D. M. De Leeuw, E. Cantatore, J. E. Anthony, I. McCulloch, D. D. C. Bradley, T. D. Anthopoulos, *Applied Physics Letters* **2008**, *93*, 253301.
- [43] W.-S. Lee, G.-W. Choi, Y.-J. Seo, *physica status solidi (c)* **2008**, *5*, 3401.
- [44] M. P. Hong, B. S. Kim, Y. U. Lee, K. K. Song, J. H. Oh, J. H. Kim, T. Y. Choi, M. S. Ryu, K. Chung, S. Y. Lee, B. W. Koo, J. Shin, H., E. J. Jeong, L. S. Pu, *International symposium digest of technical papers* **2005**, *36*, 23.
- [45] S. K. Park, T. N. Jackson, J. E. Anthony, D. A. Mourey, *Applied physics letters* **2007**, *91*, 063514.
- [46] V. C. Sundar, J. Zaumseil, V. Podzorov, E. Menard, R. L. Willett, T. Someya, M. E. Gershenson, J. A. Rogers, *Science* **2004**, *303*, 1644.
- [47] M. M. Payne, S. A. Odom, S. R. Parkin, J. E. Anthony, *Organic Letters* **2004**, *6*, 3325.
- [48] M. M. Payne, S. R. Parkin, J. E. Anthony, C.-C. Kuo, T. N. Jackson, *Journal of the American Chemical Society* **2005**, *127*, 4986.
- [49] S. Subramanian, S. K. Park, S. R. Parkin, V. Podzorov, T. N. Jackson, J. E. Anthony, *Journal of the American Chemical Society* **2008**, *130*, 2706.

- [50] J. E. Anthony, *Chemical Reviews* **2006**, *106*, 5028.
- [51] B. A. Brown, J. veres, R. M. Anemian, R. T. Williams, S. Ogier, S. W. Leeming, *Vol. WO 2005055248* (Ed.: P. I. Appl), **2005**.
- [52] R. M. Anemian, S. W. Leeming, *Vol. WO2006119853* (Ed.: P. I. Appl.), **2006**.
- [53] C. R. Swartz, S. R. Parkin, J. E. Bullock, J. E. Anthony, A. C. Mayer, G. G. Malliaras, *Organic Letters* **2005**, *7*, 3163.
- [54] J. E. Anthony, D. L. Eaton, S. R. Parkin, *Organic Letters* **2001**, *4*, 15.
- [55] J. E. Anthony, C. R. Swartz, C. A. Landis, S. R. Parkin, *Proceedings of SPIE-The international society of optical engineering* **2005**, 594.
- [56] J. Jiang, B. R. Kaafarani, D. C. Neckers, *Journal of Organic Chemistry* **2006**, *71*, 2155.
- [57] A. Maliakal, K. Raghavachari, H. Katz, E. Chandross, T. Siegrist, *Chemistry of Materials* **2004**, *16*, 4980.
- [58] I. Kaur, W. Jia, R. P. Kopreski, S. Selvarasah, M. R. Dokmeci, C. Pramanik, N. E. McGruer, G. P. Miller, *Journal of the American Chemical Society* **2008**, *130*, 16274.
- [59] D. Lehnherr, R. McDonald, R. R. Tykwinski, *Organic Letters* **2008**, *10*, 4163.
- [60] Y. Kim, J. E. Whitten, T. M. Swager, *Journal of the American Chemical Society* **2005**, *127*, 12122.
- [61] P. Coppo, S. G. Yeates, *Advanced Materials* **2005**, *17*, 3001.
- [62] F. De Angelis, M. Gaspari, A. Procopio, G. Cuda, E. Di Fabrizio, *Chemical Physics Letters* **2009**, *468*, 193.
- [63] S. K. Park, D. A. Mourey, J.-I. Han, J. E. Anthony, T. N. Jackson, *Organic Electronics* **2009**, *10*, 486.
- [64] M. P. Cava, A. A. Deana, K. Muth, *Journal of the American Chemical Society* **2002**, *81*, 6458.
- [65] M. J. Cook, S. J. Cracknell, *Tetrahedron* **1994**, *50*, 12125.
- [66] G. M. Rubottom, J. E. Way, *Synthetic Communications: An International Journal for Rapid Communication of Synthetic Organic Chemistry* **1984**, *14*, 507
- [67] O. Farooq, *Synthesis* **1994**, *1994*, 1035.

- [68] J. Kagan, *Tetrahedron Letters* **1966**, 7, 6097.
- [69] L. P. Kyrides, *Journal of the American Chemical Society* **2002**, 59, 206.
- [70] K. Inoue, M. Yasuda, I. Shibata, A. Baba, *Tetrahedron Letters* **2000**, 41, 113.
- [71] G. Rincon Llorente, M.-B. Dufourg-Madec, D. J. Crouch, S. Ogier, S. G. Yeates, *Chemical Communications* **2009**, 3.
- [72] C. A. Landis, S. R. Parkin, J. E. Anthony, *Japanese Journal of Applied Physics* **2005**, 44, 3921.
- [73] J.-i. Aihara, *Physical chemistry, chemical physics* **1999**, 1, 3193.
- [74] K. Takimiya, T. Yamamoto, H. Ebata, T. Izawa, *Science and Technology of Advanced Materials* **2007**, 8, 273.
- [75] J. Chen, D. C. Martin, J. E. Anthony, *Journal of Material Research* **2007**, 22, 1701.
- [76] R. Li, W. Hu, Y. Liu, D. Zhu, *Accounts of Chemical Research* **2010**.
- [77] D. Kim, S. Jeong, S. H. Lee, J. Moon, J. K. Song, *Synthetic Metals* **2009**, 159, 1381.
- [78] T. Okamoto, M. L. Senatore, M.-M. Ling, A. B. Mallic, M. L. Tang, Z. Bao, *Advanced Materials* **2007**, 19, 3381.
- [79] M. C. Scharber, D. Muehler, M. Koppe, P. Denk, C. Waldauf, A. J. Heeger, C. J. Brabec, *Advanced Materials* **2006**, 118, 789.
- [80] K. Kawakami, *Journal of Pharmaceutical Sciences* **2007**, 96, 982.
- [81] M. Pope, C. E. Swenberg, *Electronic processes in organic crystals and polymers*, Oxford University press, New york, **1982**.
- [82] D. H. Kim, D. Y. Lee, H. S. Lee, W. H. Lee, Y. H. Kim, J. I. Han, K. Cho, *Advanced Materials* **2007**, 19, 678.
- [83] J. Veres, S. Ogier, G. Lloyd, D. de Leeuw, *Chemistry of Materials* **2004**, 16, 4543.
- [84] J. Xiang, P. Zhu, Y. Masuda, K. Koumoto, *Langmuir* **2004**, 20, 3278.
- [85] A. R. Brown, C. P. Jarrett, D. M. de Leeuw, M. Matters, *Synthetic Metals* **1997**, 88, 37.
- [86] C. Jihua, T. Chee Keong, S. Max, A. John, C. M. David, *Journal of Applied Physics* **2008**, 103, 114513.

- [87] M.-B. Madec, D. Crouch, G. Rincon Llorente, T. J. Whittle, M. Geoghegan, S. G. Yeates, *Journal of Materials Chemistry* **2008**, *18*, 3230.
- [88] G. Rincon Llorente, M.-B. Madec, D. Crouch, R. G. Pritchard, S. G. Yeates, *Materials Research Society Symposium Proceedings* **2009**, *1114*, no page given.
- [89] M.-b. Madec, D. J. Crouch, G. Rincon-LLorente, T. Whitte, M. Geoghegan, S. G. Yeates, *Electronic Journal of Surface Science and nanotechnology* **2009**, *7*.
- [90] P. W. M. Blom, N. C. Greenham, C. D. Dimitrakopoulos, C. D. Frisbie, *Materials Research Society* **2003**, *771*, no page given.
- [91] V. Subramanian, P. C. Chang, J. B. Lee, S. E. Molesa, S. K. Volkman, *IEEE transactions on components and packaging technologies* **2005**, *28*, 742.
- [92] A. Babel, S. A. Jenekhe, *Macromolecules* **2004**, *37*, 9835.
- [93] B. A. Brown, D. C. Cupertino, S. Leeming, J. Veres, J. D. Schofield, S. G. Yeates, *Vol. EP 1340270*, **2002**.
- [94] N. Stingelin-Stutzmann, E. Smits, H. Wondergem, C. Tanase, P. Blom, P. Smith, D. de Leeuw, *Nat Mater* **2005**, *4*, 601.
- [95] S. Goffri, C. Muller, N. Stingelin-Stutzmann, D. W. Breiby, C. P. Radano, J. W. Andreasen, R. Thompson, R. A. J. Janssen, M. M. Nielsen, P. Smith, H. Sirringhaus, *Nat Mater* **2006**, *5*, 950.
- [96] a)H. S. Byun, Y.-X. Xu, C. K. Song, *Thin Solid Films* **2005**, *493*, 278; b)P. C. chang, S. E. Molesa, A. R. Murphy, J. M. J. Frechet, V. Subramanian, *IEEE Transactions on electron devices* **2006**, *53*, 594; c)I. Torres, D. M. Taylor, *Journal of applied physics* **2005**, *98*, 073710; d)M. Iwamoto, T. Manaka, E. Lim, R. Tamura, *Current Applied Physics* **2007**, *7*, 334.
- [97] K. Ryu, I. Kymisis, V. Bulovic, C. G. Sodini, *IEEE Transactions on electron devices* **2005**, *26*, 716.
- [98] H. Sirringhaus, *Advanced Materials* **2005**, *17*, 2411.
- [99] D. B. Holt, B. G. Yacobi, *Extended defects in semiconductors*, Cambridge University Press, **2007**.
- [100] F. A. Castro, C. F. O. Graeff, J. Heier, R. Hany, *Polymer* **2007**, *48*, 2380.
- [101] R. Jaszek, *Journal of materials science: materials in electronics* **2001**, *12*, 1.

- [102] D. Briggs, *Surface analysis of polymers by XPS and static SIMS*, Cambridge University Press, **2005**.
- [103] G. Beamson, D. Briggs, *High resolution XPS of organic polymers: the Scienta ESCA300 database* John Wiley & Sons, **1992**.
- [104] a)C. Lay-Lay, K. H. H. Peter, S. Henning, H. F. Richard, *Applied Physics Letters* **2004**, *84*, 3400; b)A. C. Arias, J. D. MacKenzie, R. Stevenson, J. J. M. Halls, M. Inbasekaran, E. P. Woo, D. Richards, R. H. Friend, *Macromolecules* **2001**, *34*, 6005.
- [105] T. Ohe, M. Kuribayashi, R. Yasuda, A. Tsuboi, K. Nomoto, K. Satori, M. Itabashi, J. Kasahara, *Applied Physics Letters* **2008**, *93*, 053303.
- [106] J. Smith, R. Hamilton, I. McCulloch, M. Heeney, J. E. Anthony, D. D. C. Bradley, T. D. Anthopoulos, *Synthetic Metals* **2009**, *159*, 2365.
- [107] S. Iijima, *Nature* **1991**, *354*, 56.
- [108] T. Hayashi, Y. A. Kim, T. Natsuki, M. Endo, *ChemPhysChem* **2007**, *8*, 999.
- [109] V. Derycke, S. Auvray, J. Borghetti, C.-L. Chung, R. Lefèvre, A. Lopez-Bezanilla, K. Nguyen, G. Robert, G. Schmidt, C. Anghel, N. Chimot, S. Lyonnais, S. Streiff, S. Campidelli, P. Chenevier, A. Filoramo, M. F. Goffman, L. Goux-Capes, S. Latil, X. Blase, F. Triozon, S. Roche, J.-P. Bourgoin, *Comptes Rendus Physique* **2009**, *10*, 330.
- [110] <http://www.nanotech-now.com/nanotube-buckyball-sites.htm>.
- [111] S. Reich, C. Thomsen, J. Maultzch, *Carbon nanotubes, Basic concepts and physical properties*, Wiley-VCH, **2004**.
- [112] M. C. Hersam, *Nat Nano* **2008**, *3*, 387.
- [113] R. Krupke, F. Hennrich, *Advanced Engineering Materials* **2005**, *7*, 111.
- [114] D. Tasis, N. Tagmatarchis, A. Bianco, M. Prato, *Chemical Reviews* **2006**, *106*, 1105.
- [115] a)A. Koshio, M. Yudasaka, M. Zhang, S. Iijima, *Nano Letters* **2001**, *1*, 361; b)M. Holzinger, O. Vostrowsky, A. Hirsch, F. Hennrich, M. Kappes, R. Weiss, F. Jellen, *Angewandte Chemie International Edition* **2001**, *40*, 4002.
- [116] a)M. Zheng, A. Jagota, E. D. Semke, B. A. Diner, R. S. McLean, S. R. Lustig, R. E. Richardson, N. G. Tassi, *Nat Mater* **2003**, *2*, 338; b)T. G. Hedderman, S.



- M. Keogh, G. Chambers, H. J. Byrne, *The Journal of Physical Chemistry B* **2004**, *108*, 18860.
- [117] R. J. Chen, Y. Zhang, D. Wang, H. Dai, *Journal of the American Chemical Society* **2001**, *123*, 3838.
- [118] S. M. Keogh, T. G. Hedderman, E. Gregan, G. Farrell, G. Chambers, H. J. Byrne, *The Journal of Physical Chemistry B* **2004**, *108*, 6233.
- [119] Y. Asada, T. Sugai, R. Kitaura, H. Shinohara, *Journal of nanomaterials* **2009**, *2009*.
- [120] L. Zhang, S. Zaric, X. Tu, X. Wang, W. Zhao, H. Dai, *Journal of the American Chemical Society* **2008**, *130*, 2686.
- [121] a)B. Z. Tang, H. Xu, *Macromolecules* **1999**, *32*, 2569; b)P. Fournet, J. N. Coleman, B. Lahr, A. Drury, W. J. Blau, D. F. O'Brien, H.-H. Horhold, *Journal of applied physics* **2001**, *90*, 969; c)P. Fournet, D. F. O'Brien, J. N. Coleman, H. H. Hörhold, W. J. Blau, *Synthetic Metals* **2001**, *121*, 1683; d)I. Alexandrou, E. Kymakis, G. A. J. Amaratunga, *Applied Physics Letters* **2002**, *80*, 1435; e)X. Liu, M. B. Chan-Park, *Journal of Applied Polymer Science* **2009**, *114*, 3414.
- [122] B. Mc Carthy, J. N. Coleman, R. Czerw, A. B. Dalton, D. L. Carroll, W. J. Blau, *Synthetic Metals* **2001**, *121*, 1225.
- [123] J. Chen, H. Liu, W. A. Weimer, M. D. Halls, D. H. Waldeck, G. C. Walker, *Journal of the American Chemical Society* **2002**, *124*, 9034.
- [124] J. Lu, S. Nagase, X. Zhang, D. Wang, M. Ni, Y. Maeda, T. Wakahara, T. Nakahodo, T. Tsuchiya, T. Akasaka, Z. Gao, D. Yu, H. Ye, W. N. Mei, Y. Zhou, *Journal of the American Chemical Society* **2006**, *128*, 5114.
- [125] T. G. Hedderman, S. M. Keogh, G. Chambers, H. J. Byrne, *The Journal of Physical Chemistry B* **2006**, *110*, 3895.
- [126] E. Gregan, S. M. Keogh, A. Maguire, T. G. Hedderman, L. O. Neill, G. Chambers, H. J. Byrne, *Carbon* **2004**, *42*, 1031.
- [127] <http://www.olympusmicro.com/primer/java/jablonski/jabintro/index.html>.
- [128] J. R. Lackowicz, *Principles of fluorescence spectroscopy*, Springer science, **1983**.

- [129] A. Sharma, S. G. Shulman, *Introduction to fluorescence spectroscopy*, Wiley, **1999**.
- [130] E. Wyn-Jones, J. Gormally, *Aggregation processes in solution*, Elsevier, **1983**.
- [131] W. Ried, F. Anthöfer, *Angewandte Chemie* **1953**, *65*, 601.
- [132] S. Kotha, R. J. Stoodley, *Bioorganic & Medicinal Chemistry* **2002**, *10*, 621.

## **9 Appendix**

## 9.1 X-rays crystallographic data for TMTES-pentacene (4).

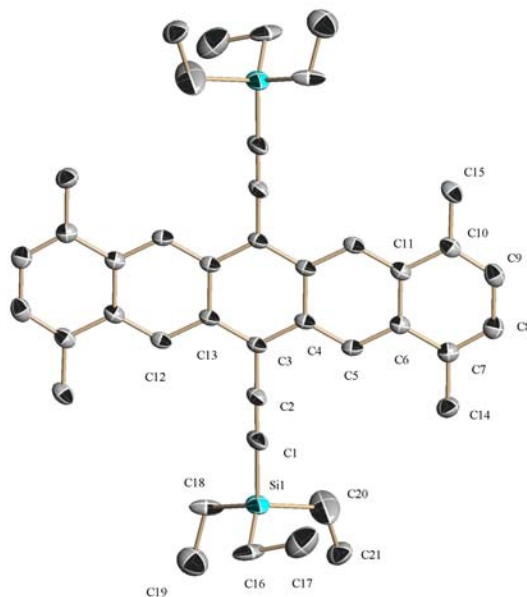


**Table 1.** Crystal data and structure refinement for TMTES-pentacene

Identification code	new	
Empirical formula	C <sub>42</sub> H <sub>50</sub> Si <sub>2</sub>	
Formula weight	611	
Temperature	150(2) K	
Wavelength	0.71073 Å	
Crystal system	Triclinic	
Space group	P -1	
Unit cell dimensions	a = 7.3024(2) Å	a = 74.402(3)°.
	b = 10.9762(3) Å	b = 89.953(2)°.
	c = 12.1090(4) Å	g = 73.746(2)°.
Volume	894.55(5) Å <sup>3</sup>	
Z	1	
Density (calculated)	1.134 Mg/m <sup>3</sup>	
Absorption coefficient	0.127 mm <sup>-1</sup>	
F(000)	330	
Crystal size	0.25 x 0.18 x 0.18 mm <sup>3</sup>	
Theta range for data collection	3.02 to 25.49°.	

Index ranges	-6<=h<=8, -13<=k<=12, -12<=l<=14
Reflections collected	13549
Independent reflections	3297 [R(int) = 0.0774]
Completeness to theta = 25.49°	99.2 %
Absorption correction	Semi-empirical from equivalents
Max. and min. transmission	0.9775 and 0.969
Refinement method	Full-matrix least-squares on F <sup>2</sup>
Data / restraints / parameters	3297 / 186 / 258
Goodness-of-fit on F <sup>2</sup>	0.967
Final R indices [I>2sigma(I)]	R1 = 0.0771, wR2 = 0.1697
R indices (all data)	R1 = 0.1162, wR2 = 0.1991
Largest diff. peak and hole	0.343 and -0.268 e.Å <sup>-3</sup>

**Table 2.** Atomic coordinates ( $\times 10^4$ ) and equivalent isotropic displacement parameters ( $\text{\AA}^2 \times 10^3$ ) for TMTES-pentacene.  $U(\text{eq})$  is defined as one third of the trace of the orthogonalized  $U_{ij}$  tensor.

	x	y	z	$U(\text{eq})$
C(1)	4539(3)	7179(2)	7272(2)	57(1)
C(2)	4720(3)	6514(2)	6599(2)	46(1)
C(3)	4877(3)	5745(2)	5805(2)	39(1)
C(4)	3653(3)	4937(2)	5854(2)	38(1)
C(5)	2311(3)	4851(2)	6678(2)	42(1)
C(6)	1065(3)	4087(2)	6725(2)	41(1)
C(7)	-337(3)	4041(2)	7563(2)	47(1)
C(8)	-1516(3)	3285(2)	7558(2)	53(1)
C(9)	-1401(3)	2538(2)	6753(2)	54(1)
C(10)	-121(3)	2548(2)	5942(2)	47(1)
C(11)	1181(3)	3331(2)	5900(2)	42(1)
C(12)	7477(3)	6603(2)	4905(2)	41(1)
C(13)	6224(3)	5822(2)	4965(2)	39(1)
C(14)	-498(4)	4853(2)	8408(2)	58(1)
C(15)	-41(3)	1761(2)	5081(2)	56(1)
Si(1)	4217(1)	8252(1)	8225(1)	66(1)
C(16)	5819(10)	7420(5)	9479(4)	79(2)
C(17)	4912(11)	6249(8)	9973(7)	117(3)
C(18)	4515(8)	9912(4)	7410(4)	65(2)
C(19)	4710(11)	10856(6)	8120(7)	105(2)
C(20)	1585(9)	8503(7)	8527(8)	147(3)
C(21)	669(8)	9426(6)	9222(5)	72(2)
C(16B)	5375(9)	7223(6)	9725(5)	75(2)
C(17B)	5605(8)	8028(4)	10578(4)	69(2)
C(18B)	5900(9)	9286(6)	7658(6)	114(2)
C(19B)	5518(8)	9985(5)	6490(5)	70(2)
C(20B)	1792(7)	9101(5)	8273(4)	68(2)
C(21B)	532(10)	8326(8)	8697(8)	119(3)

**Table 3.** Bond lengths [ $\text{\AA}$ ] and angles [ $^\circ$ ] for TMTES-pentacene.

---

C(1)-C(2)	1.217(3)
C(1)-Si(1)	1.830(3)
C(2)-C(3)	1.425(3)
C(3)-C(4)	1.416(3)
C(3)-C(13)	1.417(3)
C(4)-C(5)	1.402(3)
C(4)-C(13)#1	1.444(3)
C(5)-C(6)	1.390(3)
C(5)-H(5)	0.95
C(6)-C(7)	1.443(3)
C(6)-C(11)	1.449(3)
C(7)-C(8)	1.354(3)
C(7)-C(14)	1.512(3)
C(8)-C(9)	1.422(4)
C(8)-H(8)	0.95
C(9)-C(10)	1.354(3)
C(9)-H(9)	0.95
C(10)-C(11)	1.443(3)
C(10)-C(15)	1.514(3)
C(11)-C(12)#1	1.384(3)
C(12)-C(11)#1	1.384(3)
C(12)-C(13)	1.408(3)
C(12)-H(12)	0.95
C(13)-C(4)#1	1.444(3)
C(14)-H(14A)	0.98
C(14)-H(14B)	0.98
C(14)-H(14C)	0.98
C(15)-H(15A)	0.98
C(15)-H(15B)	0.98
C(15)-H(15C)	0.98
Si(1)-C(20B)	1.764(5)
Si(1)-C(16)	1.780(5)
Si(1)-C(18)	1.897(5)
Si(1)-C(18B)	1.906(6)

Si(1)-C(16B)	1.911(6)
Si(1)-C(20)	1.913(7)
C(16)-C(17)	1.584(10)
C(16)-H(16A)	0.99
C(16)-H(16B)	0.99
C(17)-H(17A)	0.98
C(17)-H(17B)	0.98
C(17)-H(17C)	0.98
C(18)-C(19)	1.548(8)
C(18)-H(18A)	0.99
C(18)-H(18B)	0.99
C(19)-H(19A)	0.98
C(19)-H(19B)	0.98
C(19)-H(19C)	0.98
C(20)-C(21)	1.504(9)
C(20)-H(20A)	0.99
C(20)-H(20B)	0.99
C(21)-H(21A)	0.98
C(21)-H(21B)	0.98
C(21)-H(21C)	0.98
C(16B)-C(17B)	1.566(8)
C(16B)-H(16C)	0.99
C(16B)-H(16D)	0.99
C(17B)-H(17D)	0.98
C(17B)-H(17E)	0.98
C(17B)-H(17F)	0.98
C(18B)-C(19B)	1.402(8)
C(18B)-H(18C)	0.99
C(18B)-H(18D)	0.99
C(19B)-H(19D)	0.98
C(19B)-H(19E)	0.98
C(19B)-H(19F)	0.98
C(20B)-C(21B)	1.427(9)
C(20B)-H(20C)	0.99
C(20B)-H(20D)	0.99
C(21B)-H(21D)	0.98



C(21B)-H(21E)	0.98
C(21B)-H(21F)	0.98
C(2)-C(1)-Si(1)	177.2(2)
C(1)-C(2)-C(3)	178.4(2)
C(4)-C(3)-C(13)	121.05(19)
C(4)-C(3)-C(2)	119.34(19)
C(13)-C(3)-C(2)	119.60(19)
C(5)-C(4)-C(3)	121.80(19)
C(5)-C(4)-C(13)#1	118.61(19)
C(3)-C(4)-C(13)#1	119.58(19)
C(6)-C(5)-C(4)	122.7(2)
C(6)-C(5)-H(5)	118.6
C(4)-C(5)-H(5)	118.6
C(5)-C(6)-C(7)	121.7(2)
C(5)-C(6)-C(11)	118.65(19)
C(7)-C(6)-C(11)	119.6(2)
C(8)-C(7)-C(6)	118.8(2)
C(8)-C(7)-C(14)	121.3(2)
C(6)-C(7)-C(14)	119.9(2)
C(7)-C(8)-C(9)	121.7(2)
C(7)-C(8)-H(8)	119.2
C(9)-C(8)-H(8)	119.2
C(10)-C(9)-C(8)	122.2(2)
C(10)-C(9)-H(9)	118.9
C(8)-C(9)-H(9)	118.9
C(9)-C(10)-C(11)	119.0(2)
C(9)-C(10)-C(15)	121.3(2)
C(11)-C(10)-C(15)	119.6(2)
C(12)#1-C(11)-C(10)	122.5(2)
C(12)#1-C(11)-C(6)	118.9(2)
C(10)-C(11)-C(6)	118.7(2)
C(11)#1-C(12)-C(13)	122.8(2)
C(11)#1-C(12)-H(12)	118.6
C(13)-C(12)-H(12)	118.6
C(12)-C(13)-C(3)	122.30(19)

C(12)-C(13)-C(4)#1	118.33(19)
C(3)-C(13)-C(4)#1	119.37(19)
C(7)-C(14)-H(14A)	109.5
C(7)-C(14)-H(14B)	109.5
H(14A)-C(14)-H(14B)	109.5
C(7)-C(14)-H(14C)	109.5
H(14A)-C(14)-H(14C)	109.5
H(14B)-C(14)-H(14C)	109.5
C(10)-C(15)-H(15A)	109.5
C(10)-C(15)-H(15B)	109.5
H(15A)-C(15)-H(15B)	109.5
C(10)-C(15)-H(15C)	109.5
H(15A)-C(15)-H(15C)	109.5
H(15B)-C(15)-H(15C)	109.5
C(20B)-Si(1)-C(16)	123.1(3)
C(20B)-Si(1)-C(1)	112.6(2)
C(16)-Si(1)-C(1)	108.7(2)
C(20B)-Si(1)-C(18)	86.7(2)
C(16)-Si(1)-C(18)	114.2(3)
C(1)-Si(1)-C(18)	109.54(16)
C(20B)-Si(1)-C(18B)	117.5(3)
C(16)-Si(1)-C(18B)	89.2(3)
C(1)-Si(1)-C(18B)	102.0(2)
C(18)-Si(1)-C(18B)	31.8(2)
C(20B)-Si(1)-C(16B)	111.4(3)
C(16)-Si(1)-C(16B)	14.9(3)
C(1)-Si(1)-C(16B)	109.1(2)
C(18)-Si(1)-C(16B)	125.7(3)
C(18B)-Si(1)-C(16B)	103.4(3)
C(20B)-Si(1)-C(20)	21.6(3)
C(16)-Si(1)-C(20)	113.2(3)
C(1)-Si(1)-C(20)	102.3(3)
C(18)-Si(1)-C(20)	108.2(3)
C(18B)-Si(1)-C(20)	139.1(3)
C(16B)-Si(1)-C(20)	99.1(3)
C(17)-C(16)-Si(1)	97.8(4)

C(17)-C(16)-H(16A)	112.2
Si(1)-C(16)-H(16A)	112.2
C(17)-C(16)-H(16B)	112.2
Si(1)-C(16)-H(16B)	112.2
H(16A)-C(16)-H(16B)	109.8
C(16)-C(17)-H(17A)	109.5
C(16)-C(17)-H(17B)	109.5
H(17A)-C(17)-H(17B)	109.5
C(16)-C(17)-H(17C)	109.5
H(17A)-C(17)-H(17C)	109.5
H(17B)-C(17)-H(17C)	109.5
C(19)-C(18)-Si(1)	117.4(4)
C(19)-C(18)-H(18A)	107.9
Si(1)-C(18)-H(18A)	107.9
C(19)-C(18)-H(18B)	107.9
Si(1)-C(18)-H(18B)	107.9
H(18A)-C(18)-H(18B)	107.2
C(18)-C(19)-H(19A)	109.5
C(18)-C(19)-H(19B)	109.5
H(19A)-C(19)-H(19B)	109.5
C(18)-C(19)-H(19C)	109.5
H(19A)-C(19)-H(19C)	109.5
H(19B)-C(19)-H(19C)	109.5
C(21)-C(20)-Si(1)	119.9(5)
C(21)-C(20)-H(20A)	107.3
Si(1)-C(20)-H(20A)	107.3
C(21)-C(20)-H(20B)	107.3
Si(1)-C(20)-H(20B)	107.3
H(20A)-C(20)-H(20B)	106.9
C(20)-C(21)-H(21A)	109.5
C(20)-C(21)-H(21B)	109.5
H(21A)-C(21)-H(21B)	109.5
C(20)-C(21)-H(21C)	109.5
H(21A)-C(21)-H(21C)	109.5
H(21B)-C(21)-H(21C)	109.5
C(17B)-C(16B)-Si(1)	115.6(4)

C(17B)-C(16B)-H(16C)	108.4
Si(1)-C(16B)-H(16C)	108.4
C(17B)-C(16B)-H(16D)	108.4
Si(1)-C(16B)-H(16D)	108.4
H(16C)-C(16B)-H(16D)	107.4
C(16B)-C(17B)-H(17D)	109.5
C(16B)-C(17B)-H(17E)	109.5
H(17D)-C(17B)-H(17E)	109.5
C(16B)-C(17B)-H(17F)	109.5
H(17D)-C(17B)-H(17F)	109.5
H(17E)-C(17B)-H(17F)	109.5
C(19B)-C(18B)-Si(1)	114.3(4)
C(19B)-C(18B)-H(18C)	108.7
Si(1)-C(18B)-H(18C)	108.7
C(19B)-C(18B)-H(18D)	108.7
Si(1)-C(18B)-H(18D)	108.7
H(18C)-C(18B)-H(18D)	107.6
C(18B)-C(19B)-H(19D)	109.5
C(18B)-C(19B)-H(19E)	109.5
H(19D)-C(19B)-H(19E)	109.5
C(18B)-C(19B)-H(19F)	109.5
H(19D)-C(19B)-H(19F)	109.5
H(19E)-C(19B)-H(19F)	109.5
C(21B)-C(20B)-Si(1)	117.5(4)
C(21B)-C(20B)-H(20C)	107.9
Si(1)-C(20B)-H(20C)	107.9
C(21B)-C(20B)-H(20D)	107.9
Si(1)-C(20B)-H(20D)	107.9
H(20C)-C(20B)-H(20D)	107.2
C(20B)-C(21B)-H(21D)	109.5
C(20B)-C(21B)-H(21E)	109.5
H(21D)-C(21B)-H(21E)	109.5
C(20B)-C(21B)-H(21F)	109.5
H(21D)-C(21B)-H(21F)	109.5
H(21E)-C(21B)-H(21F)	109.5

Symmetry transformations used to generate equivalent atoms:

#1  $-x+1,-y+1,-z+1$

**Table 4.** Hydrogen coordinates ( $\times 10^4$ ) and isotropic displacement parameters ( $\text{\AA}^2 \times 10^3$ ) for TMTES-pentacene.

	x	y	z	U(eq)
H(5)	2250	5334	7227	50
H(8)	-2445	3253	8107	64
H(9)	-2248	2014	6784	65
H(12)	7399	7105	5441	49
H(14A)	-1509	4707	8914	87
H(14B)	-811	5792	7986	87
H(14C)	723	4587	8870	87
H(15A)	-1016	1292	5222	84
H(15B)	1228	1121	5164	84
H(15C)	-282	2362	4300	84
H(16A)	7156	7098	9290	94
H(16B)	5758	7976	10008	94
H(17A)	5625	5673	10699	175
H(17B)	4979	5736	9417	175
H(17C)	3572	6613	10108	175
H(18A)	5664	9748	6975	78
H(18B)	3399	10378	6839	78
H(19A)	5502	11405	7733	157
H(19B)	5313	10336	8889	157
H(19C)	3439	11424	8187	157
H(20A)	828	8813	7775	176
H(20B)	1439	7624	8921	176
H(21A)	-710	9535	9206	108
H(21B)	890	10288	8894	108
H(21C)	1231	9058	10019	108
H(16C)	4598	6631	10071	90
H(16D)	6658	6657	9642	90
H(17D)	6158	7417	11329	104
H(17E)	4349	8602	10664	104
H(17F)	6452	8571	10275	104

H(18C)	5817	9925	8112	137
H(18D)	7229	8696	7782	137
H(19D)	5590	10887	6383	105
H(19E)	4233	10016	6227	105
H(19F)	6463	9540	6043	105
H(20C)	1740	9707	8755	82
H(20D)	1288	9655	7484	82
H(21D)	-763	8911	8681	179
H(21E)	976	7792	9489	179
H(21F)	518	7743	8212	179

---

## 9.2 X-rays crystallographic data for TMTIPS-pentacene (5).

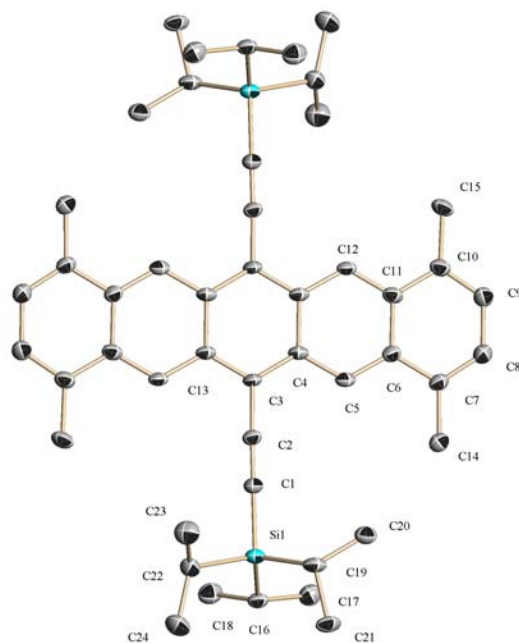


**Table 1.** Crystal data and structure refinement for TMTIPS-pentacene.

Identification code	shelxl	
Empirical formula	C <sub>48</sub> H <sub>62</sub> Si <sub>2</sub>	
Formula weight	695.16	
Temperature	173(2) K	
Wavelength	0.71073 Å	
Crystal system	Triclinic	
Space group	P -1	
Unit cell dimensions	a = 9.0135(6) Å	a = 70.694(2)°.
	b = 10.2107(5) Å	b = 84.900(2)°.
	c = 11.7743(8) Å	g = 82.342(5)°.
Volume	1012.41(11) Å <sup>3</sup>	
Z	1	
Density (calculated)	1.14 Mg/m <sup>3</sup>	
Absorption coefficient	0.12 mm <sup>-1</sup>	
F(000)	378	



Crystal size	0.3 x 0.12 x 0.04 mm <sup>3</sup>
Theta range for data collection	3.02 to 25.5°.
Index ranges	0<=h<=10, -12<=k<=12, -14<=l<=14
Reflections collected	5600
Independent reflections	3548 [R(int) = 0.098]
Completeness to theta = 25.5°	93.9 %
Absorption correction	Semi-empirical from equivalents
Max. and min. transmission	0.9952 and 0.965
Refinement method	Full-matrix least-squares on F <sup>2</sup>
Data / restraints / parameters	3548 / 0 / 229
Goodness-of-fit on F <sup>2</sup>	1.025
Final R indices [I>2sigma(I)]	R1 = 0.118, wR2 = 0.2393
R indices (all data)	R1 = 0.1849, wR2 = 0.2784
Extinction coefficient	0.042(8)
Largest diff. peak and hole	0.647 and -0.668 e.Å <sup>-3</sup>

**Table 2.** Atomic coordinates ( $\times 10^4$ ) and equivalent isotropic displacement parameters ( $\text{\AA}^2 \times 10^3$ ) for TMTIPS-pentacene.  $U(\text{eq})$  is defined as one third of the trace of the orthogonalized  $U_{ij}$  tensor.

	x	y	z	$U(\text{eq})$
C(1)	4857(7)	2226(6)	2294(5)	41(1)
C(2)	4928(6)	1505(6)	1650(5)	36(1)
C(3)	4982(6)	731(6)	822(5)	36(1)
C(4)	6220(6)	723(5)	23(5)	35(1)
C(5)	7456(7)	1436(5)	1(5)	37(1)
C(6)	8669(7)	1470(6)	-798(5)	38(1)
C(7)	9929(7)	2199(6)	-793(5)	40(1)
C(8)	11095(7)	2172(6)	-1594(6)	48(2)
C(9)	11110(8)	1457(6)	-2439(6)	49(2)
C(10)	9949(7)	761(6)	-2500(5)	44(2)
C(11)	8709(7)	735(6)	-1664(5)	40(1)
C(12)	7501(7)	18(5)	-1647(5)	37(1)
C(13)	3756(6)	14(5)	835(5)	35(1)
C(14)	9920(7)	2984(6)	90(6)	46(2)
C(15)	9976(8)	47(7)	-3434(6)	53(2)
C(16)	5729(7)	3039(6)	4388(5)	41(1)
C(17)	7404(8)	3110(7)	4012(6)	55(2)
C(18)	5513(9)	1616(6)	5313(6)	56(2)
C(19)	4817(8)	5253(6)	1957(5)	47(2)
C(20)	6210(8)	5227(7)	1089(6)	52(2)
C(21)	4908(9)	6373(6)	2554(6)	54(2)
C(22)	2485(7)	3428(7)	3658(6)	48(2)
C(23)	1428(8)	3862(8)	2600(7)	64(2)
C(24)	1987(9)	4226(8)	4531(7)	66(2)
Si(1)	4502(2)	3516(2)	3088(2)	40(1)

**Table 3.** Bond lengths [Å] and angles [°] for TMTIPS-pentacene.

---

C(1)-C(2)	1.213(7)
C(1)-Si(1)	1.832(6)
C(2)-C(3)	1.438(7)
C(3)-C(4)	1.395(8)
C(3)-C(13)	1.401(8)
C(4)-C(5)	1.403(8)
C(4)-C(13)#1	1.443(7)
C(5)-C(6)	1.374(8)
C(5)-H(5)	0.95
C(6)-C(7)	1.440(8)
C(6)-C(11)	1.447(7)
C(7)-C(8)	1.352(8)
C(7)-C(14)	1.507(8)
C(8)-C(9)	1.413(8)
C(8)-H(8)	0.95
C(9)-C(10)	1.360(9)
C(9)-H(9)	0.95
C(10)-C(11)	1.420(8)
C(10)-C(15)	1.504(8)
C(11)-C(12)	1.387(8)
C(12)-C(13)#1	1.412(8)
C(12)-H(12)	0.95
C(13)-C(12)#1	1.412(8)
C(13)-C(4)#1	1.443(7)
C(14)-H(14A)	0.98
C(14)-H(14B)	0.98
C(14)-H(14C)	0.98
C(15)-H(15A)	0.98
C(15)-H(15B)	0.98
C(15)-H(15C)	0.98
C(16)-C(18)	1.526(8)
C(16)-C(17)	1.540(9)
C(16)-Si(1)	1.862(6)
C(16)-H(16)	1

C(17)-H(17A)	0.98
C(17)-H(17B)	0.98
C(17)-H(17C)	0.98
C(18)-H(18A)	0.98
C(18)-H(18B)	0.98
C(18)-H(18C)	0.98
C(19)-C(21)	1.540(7)
C(19)-C(20)	1.550(9)
C(19)-Si(1)	1.872(6)
C(19)-H(19)	1
C(20)-H(20A)	0.98
C(20)-H(20B)	0.98
C(20)-H(20C)	0.98
C(21)-H(21A)	0.98
C(21)-H(21B)	0.98
C(21)-H(21C)	0.98
C(22)-C(24)	1.517(8)
C(22)-C(23)	1.546(9)
C(22)-Si(1)	1.885(6)
C(22)-H(22)	1
C(23)-H(23A)	0.98
C(23)-H(23B)	0.98
C(23)-H(23C)	0.98
C(24)-H(24A)	0.98
C(24)-H(24B)	0.98
C(24)-H(24C)	0.98
C(2)-C(1)-Si(1)	169.9(6)
C(1)-C(2)-C(3)	176.2(6)
C(4)-C(3)-C(13)	121.7(5)
C(4)-C(3)-C(2)	120.2(5)
C(13)-C(3)-C(2)	118.1(5)
C(3)-C(4)-C(5)	122.3(5)
C(3)-C(4)-C(13)#1	119.9(5)
C(5)-C(4)-C(13)#1	117.8(5)
C(6)-C(5)-C(4)	123.2(5)

C(6)-C(5)-H(5)	118.4
C(4)-C(5)-H(5)	118.4
C(5)-C(6)-C(7)	122.1(5)
C(5)-C(6)-C(11)	119.6(5)
C(7)-C(6)-C(11)	118.3(5)
C(8)-C(7)-C(6)	118.9(5)
C(8)-C(7)-C(14)	121.4(5)
C(6)-C(7)-C(14)	119.7(5)
C(7)-C(8)-C(9)	122.0(6)
C(7)-C(8)-H(8)	119
C(9)-C(8)-H(8)	119
C(10)-C(9)-C(8)	122.0(6)
C(10)-C(9)-H(9)	119
C(8)-C(9)-H(9)	119
C(9)-C(10)-C(11)	118.2(5)
C(9)-C(10)-C(15)	120.9(6)
C(11)-C(10)-C(15)	121.0(6)
C(12)-C(11)-C(10)	121.6(5)
C(12)-C(11)-C(6)	117.8(5)
C(10)-C(11)-C(6)	120.5(5)
C(11)-C(12)-C(13)#1	122.9(5)
C(11)-C(12)-H(12)	118.5
C(13)#1-C(12)-H(12)	118.5
C(3)-C(13)-C(12)#1	123.0(5)
C(3)-C(13)-C(4)#1	118.3(5)
C(12)#1-C(13)-C(4)#1	118.6(5)
C(7)-C(14)-H(14A)	109.5
C(7)-C(14)-H(14B)	109.5
H(14A)-C(14)-H(14B)	109.5
C(7)-C(14)-H(14C)	109.5
H(14A)-C(14)-H(14C)	109.5
H(14B)-C(14)-H(14C)	109.5
C(10)-C(15)-H(15A)	109.5
C(10)-C(15)-H(15B)	109.5
H(15A)-C(15)-H(15B)	109.5
C(10)-C(15)-H(15C)	109.5

H(15A)-C(15)-H(15C)	109.5
H(15B)-C(15)-H(15C)	109.5
C(18)-C(16)-C(17)	109.5(5)
C(18)-C(16)-Si(1)	113.4(4)
C(17)-C(16)-Si(1)	113.4(4)
C(18)-C(16)-H(16)	106.7
C(17)-C(16)-H(16)	106.7
Si(1)-C(16)-H(16)	106.7
C(16)-C(17)-H(17A)	109.5
C(16)-C(17)-H(17B)	109.5
H(17A)-C(17)-H(17B)	109.5
C(16)-C(17)-H(17C)	109.5
H(17A)-C(17)-H(17C)	109.5
H(17B)-C(17)-H(17C)	109.5
C(16)-C(18)-H(18A)	109.5
C(16)-C(18)-H(18B)	109.5
H(18A)-C(18)-H(18B)	109.5
C(16)-C(18)-H(18C)	109.5
H(18A)-C(18)-H(18C)	109.5
H(18B)-C(18)-H(18C)	109.5
C(21)-C(19)-C(20)	109.0(5)
C(21)-C(19)-Si(1)	112.3(4)
C(20)-C(19)-Si(1)	114.5(4)
C(21)-C(19)-H(19)	106.9
C(20)-C(19)-H(19)	106.9
Si(1)-C(19)-H(19)	106.9
C(19)-C(20)-H(20A)	109.5
C(19)-C(20)-H(20B)	109.5
H(20A)-C(20)-H(20B)	109.5
C(19)-C(20)-H(20C)	109.5
H(20A)-C(20)-H(20C)	109.5
H(20B)-C(20)-H(20C)	109.5
C(19)-C(21)-H(21A)	109.5
C(19)-C(21)-H(21B)	109.5
H(21A)-C(21)-H(21B)	109.5
C(19)-C(21)-H(21C)	109.5

H(21A)-C(21)-H(21C)	109.5
H(21B)-C(21)-H(21C)	109.5
C(24)-C(22)-C(23)	111.1(6)
C(24)-C(22)-Si(1)	114.8(5)
C(23)-C(22)-Si(1)	110.9(5)
C(24)-C(22)-H(22)	106.5
C(23)-C(22)-H(22)	106.5
Si(1)-C(22)-H(22)	106.5
C(22)-C(23)-H(23A)	109.5
C(22)-C(23)-H(23B)	109.5
H(23A)-C(23)-H(23B)	109.5
C(22)-C(23)-H(23C)	109.5
H(23A)-C(23)-H(23C)	109.5
H(23B)-C(23)-H(23C)	109.5
C(22)-C(24)-H(24A)	109.5
C(22)-C(24)-H(24B)	109.5
H(24A)-C(24)-H(24B)	109.5
C(22)-C(24)-H(24C)	109.5
H(24A)-C(24)-H(24C)	109.5
H(24B)-C(24)-H(24C)	109.5
C(1)-Si(1)-C(16)	110.9(3)
C(1)-Si(1)-C(19)	107.0(3)
C(16)-Si(1)-C(19)	112.3(3)
C(1)-Si(1)-C(22)	104.6(3)
C(16)-Si(1)-C(22)	109.5(3)
C(19)-Si(1)-C(22)	112.3(3)

---

Symmetry transformations used to generate equivalent atoms:

#1 -x+1,-y,-z

**Table 4.** Hydrogen coordinates ( $\times 10^4$ ) and isotropic displacement parameters ( $\text{\AA}^2 \times 10^3$ ) for TMTIPS-pentacene.

	x	y	z	U(eq)
H(5)	7454	1918	567	44
H(8)	11930	2648	-1589	57
H(9)	11958	1463	-2981	59
H(12)	7519	-474	-2207	44
H(14A)	10887	3349	25	68
H(14B)	9750	2352	911	68
H(14C)	9117	3760	-90	68
H(15A)	10944	113	-3887	79
H(15B)	9171	500	-3987	79
H(15C)	9830	-938	-3036	79
H(16)	5434	3747	4808	49
H(17A)	7544	4026	3422	82
H(17B)	7762	2378	3653	82
H(17C)	7973	2969	4723	82
H(18A)	4449	1577	5563	84
H(18B)	6095	1475	6017	84
H(18C)	5856	882	4955	84
H(19)	3923	5565	1450	56
H(20A)	6158	4520	702	79
H(20B)	7121	4999	1544	79
H(20C)	6232	6146	471	79
H(21A)	4026	6402	3099	81
H(21B)	4939	7286	1930	81
H(21C)	5817	6143	3011	81
H(22)	2381	2423	4110	57
H(23A)	1763	3320	2058	96
H(23B)	1445	4859	2157	96
H(23C)	405	3683	2915	96
H(24A)	2674	3931	5193	99
H(24B)	971	4036	4856	99



H(24C)

1997

5229

4110

99

---